Multinuclear Solid-State NMR Studies of Phosphate Uptake by Aluminum (Hydr)oxides

A Dissertation Presented

by

Wei Li

to
The Graduate School
in Partial Fulfillments of the Requirements
for the Degree of

Doctor of Philosophy
in
Geosciences

Stony Brook University
December 2010

Stony Brook University

The Graduate School

Wei Li

We, the dissertation committee for the above candidate for the
Doctor of Philosophy degree, hereby recommend
acceptance of this dissertation.

Dr. Brian L. Phillips – Dissertation Advisor
Associate professor, Department of Geosciences

Dr. Richard J. Reeder - Chairperson of Defense
Chair and Professor, Department of Geosciences

Dr. Martin A.A. Schoonen – Committee Member
Professor, Department of Geosciences

Dr. Michael Sperazza – Committee Member
Assistant professor, Department of Geosciences

Dr. R. James Kirkpatrick – Outside Member
Dean and Professor, College of Natural Science, Michigan State University

This dissertation is accepted by the Graduate School

Lawrence Martin
Dean of the Graduate School

Abstract of the Dissertation

Multinuclear Solid State NMR Studies of Phosphate Uptake by Aluminum (Hydr)oxides

by

Wei Li

Doctor of Philosophy

In

Geosciences

Stony Brook University

2010

Phosphorus is an essential nutrient for plant growth and agriculture. In aqueous environments, interaction of dissolved phosphate with the surfaces of Al oxyhydroxides and clays is important for controlling its transport, fate and bioavailability. Understanding the reaction mechanisms responsible for phosphate uptake at the molecular level can provide significant insight and improved prediction of phosphate uptake behavior, leading to better strategies for phosphate fertilization and regulation.

In this research, I examined the specific adsorption of phosphate on boehmite (γ-AlOOH) and other Al (hydr)oxides by combining mainly batch sorption techniques, solid-state ^{31}P NMR spectroscopy, quantum chemical calculations and Fourier transform infrared (FTIR) spectroscopy. Solid state NMR spectroscopy is sensitive with phosphate species that adsorb on mineral surfaces, such that outer-sphere complexes, inner-sphere complexes and surface precipitates can be distinguished. Using novel solid state NMR techniques, such as ^{31}P{^{1}H} cross-polarization magic-angle-spinning (CP/MAS) and ^{31}P{^{27}Al} dephasing curves from rotational echo adiabatic passage double resonance (REAPDOR) experiments, formation of bridging bidentate or monodentate mononuclear surface complexes can be readily determined. In particular, solid state NMR results indicate that bridging bidentate surface complexes is responsible for the dominant uptake mechanism for all Al-oxyhydroxides under all conditions (0.1 – 10 mM P; pH 4-10, etc.). Furthermore, two distinct bidentate surface complexes are resolved for adsorbed phosphate on boehmite, even though macroscopic adsorption isotherm is well fitted by a single-site Langmuir isotherm. The two species exhibit distinct pH-dependence and different protonation states, and further examination of their reaction stoichiometry suggests they might adsorb at different surface sites. In addition, I found that in the presence of dissolved calcium, the mechanism of phosphate uptake is dominant by surface precipitation of calcium phosphates (Ca-P). The Ca-P surface precipitate is identified as poorly crystalline hydroxylapatite by two-dimensional $^{31}P\{^{1}H\}$ heteronuclear correlation (HetCor) experiments,. To summarize, this dissertation shows ^{31}P solid state NMR is significant sensitivity to the chemical environment and motional property of phosphate adsorbed on different Al (hydr)oxides, from which a better understanding of mineral surfaces can be achieved by using ^{31}P nuclei as a molecular probe.

Table of contents

Chapter 1. Introduction

Chapter 2. Surface speciation of phosphate on boehmite (γ-AlOOH) determined from NMR spectroscopy

Chapter 3. ^{31}P solid state NMR investigation phosphate sorption on aluminum hydroxides

Chapter 6. General conclusion: promises and constrains of solid state NMR in interfacial geochemistry

List of Figures

List of Tables

Acknowledgments

Achieving the doctoral degree at the Department of Geosciences of Stony Brook University has been a challenging and exciting experience in my life. There were a lot of sufferings, stresses and frustration, but finally all become funs, confidence and stronger heart. While looking back, I feel extremely honored to meet and work with so many fascinating faculty members. Especially, I would like to thank my thesis advisor Dr. Brian L. Phillips for having me to in his solid-state NMR group. Without his academic training, financial support, and fatherhood encouragement, I can not complete this dissertation. He gave much freedom to me, which turns doing research not a boring and tough work any longer, but more like enjoyable games. So I strongly agree with what Dr. John Loring has ever commented in our correspondences, that I was very fortunate to be Brian's student. In the last four years with him, I learned so much from him, not only the knowledge of sciences, but also the wisdom of life. I just wish someday I could be a great scientist and mentor like him, as an appreciation. I also want to thank his wife, Mrs. Katherine Sugg for her kindness and warmness, and particularly for her annual Christmas party!

I would also like to thank my committee members, Prof. R. James Kirkpatrick from Michigan State University for serving as the outside member, and Prof. Richard J. Reeder, Prof. Martin A.A. Schoonen and Prof. Michael Sperazza for their help, encouragement and mentoring in the past four years.

During the four years at Stony Brook, my labmates, Dr. Jian Feng, Dr. Harris E. Mason, Dr. Stacey Cochiara and Miss Laura Kubista have given me a lot of helps and supports in both experiments and daily life, which I am greatly appreciated. Special thanks are given to Jian for his teaching me NMR skills in the early time and the collaboration on the boehmite project. I appreciate the saying that *a group is a family*, and in the mean time I would like to express my gratitude to Prof. Clare P. Gray and all the members in Grey group in Chemistry department for the joint group meeting. Also, I would like to say thanks to my collaborators in the CRC project.

Particular thanks to Prof. James Kubicki at Pennsylvania State University and his former student Dr. Kideok Kwon for their help in quantum chemical calculation, Prof. Daniel Strongin and his student Andro-Marc Pierre-Louis at Temple University for collecting the IR spectra, and Prof. John Parise and his student Wenqian for the collection of X-ray diffraction data.

In addition, I want to acknowledge all the faculty members, staff, graduate students and postdocs in Geosciences department. They are making really a wonderful atmosphere for working enjoyably in this department.

The text of this dissertation in Chapter 2 is a reprint of the material as it appears in *Langmuir*. The co-authors listed in the publication were acknowledged for their help.

Finally, I would like to express my deep appreciation to my beloved parents, Mr. Sanding Li and Ms. Baozhen Yu, and my wife Ms. Fang Wang for their endless love, encouragement, and support to me through my PhD time.

Chapter 1

Introduction

1. Motivation

Phosphorus is an essential element in biological systems, occurring in critical compounds such as adenosine triphosphate (ATP), the energy source for metabolic processes, and phosphate lipid in cell membranes. Thus, its biogeochemical cycle is of significant geochemical, environmental and agricultural importance. In the natural environment, the principal phosphorus species are inorganic phosphates (PO_4^{3-}), among which the most abundant phosphate mineral is hydroxylapatite (Hap) [1], whereas organic phosphorus compounds dominate in the biological systems. Inorganic phosphate can be transformed to organic phosphate, phosphonate, and esters through the uptake of dissolved phosphate by plants, allowing phosphorus to enter the food chain and start its biological cycle in ecological systems.

In the last four decades, phosphorus has received more attention as a pollutant than as a nutrient, due to input of long term run-off from over-fertilization of soils systems and municipal sewage to lakes and rivers [2]. A severe consequence is eutrophication, the process by which excess P in water stimulates the overgrowth of algae and cyanobacteria, leading to a shortage of dissolved oxygen and subsequent death of aquatic organisms. The resulting degradation of aquatic systems brings a series of environmental problems such as water quality that threatens human health. To rationally regulate the overuse of phosphorus, a better understanding of the fate and transport of phosphorus compounds in aqueous and soil environment is needed.

Surface-charged minerals, such as iron (Fe-) and aluminum (Al-) (hydr)oxides, are major constituents of soils and sediments, and tend to strongly adsorb dissolved phosphate, contributing significantly to phosphate immobilization. To understand the uptake mechanism, extensive studies have been undertaken using well-defined minerals (e.g. goethite) as models in laboratories. Methods used to explore the phosphate uptake mechanisms involve batch techniques (i.e. adsorption isotherm and kinetics), surface complexation modeling, spectroscopy such as infrared (IR) and X-ray absorption spectroscopy (XAFS), and quantum chemical calculations. It is well accepted in the literature that dissolved orthophosphate can replace surface hydroxyl groups on Fe- and Al-(hydr)oxides and form stable inner sphere surface complexes [2-3]. Nonetheless, many uncertainties in the details of the bonding configuration remain unresolved. One long-standing controversy is whether the phosphate binds on oxide surface as bidentate coordination or monodentate mononuclear coordination with surface metal atoms [4-5]. Another question is whether the conclusions obtained from studies of metal hydroxides like goethite (α-FeOOH) can be extrapolated to other minerals such as hematite and magnetite. If so, what is the mechanism? If not, then what is the relationship between the atomic arrangement of mineral surface and its corresponding phosphate bonding structure? Since dissolved phosphate is protonated under in most environments (i.e., pH 4 to pH 9), are those phosphate surface complexes adsorbed on minerals protonated as well? In addition, since natural environments are complex and heterogeneous, how do the co-existing anions and cations influence phosphate bonding environment?

To answer these questions, a reliable experimental method to characterize and/or identify the phosphate bonding structures on mineral surface must be established, since most of the controversies are caused by the inability to determine unambiguously structure of the surface adsorbed species. In this dissertation, solid state NMR spectroscopy along with traditional FTIR and batch techniques are used to systematically investigate the mechanism of phosphate adsorption by well-crystalline Al-(hydr)oxides such as boehmite (γ-AlOOH) and corundum (α-Al_2O_3). The first chapter provides an overview of prior phosphate adsorption studies and briefly introduces the NMR techniques that will be used in the following chapters. In Chapter 2, I establish a solid state NMR method for determining the coordination environment of phosphate bonds to boehmite surface, especially the differentiation between bridging bidentate complexes and monodentate mononuclear complexes. Chapter 3 continues the study of phosphate uptake by boehmite, but focuses mainly on the impact of environmental factors such as concentration, pH, ionic strength, moisture. Chapter 4 describes phosphate uptake by corundum (α-Al_2O_3), for the purpose of allowing investigation by both attenuation total reflectance Fourier-transform infrared (ATR-FTIR) and solid state NMR, so that results obtained from two techniques can be compared. Chapter 5 expands the application of solid state NMR to a more heterogeneous system, where the presence of dissolved calcium is added into the phosphate uptake experiments to investigate the effect of dissolved calcium on phosphate adsorption. Finally, in Chapter 6, I summarize the findings in the proceeding chapters and discuss the promise and constraints of the NMR techniques for investigating surface adsorption phenomena.

The goal of this dissertation is to study phosphate adsorption at a molecular level, and provides insight into phosphate interaction with Al (hydr)oxides for better understanding of the phosphorus sequestration in aqueous environments. In the process, it will show that advanced solid state NMR techniques developed from solid state chemistry can be applied to difficult and heterogeneous systems relevant to low temperature aqueous and interfacial geochemistry.

1.2. Overview of phosphate uptake by metal oxides

1.2.1. Phosphorus geochemistry and mineralogy

Phosphorus (P) is the 11th most abundant element in the crust. It occurs mainly in the form of inorganic phosphate minerals and organic phosphate derivatives in rocks and soil. The most common naturally occurring P-bearing mineral is apatite ($Ca_5(PO_4)_3(F,Cl,OH)$), accounting for over 95% of P in the Earth's crust. Dissolution and transport of terrestrial apatite to the oceans contribute the major source of aqueous phosphate [6].

In the periodic table, P belongs to the Group V; the electronic configuration is [Ne] $3s^2 3p_x^1\ p_y^1\ p_z^1$, a state that supplies up to five valence electrons for chemical bonding. This electron configuration gives P three possible oxidation states from +5 to -3; the +5 valence forms orthophosphates as the most stable. The solution chemistry of P is similar to that of arsenate, due to the similar tetrahedral coordination with oxygen. As a results, the three acid dissociation constants for phosphoric acid are very close to those for arsenic acid, with pK_{a1} = 2.1, pK_{a2} = 7.2, and pK_{a3} = 12.3 for phosphate (Figure 1.1) and 2.1, 7.0, 11.5 for arsenate. The ^{31}P NMR chemical shift for phosphate in solution is dependent on pH, with the chemical shift increasing as the phosphate group becomes depronated [7]. Some important organic phosphorus compounds are listed in Figure 1.2.

There are over 300 minerals containing phosphate (PO_4^{3-}) besides the apatite family [6]. Table 1 lists some phosphorus minerals/compounds with relevance to this dissertation and their ^{31}P chemical shift [8]. Aluminum phosphates, including wavellite ($Al_3(PO_4)_2(OH)_3 \cdot 5H_2O$) and variscite ($AlPO_4 \cdot 2H_2O$), are introduced as model structures for aluminum phosphate surface precipitates. Alkali phosphates and alkaline-earth phosphates are listed as potential models of outer-sphere complexes. Calcium phosphates, such as hydroxylapatite and brushite ($CaHPO_4 \cdot 2H_2O$), are useful to understand the possible phosphate-calcium-oxide ternary surface complexes. Systematic examination of ^{31}P chemical shift of these P-containing solids is very useful for understanding variation in magnetic shielding effect and its ability to serve as an indication of chemical environment [9-10].

1.2.2. Advance in phosphate uptake mechanism

There is a broad consensus that orthophosphate is specifically adsorbed onto metal oxides via a ligand-exchange mechanism, as shown by the increase of solution pH observed during P adsorbing onto the oxides from solution [11-13]. A general chemical reaction was provided by Goldberg and Sposito (1985) [3]

$a{\equiv}MeOH(s) + H_bPO_4^{b-3}(aq) + cH^+(aq) \rightarrow {\equiv}Me_aH_cPO_4(s) + bH_2O + (a-b)OH^-(aq)$ (1).

The adsorption products ${\equiv}Me_aH_cPO_4(s)$ are very stable, and can be formed at even very high pH. This is referred as specific adsorption because it cannot be explained by conventional electrostatic attraction. The concept of inner-sphere complexation was proposed to explain specific adsorption, which inner-sphere phosphate complexes bind on mineral surfaces directly with no oxygen atoms or water molecules between surface cations and phosphate, showing covalent or ionic bonding character. This idea was against the traditional outer-sphere complexation, in which phosphate binds on metal oxides via electrostatic interaction, with water or hydrogen bond between mineral surface and phosphate. With respect to molecular dynamics, it is believed that outer-sphere complexes experience rapid exchange (> 10^6 s^{-1}) with free phosphate anions in bulk solution, whereas adsorbed phosphate inner-sphere complexes exchange very slowly with bulk solution. Kinetic evidence for inner-sphere P surface complexes was provided from isotopic exchange experiments by Atkindon et al. (1972) [14], who studied the exchange rates of ^{32}P-labelled phosphate solution and ^{31}P phosphate surface complexes on goethite. The rate constants were reported as 1.7 to 46 $\times$ 10^{-5} s^{-1}, corresponding to a half life for phosphate exchange ranging from 25 minutes to 11 hours. Kyle et al. (1975) [15] performed a similar study for phosphate adsorption on gibbsite, suggesting the half-lives of phosphate on gibbsite range from 27 s to a much long value. The mobile nature of outer-sphere complexes would generate a rapid exchange rate comparable to molecular motion or Brownian diffusive motion in solution.

Structural evidence for inner-sphere phosphate complexes was first provided by IR spectroscopy, and later by NMR spectroscopy. Atkinson (1974) [16] provided the first IR evidence for the formation of inner-sphere complexes and reduced hydroxyl density on the goethite surfaces for supporting the ligand-exhcange mechanism. Bleam et al (1991) [17] used solid state NMR to study the hydrolysis of phosphate on boehmite and reached the same conclusion for the existence of inner-sphere complexes based on their observation of a strong CP/MAS signal. The cross polarization (CP) process requires a rigid structure on the millisecond timescale to sustain the ^{1}H-^{31}P dipolar coupling. The rapid motion and molecular tumbling of outer-sphere complexes will average the ^{1}H-^{31}P dipolar coupling to zero such that no signal would be observed. Although arguing that ex-situ experimental conditions cannot reflect the real situation of phosphate adsorption, in-situ studies using cylindrical internal reflectance Fourier transform infrared (CIR-FTIR) [18] or ATR-FTIR [19-22] still agree with inner-sphere complexes. Phosphate outer-sphere complexes have not been observed experimentally yet, although their existence remains in question. Recently, Catalano et al. (2008) [23] reported observation of simultaneous occurrence of inner-sphere complexes and outer-sphere complexes for arsenate sorption on single-crystal hematite (001) surface, which implies that phosphate may form outer-sphere complexes on metal oxides surface.

The configuration of inner-sphere complexes possibly involves either bidentate binuclear and/or monodentate mononuclear phosphate coordination with surface cations on metal oxides. Taking the protonation states into consideration, six possible bonding structures (Figure 1.3) are proposed by Kwon and Kubicki (2004) [4]. Experimentally distinguishing among these possible structures, especially between bidentate and monodentate coordination, is a long-term topic in the study of phosphate sorption. Spectroscopic studies on this topic are reviewed in 2.3.

In addition to surface complexes, the formation of surface precipitates on metal hydroxides is a possible mechanism for uptake of phosphate from solution, especially considering the low solubility of many Ca-, Al- and Fe-phosphates. Surface precipitation is the three-dimensional growth of a distinct phase containing the adsorbate on the metal (hydr)oxides, whereas surface complexes usually are regarded as two-dimensional. It should be noted that surface precipitates are conceptually different from traditional precipitates that form in supersaturated fluids, because surface precipitates are believed to form in the near surface environment induced by the solid surface, whereas the bulk fluid remains under saturated. Direct observation of surface precipitates is difficult, owing to the small fraction of the total solid products, potentially small crystal size and disordered structure. Indirect evidence for phosphate surface precipitates on goethite was provided by Ler and Stanforth (2003) [24] from monitoring of Zeta potential over a long period. They proposed a possible mechanism which involves dissolution of goethite and interaction of dissolved iron with inner-sphere phosphate complexes. Microscopic techniques could give some clues for the presence of a wavellite-like surface precipitates, as reported by van Riemsdijk et al (1980) [25] using electronmicroscopy and electron diffraction to study phosphate interaction with gibbsite. Kim and Kirkpatrick (2004) [26] also reported the observation of surface precipitates on aluminum oxides by solid state NMR. Using XANES, Khare et al. (2005) observed a special feature in the pre-edge white lines and ascribed it to surface precipitates [27]. Overall, evidence for surface precipitation and the conditions with which it is an important uptake process remain poorly understood.

1.2.3. Spectroscopic studies of phosphate uptake by metal (hydr)oxides

1.2.3.1. IR studies

Infrared (IR) spectroscopy has been applied to study phosphate adsorption for almost four decades [2, 16, 18-22, 28-35]. It is sensitive to the molecular symmetry of the phosphate group, and thus can be used in principle to distinguish between bidentate and monodentate coordination to the surface of metal (hydr)oxides. For instance, aqueous PO_4^{3-} has T_d symmetry, which yields a single degenerate ν_3 asymmetrical vibration and no activation of the ν_1 (symmetric stretching) vibration [34]. A reduction in symmetry occurs when phosphate is protonated to HPO_4^{2-} and $H_2PO_4^-$, leading to three bands for the ν_3 vibrations, along with the activated ν_1 band. Thus HPO_4^{2-} and H_3PO_4 each give rise to two IR frequencies (1077, 989 and 1174-1179, 1006 cm^{-1} respectively) for the ν_3 vibrations and (847-850 and 890 cm^{-1} respectively) for the activated ν_1 band. Adsorption on metal (hydr)oxides as inner-sphere surface complexes, their symmetry is further reduced to mainly C_{2v} or lower (C_1), leading to four vibrational peaks.

The earliest surface phosphate IR studies were conducted by Atkinson (1974) [16] and Parfitt [28] who investigated phosphate adsorption on goethite by ex-situ IR. These IR data support the ligand-exchange mechanism with the disappearance of IR features for physically adsorbed surface water and terminal hydroxyl groups, and provides evidence of inner-sphere complexes with IR peaks for surface adsorbed phosphate that are distinct from those for pure alkali phosphate. A bridging bidentate structure for phosphate can be deduced by comparing the observed frequencies with those of model compounds, $Co(NH_3)_5PO_4$ for monodentate complexes and $Co(NH_2CH_2CH_2NH_2)PO_4$ for bidentate complexes.

Although ex-situ IR provided valuable information about the phosphate sorption mechanism, it was subsequently argued that the drying process during sample preparation could change the real phosphate environment on the surface [2]. Thus in-situ IR was carried out using cylindrical internal reflectance (CIR) FTIR to study phosphate sorption in goethite slurries [18]. With the development of the attenuation total reflectance (ATR) accessory, ATR-FTIR investigations of phosphate adsorption on TiO_2 [19], ferrihydrite suspensions [20], and hematite [34] were undertaken. With in-situ ATR-FTIR, real-time investigation of phosphate uptake kinetics can be approached at the molecular level [21, 33]. The in-situ IR studies suggest the existence of monodentate mononuclear surface complexes [18, 31, 34]. However, questions about whether bidentate or monodentate inner-sphere complexes are the dominant species on mineral surface are still under debate [2, 22].

1.2.3.2. Solid state NMR studies

^{31}P NMR spectroscopy is very sensitive to local phosphorus chemical and structural environment in solids and in solution, but studies on interfacial species are relatively sparse. Several difficulties hindered its application to study adsorption reactions at the mineral/water interface. The major challenge is that NMR is an insensitive technique, requiring a long time to accumulate adequate signals even for pure sample. For adsorption samples with typically low P contents, longer acquisition times are required. A second challenge is that the interpretation of NMR results is not straightforward, requiring potentially non-unique comparison with proper model compounds. Any misinterpretation of the NMR spectra will lead to incorrect conclusions. In addition, dry powders are usually required for solid state NMR, which as mentioned previously is being questioned not representing the real environment expected in soils and sediments.

Despite the difficulties listed above, several researchers have attempted to apply solid state NMR to phosphate sorption samples, mostly on Al-(hydr)oxides. Application to Fe-oxides is possible, but very difficult due to their paramagnetic properties, which will not be discussed below. Bleam et al [17] conducted the first NMR study to investigate hydrolysis of phosphate while adsorbed on boehmite (γ-AlOOH) using a method called dipolar dephasing. This technique provides a qualitative estimate of the dipolar coupling between ^{31}P and ^{1}H spins, from which proximity between protons and phosphate can be obtained. Although inner sphere complexes can be identified, detailed structure cannot be determined. Lookman et al. (1994) [36] further studied phosphate adsorption on synthetic amorphous $Al(OH)_3$ by ^{31}P magic angle spinning (MAS) NMR. With the comparison of ^{31}P NMR spectra for two amorphous aluminum phosphates, the authors assigned one peak at -6 ppm to phosphate bonded to surface octahedral aluminum as inner sphere complexes. They further studied phosphate speciation in fertilized soils using NMR spectroscopy [37-38]. Combining both batch method and NMR spectroscopy, Johnson et al (2002) [39] further investigated organic phosphate adsorption on γ-Al_2O_3, showing that phenyl phosphate forms both inner sphere and outer sphere complexes. Recently, similar studies have been reported on activated carbon [40], boehmite, γ-Al_2O_3 [26], gibbsite and kaolinite [41]. On the surface of gibbsite and kaolinate, phosphate formed a variscite-like surface precipitates as evidenced by a NMR peak at -19 ppm observed by van Emmerik et al. (2007) [41]. Although these studies could distinguish outer-sphere complexes, inner-sphere complexes and surface precipitates, they were not capable of determining monodentate and bidentate surface complexes clearly. Combining NMR results with quantum chemical calculations, Fry et al [42] interpreted the chemical shift anisotropy data, suggesting that the structure of mononucleotide 2'-deoxyadenosine 5'-monophosphate (d-AMP) adsorbed on mesophorous alumina was monodentate coordination with surface Al.

1.2.3.3. XAFS studies

The low energy of the P K-edge hinders the application of X-ray absorption fine structure spectroscopy (XAFS) to elucidate the phosphate sorption mechanism. However, several researchers have employed X-ray near edge spectroscopy (XNAES) to determine solid state phosphorus speciation at metal oxides/water interfaces. Khare et al. [43] used linear combination analysis (LCA) to quantitatively separate the signal of adsorbed PO_4 between ferrihydrite and boehmite in aqueous mixtures of these minerals. They found there is a pre-edge feature in the XANES spectrum for phosphate adsorbed on ferrihydrite, whereas no such feature was observed for phosphate adsorbed on boehmite, due to the lower electron density of Al over Fe as a backscattering atom. Using the same technique, Khare et al. [26] observed surface precipitates of phosphate on boehmite and amorphous $Al(OH)_3$ systems as evidenced by the changes of full width at half-maximum (FWHM) in the white-line peak in the pre-edge region of P K-XANES spectra. Yet no surface precipitates on goethite and ferrihydrite were detected. More recently, Arai and Sparks [2] observed changes in the first derivative of P K-edge XNAES spectra for a series of samples with different aging periods. As aging increases, the pre-edge features become more pronounced, implying the possibility of Fe-P surface precipitates. For samples aged for 30, the XANES spectrum is similar to the pre-edge doublets observed for both crystalline and amorphous strengite ($FePO_4 \bullet 2H_2O$), which provides strong evidence for P inner-sphere complexes. However, the authors did not conclude that surface precipitates formed, but the possibility is suggested. In addition to the above qualitative studies, Khare et al. (2007) [44] performed a quantitative interpretation of the P-XANES spectrum for phosphate adsorbed on ferrihydrite with the aid of molecular orbital calculations, from which they concluded that at pH 6 phosphate forms binuclear bidentate surface complexes on ferrihydrite. However, XANES spectra for phosphate adsorbed on boehmite could not be interpreted structurally.

To summarize, although the debates are not ended, spectroscopic studies certainly have provided a large amount of molecular-level information for understanding phosphate sorption on metal oxides. Importantly, these studies point out the right direction for further investigation.

1.3. Basic NMR principles

Nuclear magnetic resonance spectroscopy (NMR) is a powerful tool to determine the static structure and dynamic behavior of condensed matter. It complements diffraction methods, such as X-ray or neutron diffraction, in offering structural information in short-range orders and provides high resolution of chemical environment. A brief introduction of the basis of NMR spectroscopy will be given here before discussing the NMR techniques which are employed in this dissertation.

1.3.1. A brief introduction of solid state NMR concepts

Under an external magnetic field, nuclei possessing a magnetic moment can absorb energy from electromagnetic waves, leading to a transition between energy levels corresponding to orientations of the magnetic moment. NMR spectroscopy is a technique designed to study this phenomenon, by which the nature of nuclear spin behavior can be exploited [45]. Atomic nuclei have quantum property of spin, with spin energy quantized by its intrinsic spin quantum numbers (**I**). Some nuclei have spin quantum number of **I** = 0, such as ^{12}C and ^{16}O. These nuclei have no magnetic moment, and cannot absorb radio waves to make energy level transitions and thus do not produce NMR signals. Another group of nuclei have spin quantum number of **I** = ½ , such as ^{1}H, ^{13}C and ^{31}P. These spins allow transitions between two energy levels (2**I** +1), which can be observed by NMR spectroscopy. In addition, there are a group of nuclear spins with quantum number I > ½, which are referred as quadrupolar nuclei, such as ^{2}H, ^{23}Na and ^{27}Al. The charge distribution for quadrupolar nuclei is not sphere-symmetric, thus producing quadrupole moment besides the dipole moment that typical spin½ nuclei have. Strong quadrupolar coupling could be resulted from the interaction between quadurapole moment and electric field gradient (EFG) around the nuclei, leading to severe NMR line broadening and strange line shapes. The NMR line shapes for spin-½ nuclei are normally symmetric and could be described by a combination of Gaussian or/and Lorenzen curves, but the line shapes for quadurapolar nuclei are usually asymmetric and can not be simply described by Gaussian or Lorenzen curves.

In modern Fourier transform (FT) NMR spectrometer, radio frequency (RF) pulses [46] are used to manipulate the nuclear spin behavior. It is possible to obtain the mutual interactions between nuclear spin and other particles (i.e. electrons and/or other nuclear spins) or fields (external magnetic field or induced magnetic field by surrounding electrons), which contain a great deal of physical and chemical information. These interactions are called coupling. The most important couplings include chemical shift interaction (chemical shielding by electrons) and direct dipole-dipole interactions for spin-½ nuclei. The chemical shift interaction is the modification of the magnetic field by its surrounding electrons when an external field B_0 is applied. The direct dipole-dipole interaction, also called dipolar coupling, refers to the interaction between magnetic moments of nuclear spins. These two interactions depend directly on material structure and the details will be explained in the following paragraphs.

1.3.2. Chemical shift

The chemical shift is the primary parameter observed in NMR spectroscopy, providing highly detailed information about local molecular structure [47]. In an external magnetic field (B_0), small local magnetic fields are induced as electrons circulate around a nucleus. This induced electron circulation will exert a shielding effect on the observed nuclei, leading to a small shift in resonance frequency of the nucleus. Since the shift depends on the details of electronic structure and thus of the chemical environment of observed nuclei, thus it is called chemical shift. The induced fields (σB_0) usually oppose the applied magnetic field. In the absence of electronic shielding, the resonance frequency is given by $\nu_0 = \gamma B_0$, where γ is gyromagnetic ratio and B_0 is the external magnetic field. The ν_0 is also called Larmor frequency. The nucleus exposed to an applied magnetic field that is slightly different from external magnetic field (B_0) would give rise to a frequency different form the intrinsic Larmor frequency, as illustrated in the formula (2).

$$\nu = \gamma B_0(1- \sigma) = \nu_0 - \sigma\gamma B_0 \qquad (2)$$

Where and σ is the screening constant, which is dependent on the density and spatial distribution of electron density around the nucleus. The formula equation (2) arises because the shielding of the nucleus is proportional to the external magnetic field. NMR spectroscopy does not measure the absolute Larmor frequency for a bare nucleus; instead, a relative factor is measured by comparing with a reference compound. The resulted chemical shift indicates the signal position in NMR spectra, defined as

$$\delta = (\nu - \nu_{ref})/\nu_{ref} \times 10^6 \qquad (3)$$

Where δ is the chemical shift (ppm), ν is of observed frequency nuclear spin and ν_{ref} frequency of a reference compound. For ^{1}H, the reference compound is tetramethylsilane (TMS) as 0 ppm.

In general, the chemical shift of the nucleus of interest will increase as the electronegativity of groups adjacent to the nucleus increases and the electron density or "shielding" is reduced. For ^{31}P, the chemical shift region is roughly -60 to +40 ppm (parts per million) from polyphosphates to phosphonates, with $\delta = 0$ ppm for H_3PO_4 85% phosphoric acid. Some characteristic chemical shifts are listed in Figure 1.5 for solution species and in Table 1.1 for solids.

In solids, the chemical shift is dependent on the orientation of the molecule with respect to the external magnetic field. The shielding constant (σ) is not a scalar factor, but a second-rank tensor that is symmetric and trace-invariant. The chemical shift anisotropy (CSA) tensor in the laboratory frame can be obtained by transformation of the tensor from its principal molecular frame to the laboratory frame through a set of Euler angles (α, β, γ):

$$\sigma_{CSA} = \begin{pmatrix} \sigma_{xx} & \sigma_{xy} & \sigma_{xz} \\ \sigma_{yx} & \sigma_{yy} & \sigma_{yz} \\ \sigma_{zx} & \sigma_{zy} & \sigma_{zz} \end{pmatrix} \xleftarrow{Lab \leftarrow PAF} \begin{pmatrix} \sigma_{11} & 0 & 0 \\ 0 & \sigma_{22} & 0 \\ 0 & 0 & \sigma_{33} \end{pmatrix} \qquad (4)$$

The principal tensor values (σ_{11}, σ_{22}, σ_{33}) reflect the symmetry of the local electronic structure; thus some information on the structure of the materials of interest can be obtained. CSA is one factor causing peak broadening in solid state NMR, but such effect can be overcome by special NMR techniques, i.e. magic angle spinning (MAS). Rapid molecular tumbling in fluids on application of averaging techniques such as MAS removes the CSA, leaving a single peak at the so called isotropic chemical shift: $\delta_{iso} = -1/3\ (\sigma_{11} + \sigma_{22} + \sigma_{33})$.

There are a few methods to measure the CSA [45, 47]; the two most common ones are static powder pattern [48] and spinning sidebands analysis [49]. It should be noted that structural information cannot be directly obtained from the CSA analysis. Structural information is extracted by comparing of the experimental CSA tensors to those calculated from possible structure models.

1.3.3. Dipolar coupling

Direct dipolar coupling is the magnetic force between nuclear spins. Such interaction between the same nuclei is called homonuclear dipolar coupling, whereas heteronuclear dipolar coupling refers to the interaction between different nuclei.

Direct dipolar coupling for a spin-pair is analogous to the interaction between two bar magnets in the macroscopic world. The heteronuclear dipolar coupling is orientation dependent as

$$D_{IS} = -\left(\frac{h}{4\pi}\right)\left(\frac{\gamma^I \gamma^S}{r_{IS}^3}\right)\left(3\cos^2\theta - 1\right) \tag{5}$$

where h is the Planck constant, r_{IS} the distance between the two nuclei, γ^I, γ^S the gyromagnetic ratio for spin I and spin S, and θ the angle between the two nuclei and the z-axis of the external magnetic field. The dipolar coupling constant (d) is given by the term $\gamma^I\gamma^S/r^3$, where the r^{-3} dependence makes D_{IS} sensitive to local structure. Dipolar coupling is usually of the order of kHz. For instance, the strength of ^1H-^{31}P heteronuclear dipolar coupling strengths vary from 10 to 30 kHz.

Dipolar coupling in solids often causes severe line broadening, which makes the interpretation more difficult. High power decoupling techniques and magic angle spinning are two useful methods to eliminate the dipolar coupling and provide high spectral resolution. However, dipolar coupling also contains structural information; by measuring direct dipolar coupling, the interatomic distances can be estimated. Techniques such as cross polarization dynamics and rotational echo double resonance (REDOR) measure direct heteronuclear dipolar coupling under magic angle spinning (MAS) condition such that high spectral resolution is achieved.

1.4. NMR techniques for solids

NMR techniques refer to the experimental methods developed to measure specific NMR parameters and improve resolution or signal-to-noise (S/N) ratio. Several methods used in this dissertation will be briefly introduced. The single pulse methods usually combined with magic angle spinning aims to measure signal intensity and chemical shift. Cross polarization (CP) is a technique for signal enhancement [50-51]; CP dynamics can be used to characterize heteronuclear dipolar coupling. Rotational echo, adiabatic passage, double resonance (REAPDOR) is a method to measure dipolar coupling between a spin-½ nucleus and a quadrupolar nucleus. Heteronuclear Correlation (HetCor) is a two-dimensional NMR technique for measuring chemical shifts of two different nuclei simultaneously, providing the correlation between chemical sites of two different elements.

1.4.1. Single pulse/magic angle spinning

As mentioned above, modern FT NMR spectrometers use short radio frequency (RF) pulse sequence to excite the nucleus energy level transition and to manipulate nuclear spin behavior, by which acquisition time is greatly reduced compared to the field sweeping or frequency sweeping methods by early NMR spectrometers. Single pulse is the simplest pulse sequence (Figure 1.9a), which contains only one short pulse. The free induction decay (FID) signal is recorded after the short pulse. After waiting for a sufficiently long period (usually 3 to 5 times of spin lattice relaxation time) that allows the magnetization fully recovery during, this experiment can be repeated to accumulate adequate signal.

In modern solid state NMR experiments, the single pulse experiment is usually conducted under magic angle spinning condition. The magic angle spinning, normally short for MAS, is the most basic technique in solid state NMR to eliminate the line broadening resulted from the chemical shift anisotropy (CSA) and dipolar coupling. NMR lineshapes in liquid-state NMR spectroscopy are usually narrow, because the fast molecular motion (10^{-8} -10^{-9} s^{-1}) in solution averages the CSA and dipolar coupling. But for solid materials, the orientation dependent CSA and dipolar coupling yield a broad pattern for polycrystalline (powder) samples. Both interactions contain a geometrical term ($3\cos^2\theta - 1$), where θ is the angle between the molecular principle frame and the external magnetic field. In the late 1950s, Andrew et al. [52] and Lowe [53] independently realized that rotating the samples around an axis inclined at 54.74°, the so-called ‘magic angle’, to the external magnetic field B_0 can effectively remove dipolar coupling and CSA, leading to a much narrower line shape. Figure 1.7 shows a schematic instrumental design of a stator in NMR probe to achieve MAS experimentally.

Figure 1.8 shows a typical application of magic angle spinning for obtaining ^{13}C NMR spectra of glycine under different spinning rates. The static non-spinning spectrum contains two broad features, corresponding to the “powder patterns” due to large CSA, for the two ^{13}C chemical sites in the glycine molecular structure. The broad peaks break into a series of spinning sidebands at low spinning rate. The spinning sidebands are spaced at the spinning frequency. As spinning rate increases, the sidebands move away but the center band located at the isotropic chemical shift (δ_{iso}) stays in the same position. Also the intensities for sidebands decrease with signal concentrated in the center band, by which the signal to noise ratio is largely enhanced. The sidebands disappear only when the spinning rate is larger than the CSA, meaning that CSA is efficiently averaged.

1.4.2. Cross polarization

Cross polarization (CP) originally referred to a process by which magnetization (polarization) is exchanged between two distinct nuclear spins. Subsequently, CP was used to assistant in observing dilute spins, such as ^{13}C and ^{31}P. In NMR spectroscopy, abundant nuclear spins like ^{1}H are the easiest nuclei to be observed due to its large magnetization (or high frequency), almost 100% natural abundance and short relaxation time. In contrast, dilute nuclei such as ^{13}C and ^{31}P are more difficult to work with. First, most dilute nuclei are not 100% natural abundance. For instance, the natural abundance for ^{13}C is approximately 1%, resulting to inevitable poor signal-to noise ratio. In addition, the relaxation times for them are usually very long, which means a very long time is required to collect a spectrum with reasonable signal-to-ratio. The CP technique helps improve the resolution of dilute nuclei in two ways: 1) transferring magnetization from abundant nuclei (spins **S**) to dilute nuclei (spins **I**) utilizing the different gyromagnetic ratio and Boltzmann distribution; 2）reducing the spin-lattice relaxation time and increasing the numbers of scan possible in a fixed period.

CP is often explained thermodynamically. The spins **S** (e.g. ^{1}H) are considered to have a cold spin temperature due to their large Boltzmann population factor and the spins **I** (e.g. ^{31}P) have a high spin temperature [33]. Through an exchange of energy from the cold spins to the hot spins, the temperature of the ^{31}P spin system is cooled down until the two systems approach the same spin temperature. CP is a dynamic process in that the intensity of spins **I** (e.g. ^{31}P) is dependent on length of time that the spins I and S exchange magnetization, which is called CP contact time as illustrated in its pulse sequence (Figure 1.9b). The signal intensity for spins **I** (e.g. ^{31}P) over CP contact time could be described with by different classic models, which were reviewed by Kolodziejski and Klinowski [54]. Qualitatively, the rate constant (T_{IS}^{-1}) of the CP dynamics characterizes the strength of dipolar coupling between spins **I** (e.g. ^{31}P) and spins **S** (e.g. ^{1}H). Since the cross-polarization process depends on the heteronuclear dipolar coupling, CP can be used to estimate the strength of dipolar coupling between spin **I** (^{31}P) and **S** (^{1}H) and thus examine the spatial connectivity of two elements (e.g. P and H) in solid materials.

To allow the polarization exchange between spins I and S, the energy levels the two must be equal. But in the laboratory frame, the Zeeman energies of the two systems are different, so that experimentally a pair of radio-frequency (rf) fields are applied simultaneously at the spins **I** and **S** to ensure that their nutation rates are equal in the XZ-plane, by which polarization can be exchanged. This experimental condition is called Hartmann-Hahn match [55]: $\gamma_I B_{1I} = \gamma_S B_{1S}$, where γ_I, γ_S are the gyromagnetic ratios (intrinsic properties of the nuclei) and B_{1I}, B_{1S} are the applied magnetic fields on **I** and **S** spins respectively. In solid state NMR, CP is usually implemented under MAS condition as CP/MAS [54, 56], which slightly modifies the Hartmann-Hahn match to $\gamma_I B_{1I} = \gamma_S B_{1S} \pm \nu_{rot}$, where ν_{rot} is the spinning rate.

1.4.3. Heteronuclear correlation

Heteronuclear correlation (HetCor) is a two-dimensional (2-d) NMR technique, which is used to examine the connectivity between chemical sites of different type of nuclei. It is also a technique that relies on through–space dipolar coupling. The HetCor sequence used in this dissertation is Wideline Separation (WISE) [57] HetCor modified from the CP sequence by adding an incremental t_1 delay after the ^{1}H 90° excitation pulse, shown in Figure 1.10a. During the *t1* delay, the ^{1}H magnetization evolves under ^{1}H chemical shifts and the ^{1}H free induction decay is built indirectly from the series of ^{31}P spectra by plotting the ^{31}P peak intensity as a function of t_1 evolution time. A two-dimentional NMR spectrum is obtained by 2-d Fourier Transform (FT) of the ^{1}H FID in *t1* period and ^{31}P FID in *t2* period. The ^{1}H spectrum is generated according to the ^{31}P signals and a correlation between heteronuclear coupled ^{31}P and ^{1}H spins is established. As a result, only signals from those ^{1}H spins which are in proximity to the corresponding ^{31}P nuclei are observed, providing addition information for peak assignment in ^{1}H single pulse spectrum. An optional "mixing period" (Figure 1.10b) can be added which allows ^{1}H-^{1}H spin diffusion so that the ^{31}P-detected ^{1}H spectrum contains signal from more distant ^{1}H nuclei.

1.4.4. Rotational echo adiabatic passage double resonance

Rotational echo adiabatic passage double resonance (REAPDOR) [58-59] is a double resonance technique developed on the basis of rotational echo double resonance (REDOR) [60] and transfer of populations double resonance (TRAPDOR) [61-62]. It aims specifically to measure the dipolar coupling between spin-½ nuclei and quadrupolar nuclei. Here we take ^{31}P-^{27}Al dipolar coupling as the relevant example.

For instance, the ^{31}P/^{27}Al REAPDOR sequence (Figure 1.11) contains a series of spin echoes on the ^{31}P channel and a simultaneous short irradiation on the ^{27}Al channel. The short ^{27}Al pulse is set to be usually 1/3 or 1/5 of the rotor period, and must be strong enough to excite the ^{27}Al spins, causing a decrease of intensity in the ^{31}P free induction decay via ^{31}P-^{27}Al dipolar coupling. To achieve this, the adiabatic excitation condition should be satisfied for ^{27}Al: $\alpha' = \nu_1^2 / \nu_R \nu_Q > 1$, where α' is the adiabaticity parameter, ν_1 the radio-frequency pulse amplitude on ^{27}Al, ν_R the spinning rate and ν_Q the quadrupolar coupling constant of the ^{27}Al nuclei.

Experimentally, REAPDOR contains two ^{31}P-observed NMR spectra, one obtained with a heteronuclear dipolar dephasing sequence (S) and a control spectrum (S_0) acquired under identical conditions but without irradiation at the ^{27}Al frequency. The difference (S_0-S) in peak intensity between the dephased spectrum (S) and the control (S_0) depends on the ^{31}P-^{27}Al heteronuclear dipolar coupling and the total length of the dephasing sequence (τ_D). The REAPDOR fraction (S_0-S)/S_0 is typically measured as a function of dephasing time, yielding the so-called REAPDOR dephasing curve, which characterizes the magnitude of ^{31}P-^{27}Al heteronuclear dipolar coupling interactions. Analysis of this dephasing curve allows the determination of the dipolar couping between the two spins and to distinguish possible structures by coordination number and distance of P to nearby Al (e.g. monodentate and bidentate P/Al coordination).

To obtain specific structural information such as the P/Al coordination or P-Al distance, experiments on proper model compounds should be conducted for comparison. In some cases, when such model compounds are not available, numerical simulations using NMR simulation software packages (e.g. SIMPSON [63]) can help interpret the REAPDOR results. SIMPSON, short for simulation package for solid sate NMR, is able to calculate a theoretical REAPDOR curve for a given structural model. From the comparison of experimental and calculated REAPDOR curves, detailed structural information can be revealed. Besides SIMPSON, there are some other NMR simulation programs, such as SPINEVOLUTION [64].

Reference

[1] Slomp, C. P.; van Cappellen, P., *Biogeosciences* **2007**, *4*, 155-171.

[2] Arai, Y.; Sparks, D. L., *Adv. Agron.* **2007**, *94*, 135-179.

[3] Goldberg, S.; Sposito, G., *Commun. Soil Sci. Plant Anal.* **1985**. 16, 801-821.

[4] Kwon, K. D.; Kubicki, J. D., *Langmuir* **2004**, *20*, 9249-9254.

[5] Rahnemaie, R.; Hiemstra, T.; van Riemsdijk, W. H., *Langmuir* 2007, *23*, 3680-3689.

[6] Paytan, A.; McLaughlin, K., *Chem. Rev.* **2007**, *107*, 563-576.

[7] Mortlock, R. F.; Bell, A. T.; Radke, C. J., *J. Phys. Chem.* **1993**, *97*, 775-782.

[8] Cade-Menun, B. J., *Talanta* **2005**, *66*, 359-371.

[9] Cheetham, A. K.; Clayden, N. J.; Dobson C. M.; Jakeman, R. J. B., *Chem. Commun.* **1986**, 195-197.

[10] Turner, G. L.; Turner, G. L.; Smith, K. A.; Kirkpatrick, R. J.; Oldfield, E., *J. of Magn. Reson.* **1986**, *70*, 408-415.

[11] Rajan, S. S. S.; Perrott, K. W.; Saunders, W. M. H., *J. Soil Sci.* **1974**, *25*,

438-447.

[12] Rajan, S. S. S., *Nature* **1975**, *253*, 434-436.

[13] Rajan, S. S. S., *Nature* **1976**, *262*, 45-46.

[14] Atkinson, R. J.; Quirk, J. P.; Posner, A. M., *J. Inorg. Nucl. Chem.* **1972**, *34*, 2201-2211.

[15] Kyle, J. H.; Posner, A. M.; Quirk, J. P., *J. Soil Sci.* **1975**, *26*, 32-43.

[16] Atkinson, R. J.; Parfitt, R. L.; Smart, R. S., *J. Chem. Soc. Faraday Trans. I* **1974**, *70*, 1472-1479.

[17] Bleam, W. F.; Pfeffer, P. E.; Goldberg, S.; Taylor, R. W.; Dudley, R., *Langmuir* **1991,** *7*, 1702-1712.

[18] Tejedortejedor, M. I.; Anderson, M. A., *Langmuir* **1990**, *6*, 602-611.

[19] Connor, P. A.; McQuillan, A. J., *Langmuir* **1999**, *15*, 2916-2921.

[20] Arai, Y.; Sparks, D. L., *J. Colloid Interface Sci.* **2001**, *241*, 317-326.

[21] Gong, W. Q., *Int. J. Min. Proc.* **2001**, *63*, 147-165.

[22] Lefevre, G., *Adv. Colloid Interface Sci.* **2004,** *107*, 109-123.

[23] Catalano, J. G.; Park, C.; Fenter, P.; Zhang, Z., *Geochim. Cosmochim. Acta* **2008**, *72*, 1986-2004.

[24] Ler, A.; Stanforth, R., *Environ. Sci. Technol.* **2003**, *37*, 2694-2700.

[25] van Riemsdijk, W. H.; Lyklema, J., *J. Colloid Interface Sci.* **1980**, *76*, 55-66.

[26] Kim, Y.; Kirkpatrick, R. J., *Eur. J. Soil Sci.* **2004**, *55*, 243-251.

[27] Khare, N.; Hesterberg, D.; Martin, J. D., *Environ. Sci. Technol.* **2005**, *39*, 2152-2160.

[28] Parfitt, R. L.; Atkinson, R. J., *Nature* **1976**, *264*, 740-742.

[29] Nanzyo, M.; Watanabe, Y., *Soil Sci. Plant Nutri.* **1982**, *28*, 359-368.

[30] Nanzyo, M., *J. Soil Sci.* **1984**, *35*, 63-69.

[31] Persson, P.; Nilsson, N.; Sjoberg, S., *J. Colloid Interface Sci.* **1996**, *177*, 263-275.

[32] Ronson, T. K.; McQuillan, A. J., *Langmuir* **2002**, *18*, 5019-5022.

[33] Luengo, C.; Brigantea, M.; Antelo, J.; Avena, M., *J. Colloid Interface Sci.* **2006**, *300*, 511-518.

[34] Elzinga, E. J.; Sparks, D. L., *J. Colloid Interface Sci.* **2007**, 308, 53-70.

[35] Laiti, E.; Persson, P.; Ohman, L. O., *Langmuir* **1996**, 12, 2969-2975.

[36] Lookman, R.; Grobet, P.; Merckx, R.; Vlassak, K., *Eur. J. Soil Sci.* **1994**, 45, 37-44.

[37] Lookman, R.; Grobet, P.; Merckx, R.; Van Riemsdijk, W. H., *Geoderma* **1997**, 80, 369-388.

[38] Lookman, R.; Geerts, H.; Grobet, P.; Merckx, R.; Vlassak, K., *Eur. J. Soil Sci.* **1996**, 47, 125-130.

[39] Johnson, B. B.; Ivanov, A. V.; Antzutkin, O. N.; Forsling, W., *Langmuir* **2002**, *18*, 1104-1111.

[40] Harris R. K.; Thompson T. V.; Norman P. R.; Pottage C., *Carbon* **1999**, *37*, 1425-1430.

[41] Van Emmerik, T. J.; Sandstrom, D. E.; Antzutkin, O. N.; Angove, M. J.; Johnson, B. B., *Langmuir* **2007**, *23*, 3205-3213.

[42] Fry, R. A.; Kwon, K. D.; Komarneni, S.; Kubicki, J. D.; Mueller, K. T., *Langmuir* **2006**, *22*, 9281-9286.

[43] Khare, N.; Hesterberg, D.; Beauchemin, S.; Wang, S. L., *Soil Sci. Soc. Am. J.* **2004**, *68*, 460-469.

[44] Khare, N.; Martin, J. D.; Hesterberg, D., *Geochim. Cosmochim. Acta* **2007**, *71*, 4405-4415.

[45] Laws, D. D.; Bitter H. M. L.; Jerschow, A., *Angew. Chem. Int. Ed.* **2002,** 41, 3096-3129.

[46] Ernst, R. R.; Anderson, W. A., *Rev. Sci. Instru.* **1966**, 37, 93-102.

[47] Waugh, J. S., *Anal. Chem.* **1993**, *65*, A725-A729.

[48] Dietrich, R.; Trahms, L., *J. Magn. Reson.* **1987**, *71*, 337-341.

[49] Herzfeld, J.; Berger, A. E., *J. Chem. Phys.* **1980**, *73*, 6021-6030.

[50] Pines, A.; Waugh, J. S.; Gibby, M. G., *J. Chem. Phys.* **1972**, *56*, 1776-1787.

[51] Pines, A.; Gibby, M. G.; Waugh, J. S., *J. Chem. Phys.* **1973**, *59*, 569-590.

[52] Andrew, E. R.; Bradbury, A.; Eades, R. G., *Nature* **1958**, *182*, 1659-1659.

[53] Lowe, I. J., *Phys. Rev. Lett.* **1959**, *2*, 285-287.

[54] Kolodziejski, W.; Klinowski, J., *Chem. Rev.s* **2002**, *102*, 613-628.

[55] Hartmann, S. R.; Hahn, E. L., *Phys. Rev.* **1962**, *128*, 2042-2053.

[56] Stejskal, E. O.; Schaefer, J.; Waugh, J. S., *J. Magn. Reson.* **1977**, *28*, 105-112.

[57] Schmidt-Rohr, K.; Clauss, J.; Spiess, H. W., *Macromolecules* **1992**, *25*, 3273-3277.

[58] Gullion, T., *Chem. Phys. Lett.* 1995, *246*, 325-330.

[59] Chopin, L.; Vega, S.; Gullion, T., *J. Amer. Chem. Soc.* 1998, *120*, 4406-4409.

[60] Gullion, T.; Schaefer, J., *J. Magn. Reson.* **1989**, *81*, 196-200.

[61] Grey, C. P.; Veeman, W.S.; Vega, A. J., *J. Chem. Phys.* **1993**, *98*, 7711-7724.

[62] Haase, J.; Conradi, M. S.; Grey, C. P.; Vega, A. J., *J. Magn. Reson. A* **1994**, *109*, 90-97.

[63] Bak, M.; Rasmussen, J. T.; Nielsen, N. C., *J. Magn. Reson.* **2000,** *147*, 296-330.

[64] Veshtort, M.; Griffin, R. G., *J. Magn. Reson.* **2006**, 178, 248-282.

[65] Pilkenton, S; Raftery, D., In *Environmental Catalysis*; Grassian, V. H., Ed.; CRC press: New York, 2005; p352.

Tables and figures

Table 1.1 ^{31}P chemical shifts of selected phosphorus minerals and compounds[1]

Minerals/compound	Chemical formula	Chemical shift
Hydroxyapatite	$Ca_5(PO_4)_3OH$	3 ppm
Octacalcium phosphate	$Ca_8H_2(PO_4)_6 \bullet 5H_2O$	3 ppm
Mionetite	$CaHPO_4$	-1.9 ppm
Crandallite	$CaAl_3(OH)_5(PO_4)_2$	-5 ppm
Brazilianite	$NaAl_3(OH)_4(PO_4)_2$	-10.2 ppm
Wavellite	$Al_3(OH)_3(PO_4)_2 \bullet 5H_2O$	-11 ppm
Metavariscite	$AlPO_4 \bullet 2H_2O$	-13.2 ppm
Senegalite	$Al_2(OH)_3(PO_4) \bullet H_2O$	-16 ppm
Variscite	$AlPO_4 \bullet 2H_2O$	-19 ppm
Lazulite	$MgAl_2(OH)_2(PO_4)_2$	-20 ppm
Metaphosphate	$Na_6P_6O_{18}$	-21.7 ppm
Berlinite	$AlPO_4$	-25 ppm
Augelite	$Al_2(OH)_3(PO_4)$	-30 ppm
Li_3PO_4		10.8 ppm
K_3PO_4		10 ppm
$Na_3PO_4 \bullet 12H_2O$		7.8 ppm
Na_2HPO_4		6.6 ppm
$NaNH_4HPO_4 \bullet 4H_2O$		5.1 ppm
KH_2PO_4		4.3 ppm
$NaH_2PO_4 \bullet H_2O$		2.3 ppm
$K_2HPO_4 \bullet 3H_2O$		2.1 ppm
$(NH_4)_2HPO_4$		1.5 ppm
$NH_4H_2PO_4$		0.9 ppm
$Be_3(PO_4)_2$		-9.2 ppm
$Mg_3(PO_4)_2 \bullet 8H_2O$		4.6 ppm
$Ca_3(PO_4)_2$		3.0 ppm
$CaHPO_4$		-0.6 ppm
BPO_4		-29.5 ppm
$AlPO_4$		-24.5 ppm
$GaPO_4$		-9.8 ppm
YPO_4		-0.9 ppm

---

[1] data in this table are from the ref. [9-10].

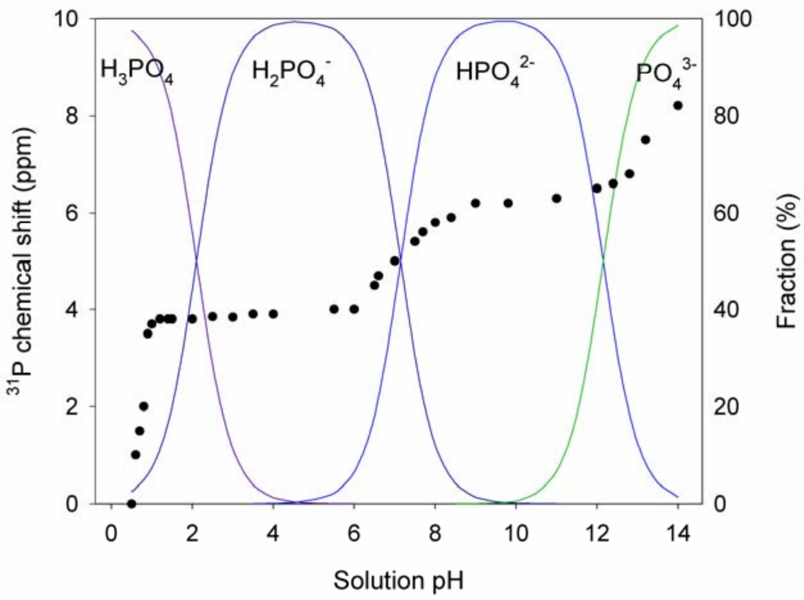

Figure 1.1 Speciation diagram for phosphate and the corresponding ^{31}P NMR chemical shift in solution as a function pH. Chemical shift values are from ref. [7].

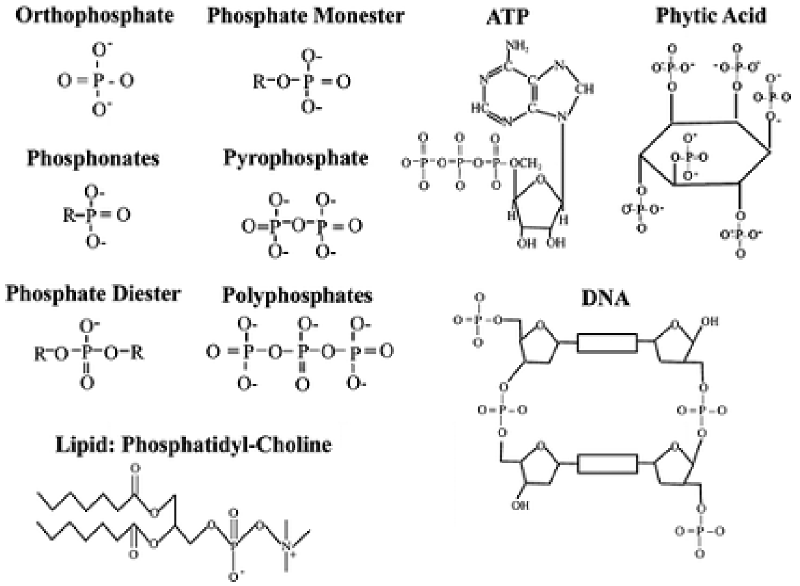

Figure 1.2 Some biologically important phosphorus compounds. This figure is obtained from ref. [6], with permission from American Chemical Society.

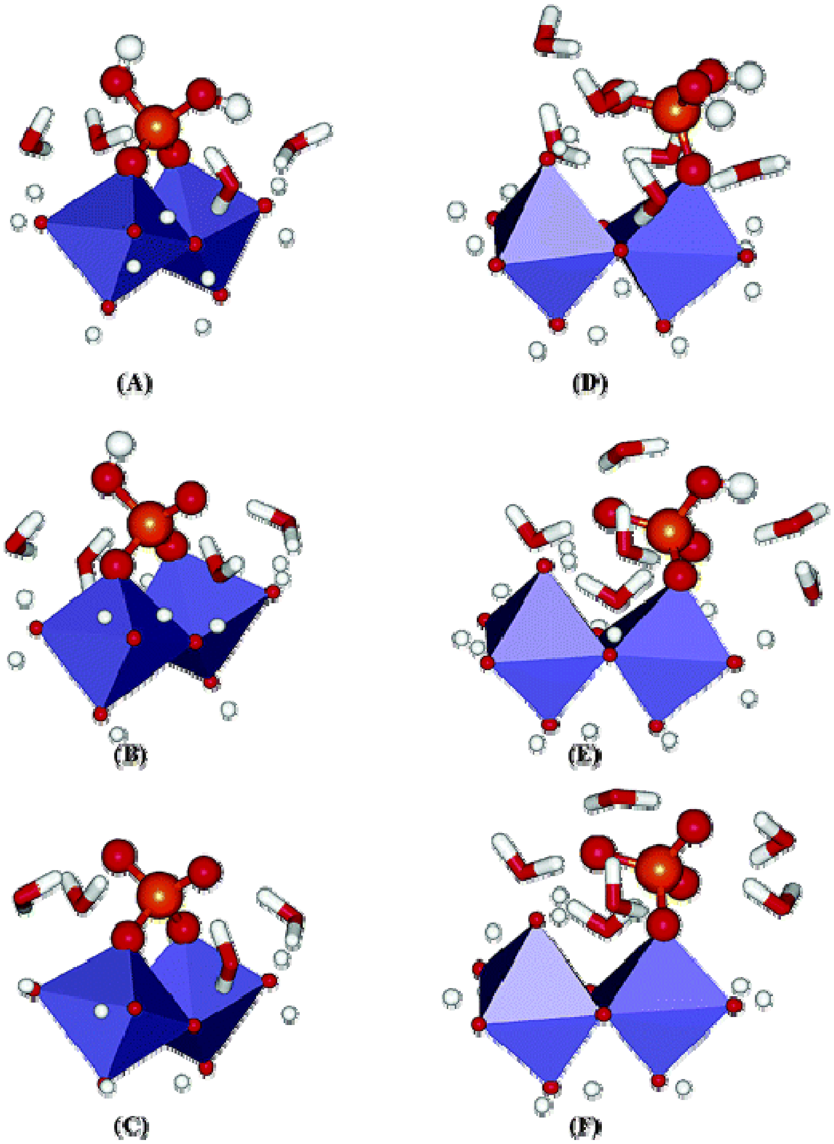

Figure 1.3 Possible bidentate and monodentate surface complexes of phosphate on iron hydroxides: (A) diprotonated bidentate (BB-H2); (B) monoprotonated bidentate (BB-H1); (C) deprotonated bidentate (BB-H0); (D) diprotonated monodentate (MM-H2); (E) monoprotonated monodentate (MM-H1); (F) deprotonated monodentate (MM-H0). H2O molecules are H-bonding to the phosphate−iron clusters. Red, oxygen; white, hydrogen; orange, phosphorus; blue, iron octahedral. This figure is obtained from ref. [4], with permission from American Chemical Society.

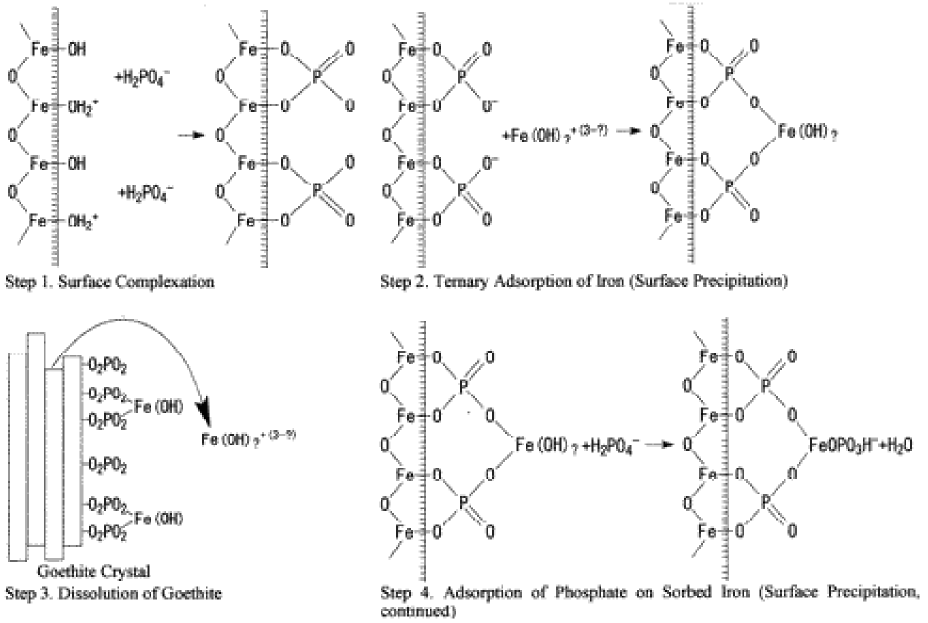

Figure 1.4 Schematic of the proposed surface precipitation process. Step 1, phosphate adsorbs on the surface. Step 2, dissolved iron adsorbs on the surface phosphate. Step 3, goethite dissolves to replenish dissolved iron. Step 4, phosphate adsorbs to the surface-bound iron. This figure is modified from ref. [24], with permission from American Chemical Society.

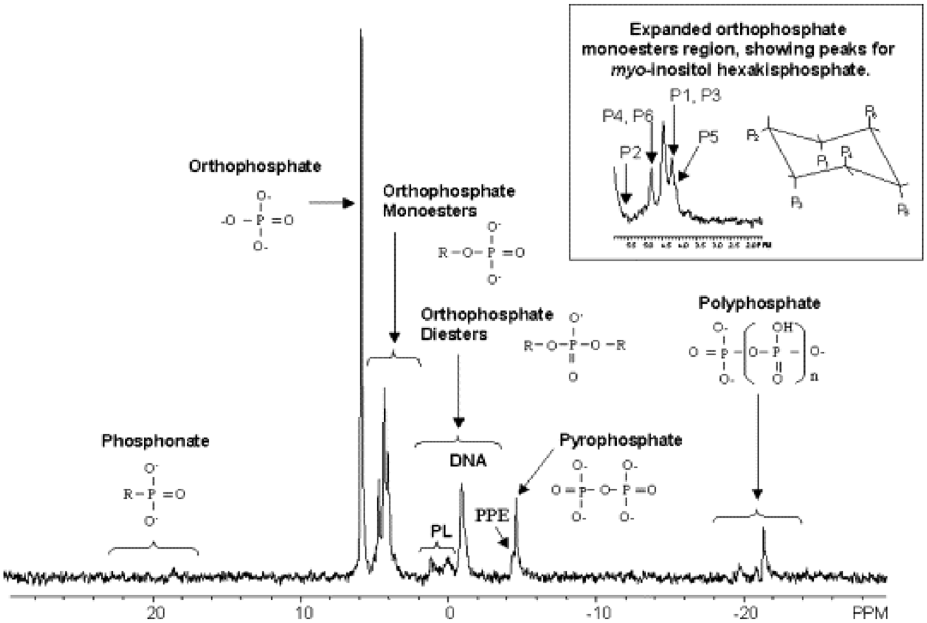

Figure 1.5 ^{31}P Chemical shifts for a series phosphorus compounds in solution, including phosphonates, orthophosphate, orthophosphate monoesters, orthophosphate diesters such as phospholipids (PL) and deoxyribonucleic acids (DNA), pyrophosphate and polyphosphate, etc. This figure is from ref [8], with permission from Elsevier.

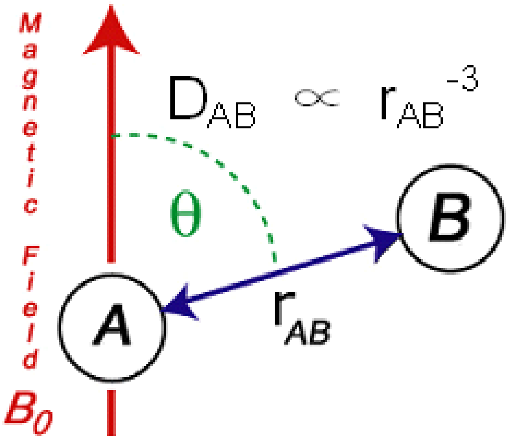

Figure 1.6 Schematic illustration of the geometrical relationship for dipolar coupling.

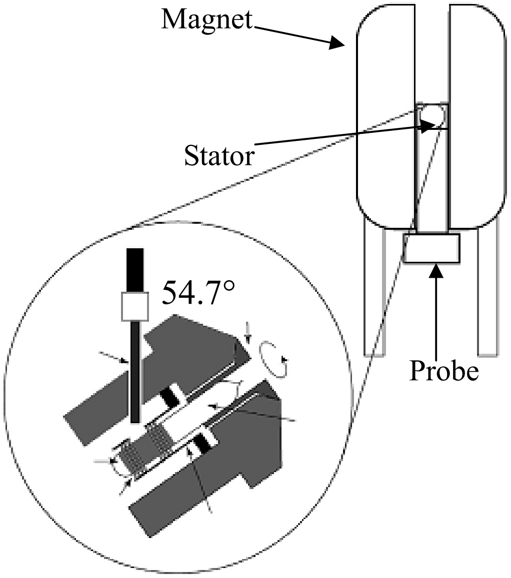

Figure 1.7 Schematic diagram of the magical angle spinning apparatus in NMR probe. This figure is modified from ref. [65].

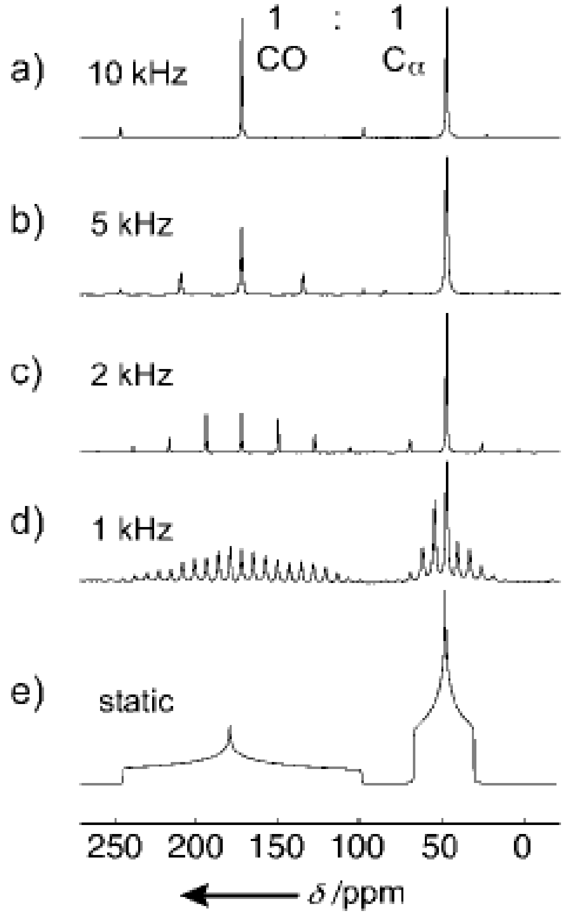

Figure 1.8 Solid state ^{13}C NMR spectra of glycine under static and MAS conditions at given spinning rate. This figure is from ref. [45], with permission from Wiley-VCH.

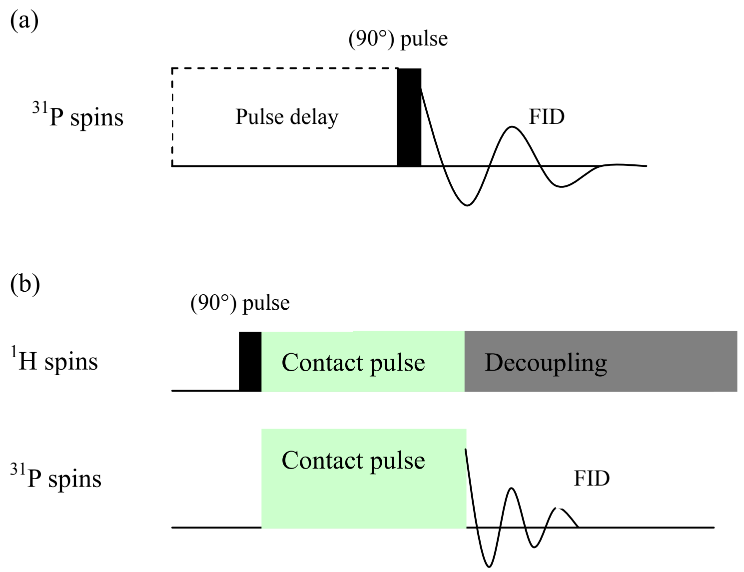

Figure 1.9 Solid state NMR Pulse sequences for single pulse (a), CP/MAS (b). ^{1}H and ^{31}P nucleus are used here to represent abundant nucleus (S) and diluted nucleus (I).

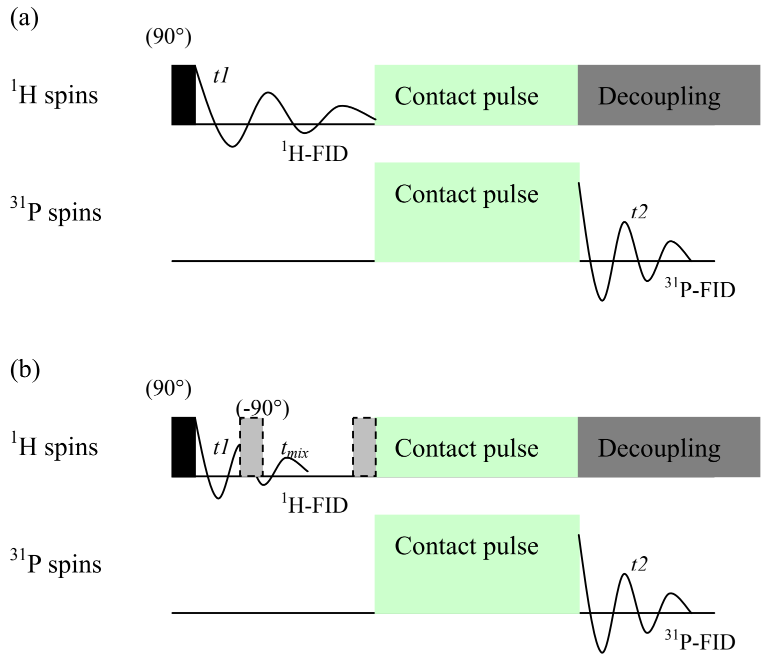

Figure 1.10 Solid state NMR Pulse sequences for CP-WISELINE heteronuclear correlation (HetCor) (a) and a modified version with a mixing time (t_{mix}) added before cross polarization. ^{1}H and ^{31}P nucleus are used here to represent abundant nucleus (**S**) and diluted nucleus (**I**).

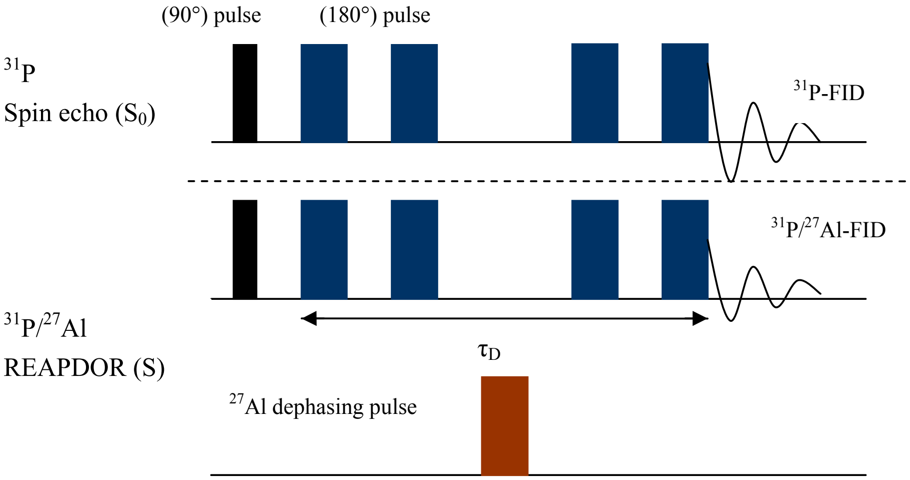

Figure 1.11 NMR pulse sequence for rotational echo adiabatic passage double resonance (REAPDOR). ^{31}P and ^{27}Al nuclei are used here for representing spin-1/2 nucleus and quadrupolar nucleus respectively. Four rotor cycles are used here as the diphasing time (τ_D), which is multiplication of rotor numbers and rotor period.

Chapter 2

Surface speciation of phosphate on boehmite (γ-AlOOH) determined from NMR spectroscopy *

*This work has been published in *Langmuir*, Li, W., Feng, J., Kwon, K.D., Kubicki, J.D., Phillips, B.L., Surface speciation of phosphate on boehmite (γ-AlOOH) determined from NMR spectroscopy, *Langmuir* 2010, 26, 4753-4761. Prof. James Kubicki and Dr. Kideok Kwon conducted the quantum chemical calculation. Reproduced with permission from *Langmuir*, Copyright 2010 American Chemical Society

Abstract

Interaction of phosphate with the surfaces of clays and metal oxyhydroxides is important for nutrient cycling in natural and agricultural systems. Here I examined the specific adsorption of phosphate to boehmite (γ-AlOOH) by solid-state ^{31}P NMR spectroscopy. The results yield evidence for the presence of two bridging bidentate surfaces complexes differing in protonation. For samples prepared along the sorption isotherm at pH 5, distinct phosphate environments are observed as two major peaks in ^{31}P NMR spectra (chemical shifts of 0 and -6 ppm) that show little change in relative intensity with adsorbate loading. Both peaks correspond to rigid phosphate in close proximity to H, as indicated by ^{31}P{^{1}H} cross-polarization magic-angle-spinning (CP/MAS) data, and yield nearly identical ^{31}P{^{27}Al} dephasing curves in rotational echo adiabatic passage double resonance (REAPDOR) experiments. The REAPDOR results indicate both phosphate environments have similar coordination to Al and are best fit by dephasing curves simulated for bridging bidentate configurations. The two resolved phosphate species exhibit distinct ^{31}P chemical shift anisotropy (CSA) and intensity variations with pH, the peak near 0 ppm being dominant at pH > 7. ^{31}P CSA's from quantum chemical calculations of hydrated bidentate cluster models with varying protonation state show that the CSA for mono-protonated phosphate is unique and closely matches that for the peak at -6 ppm. The CSA for the peak at 0 ppm is consistent with both di- and non-protonated phosphate, but assignment to the latter is suggested based on the dominance of this peak in samples prepared at high pH and with trends in ^{31}P NMR chemical shifts.

Key words: NMR; phosphate; adsorption; Al oxyhydroxide; boehmite

2.1. Introduction

To predict the mobility and bioavailability of phosphate in soils or aquatic systems, it is essential to understand the reactions at the mineral/water interface [1-2].

Macroscopic studies of phosphate uptake by oxyhydroxides and clay minerals suggest that phosphate adsorbs specifically as an inner-sphere complex via ligand-exchange processes [1, 3-4], but many uncertainties about the sorption mechanism remain, especially in the details of the bonding configuration of phosphate molecules [5] and the structural and dynamical properties of adsorption sites. Although recent advances in modeling macroscopic sorption data now allow interpretation as concentrations of specific adsorbate complexes varying in coordination (e.g., monodentate vs. bidentate) and protonation state [6], the need remains for more direct characterization of surface species by spectroscopic techniques in order to fully understand these complex interfacial systems.

Methods such as infrared (IR) [7-11], X-ray absorption spectroscopy (XAS) [5, 12-13] and X-ray photoelectron spectroscopy (XPS) [14], can provide valuable molecular information on phosphate adsorption. Of these techniques, IR methods based on asymmetric P-O vibration have proven to be particularly useful. For goethite, in-situ Cylindrical Internal Reflectance (CIR) FTIR spectroscopy provided evidence for both monodentate and bidentate phosphate surface complexes and suggested non-protonated bidentate complexes dominate at high pH and low concentration of phosphate [9]. Subsequent study reported protonated inner-sphere monodentate mononuclear complexes on goethite at pH 7.9 [10]. Recently, results from Attenuated Total Reflection (ATR) – FTIR at near-neutral pH indicate the presence of non-protonated bidentate complex on ferrihydrite [11]. However, the phosphate bonding configuration under acidic conditions (pH 4–6) could not be definitively assessed, since the protonation state of adsorbed P affects the symmetry of the surface complex and consequently the band splitting [5, 15]. By comparison, there have been fewer IR studies of phosphate adsorption on aluminum oxyhydroxides (e.g. gibbsite and boehmite), owing to interference of IR absorption bands from the substrate with those arising from P-O stretching.

In principle, ^{31}P NMR spectroscopy is well-suited to study the chemical structure of adsorbed species at the mineral-water interface, since the NMR chemical shift is sensitive to structural changes at the molecular scale, and could allow resolution of distinct adsorption complexes as well as any Al-phosphate precipitates. Several previous studies [16-21] have used NMR to study orthophosphate and organo-phosphate adsorption on aluminum oxyhydroxides and contributed better understanding of phosphate adsorption and conditions of Al-phosphate precipitation. These results suggest monodentate and bidentate complexes could be differentiated by chemical shift. However, the single pulse NMR techniques used in most studies is unable to provide direct evidence for the coordination of surface species, because the non-unique relationship between chemical shift and structure makes the chemical shift alone insufficient to identify the adsorption complexes. A wide range of double resonance NMR methods are now available that can probe spatial proximity between ^{31}P and ^{1}H (CP/MAS, HETCOR, REDOR) and between ^{31}P and ^{27}Al (TRAPDOR, REAPDOR). Although difficult to apply at low concentrations typical of adsorbed species, these methods have the potential to distinguish different types of adsorption complexes through quantitative comparison of internuclear dipolar couplings.

Here we apply solid-state NMR techniques to determine the structure of the phosphate adsorption complexes on boehmite. Quantitative ^{31}P NMR data obtained along the sorption isotherm show the presence of two main adsorbed phosphate species characterized by distinct pH-dependent concentrations. Comparison of the results of ^{31}P{^{27}Al} double-resonance experiments, rotational-echo adiabatic-passage double-resonance (REAPDOR), with those calculated from model structures indicate that both species correspond to bridging bidentate configurations. Comparison of the measured ^{31}P chemical shift anisotropy (CSA) for the two adsorbed species with those calculated via quantum chemical cluster methods strongly suggest assignment to mono-protonated and non-protonated phosphate. This result is in good qualitative agreement with the respective pH dependence of the adsorption density. These NMR measurements when combined with information from macroscopic adsorption provides insight into the mechanism of surface complexation of phosphate, leading to a better understanding of the nature of phosphate uptake by aluminum oxide and (hydr)oxide surfaces in aqueous environments.

2.2. Materials and methods

2.2.1. Materials

Boehmite was acquired from CONDEA Chemie GmbH and contained no impurity phases detectable by powder XRD analysis. The solid has a specific surface area (SSA) of 136 m^2g^{-1} determined by a five-point N_2 Brunauer–Emmett–Teller (BET) gas adsorption isotherm method. The boehmite surface has a point of zero charge (pH_{pzc}) of 9.1 based on the electrophoretic mobility (EM) method described by Nordin et al. (1999) [22].

2.2.2. Phosphate sorption

Adsorption experiments were conducted using a pH-stat method [21]. A 0.25 g aliquot of dry boehmite powder was added to 50 ml of solution at the desired pH with a 0.01M NaCl background electrolyte. One titrator (Metrohm STAT 718) was used to automatically maintain constant pH by adding increments of 0.1M HCl. A second titrator was used to add a small amount of 50 mM phosphate solution into the reaction vessel to reach the desired total phosphate concentration. After reaction, the samples were centrifuged to separate the solid and solution. The supernatant solutions were filtered by a 0.2μm-filter and then analyzed for phosphorus by the Direct Coupled Plasma-Atomic Emission Spectroscopy (DCP-AES) while the solid samples were quickly rinsed with a small volume of deionized water and then air-dried for NMR measurement.

Sorption kinetics and pH effects were tested in advance to optimize the experimental conditions for preparation of samples along the sorption isotherm. For kinetics studies, the initial phosphate concentration was 1 mM with the reaction time ranging from 5 min to 120 min at pH 5. The sorption pH edge was measured with the initial phosphate concentration at 1 mM at pH values ranging from 4 to 10, for 15 minutes. Measurement of the sorption isotherm was carried out at pH 5 with the initial concentration ranging from 100 μM to 1000 μM and 15 minute reaction times.

2.2.3. NMR data collection

Solid-state ^{31}P single-pulse (SP) and $^{31}P\{^1H\}$ cross-polarization (CP) MAS NMR spectra were collected on a 400 MHz Varian Inova spectrometer (9.4 T), at operating frequencies of 161.8 MHz and 399.8 MHz for ^{31}P and ^{1}H, respectively. Spectra were collected using a Varian/Chemagnetics T3-type probe samples contained in 3.2mm (o.d.) thin wall ZrO_2 rotors. The ^{31}P chemical shifts ($\delta_{iso,P}$) are reported relative to external 85% H_3PO_4 solution, using hydroxylapatite as a secondary reference set to $\delta_{iso,P}$ = 2.65 ppm.

The ^{31}P SP/MAS spectra were obtained with an excitation 90° pulse of 6 μs, using a 120 s relaxation delay. Spectra taken for some samples at a longer delay showed no further increase in absolute intensity. Approximately 500 scans were usually enough to provide sufficient signal-to-noise ratio for boehmite samples with adsorbed phosphate, but samples reacted at lower concentrations (e.g. 100 μM) required more scans (up to 1400). The standard ZrO_2-based rotor sleeves give ^{31}P signals in the spectral region for orthophosphate groups with the chemical shift at -12 ppm. This signal was quantified against mixtures of calcite and hydroxylapatite to allow comparison of signal intensity among samples, which is described below.

The ^{31}P{^{1}H} CP/MAS spectra were obtained at spinning rates of from 3-5 kHz and contact times that varied from 0.1 to 7 ms, using a probe assembly configured for 7.5 mm (o.d.) rotors. CP kinetics curves were measured at a spinning rate of 3 kHz with continuous wave (CW) irradiation at the n = -1 sideband match condition. For other CP/MAS spectra the transverse ^{1}H field ($\gamma B_{1,H}$) was ramped over approximately 5 kHz, centered near the first sideband match with a 42 kHz ^{31}P field. Proton decoupling (CW) was employed during acquisition of all ^{31}P{^{1}H} CP/MAS spectra.

The ^{1}H MAS NMR spectra were obtained indirectly as slices from 2-dimensional ^{31}P{^{1}H} heteronuclear correlation (HetCor) spectra. The HetCor experiments employed a spinning rate of 10 kHz and a CP contact time of 1 ms, using a linear ramp of the ^{31}P B_1 field and 42 kHz ^{1}H field. We collected 100 hypercomplex points in t_1 with a 10 μs increment, corresponding to a 100 kHz spectral window in $F1$. For each spectrum, 832 scans were added for each point at a 1 s relaxation delay, requiring approximately 2 days total. The spectra were acquired in ^{1}H-coupled mode, with no homonuclear ^{1}H decoupling pulses applied during $t1$. Some HetCor experiments included a 200 ms mixing period during which the ^{1}H magnetization was stored along B_0 between ^{1}H excitation and the CP contact time, allowing additional ^{1}H-^{1}H spin-diffusion. The 1H NMR chemical shifts (δ_{H-1}) are referenced with respect to tetramethylsilane (TMS) using adamantane as a secondary reference set to δ_{H-1} = 2.0 ppm.

$^{31}P\{^{1}H\}/^{27}Al$ REAPDOR [23] and TRAPDOR [24] NMR spectra were obtained on a 500 MHz Varian Infinity plus spectrometer (11.7 T) using a 3-channel Varian/Chemagnetics 'T3' probe assembly configured for 4 mm (o.d.) rotors. These pulse sequences employed excitation of ^{31}P signal through $^{31}P\{^{1}H\}$ cross-polarization with a linear ramp of ^{1}H B_1 field during the contact time to flatten the match condition. The ^{1}H 90°pulse length was 6 μs, the optimized contact time 1 ms, and the relaxation delay 2 s. For REAPDOR NMR experiments, the ^{31}P 180° pulse-length was 10 μs and the duration and strength of ^{27}Al pulse in the middle of the dephasing pulse train are 1/5 of the rotor period and 75 kHz, respectively.

2.2.4. NMR shielding calculations

The surface models were built from the components of an Al-hydroxide dimer ($Al_2(OH)_6(H_2O)_4$) and phosphate in different protonation states using the Cerius^2 software [25]. Phosphate was bonded to the Al atoms assuming ligand exchange with terminal OH-groups. The model phosphate surface complex was hydrated by 4 or 8 H_2O molecules to account for adsorbed H_2O in the experiments from ambient water vapor.

All calculations were performed with Gaussian 03[26]. Energy minimizations and frequency calculations were performed with the B3LYP exchange and correlation functionals [27-28] and the 6-31G(d) basis set [29]. Calculations of the NMR chemical shieldings and chemical shift anisotropy were performed using the gauge-including atomic orbital (GIAO) method [30], the Hartree-Fock approximation [31=32], and the 6-311++G(2d,2p) basis set [33]. The absolute chemical shielding values were converted to chemical shifts ($\delta_{ii} = -\sigma_{ii}$) and then shifted to make the average value of δ_{11} for each set equal to that of the observed peaks. (Note that accurately predicting ^{31}P absolute chemical shifts is a well-known problem[31], and this theoretical issue has not been solved, so we use a practical approach to address the issue here.)

2.3. Results

2.3.1. Phosphate adsorption

At a 1mM initial concentration, sorption of phosphate by boehmite follows a trend typical for most oxyanions, with the amount sorbed decreasing as pH increases (Figure 2.1). The phosphate coverage is 0.68 P nm^{-2} at pH 4, while at pH 10 this value decreased to 0.072 nm^{-2}. These results are similar to those reported previously for Al-oxyhydroxides[1]. At pH 5, approximately 71% of the phosphate was removed from the solution after 5 minutes, with the average phosphate coverage reaching 0.54 nm^{-2}. After 15 minutes the surface coverage increases 13% to 0.61 nm^{-2} and changes little with additional reaction time to 120 minutes. To avoid the formation of surface precipitates, we chose a reaction time of 15 minutes for further experiments. Under these conditions, dissolution of boehmite resulted in total dissolved Al of $9.6\cdot10^{-7}$ M at pH 5 and $9.6\cdot10^{-4}$ M at pH 4. Based on these results, we chose pH 5 and a 15 minute reaction time to prepare samples for NMR analysis.

The sorption isotherm (Figure 2.2) shows that as the initial phosphate concentration increases from 100 μM to 1000 μM, the surface coverage also increases, from 0.072 nm^{-2} to 0.63 nm^{-2}. A Langmuir isotherm, $Q = \frac{Q_m KC}{1+KC}$, was used to model the adsorption isotherm, where Q is the amount of sorbed phosphate (P nm^{-2}), C is the equilibrium phosphate concentration (μM), Q_m is the maximum adsorption amount and K is the equilibrium constant for the sorption reaction. A least-squares fit yields $Q_m = 0.79\ \mathrm{nm}^{-2}$ and $K = 0.014$, and provides a good description of the data ($R^2=0.98$), suggesting that adsorption reactions can account for the uptake of phosphate by the boehmite surface under these conditions.

2.3.2. ^{31}P SP/MAS NMR spectra.

Six phosphate-adsorbed boehmite samples prepared along the adsorption isotherm (Table 2.1 and Figure 2.2) were examined by quantitative ^{31}P single-pulse MAS NMR. Spectra of all six samples (Figure 2.3) exhibit the same three major peaks, at chemical shifts of $\delta_{iso,P} = 0$, -6 and -12 ppm and full-width at half-maximum (FWHM) of 3.5, 6.5, and 1.2 ppm respectively. A control spectrum taken of the empty rotor shows only a sharp peak at $\delta_{iso,P} = -12$ ppm, which we assign to a background signal from the rotor. Since this peak intensity should remain unchanged, we used it as an internal standard to quantify the intensity changes in the other two peaks among the samples. Quantitative comparison of the phosphate uptake by each sample with the corresponding ratio of combined intensity for the peaks at $\delta_{iso,P} = 0$ and -6 ppm to that at -12 ppm (Table 1.1) indicates a linear relationship ($r^2 = 0.99$) that intersects the origin (Figure 2.4). This result suggests that both of the peaks arise from adsorbed phosphate and represent distinct surface complexes. We found no significant contribution from aluminophosphate precipitates, which previous studies have reported to yield a broad ^{31}P NMR peak centered near -10 to -12 ppm [18-20], indicating that surface adsorption reactions are the principal process for phosphate uptake under these experimental conditions.

Additional spectra acquired for a sample prepared as a wet paste are essentially similar to those of air-dried samples, containing the same three major peaks (See Chapter 3). Due to the lack of significant differences aside from lower signals from the pastes, all subsequent NMR spectra were collected on samples dried to room humidity.

2.3.3. $^{31}P\{^{1}H\}$ CP/MAS results

The $^{31}P\{^{1}H\}$ CP/MAS NMR spectra of phosphate adsorbed on boehmite at pH 5 contain two peaks at chemical shifts near $\delta_P = 0$ and -6 ppm (Figure 2.5), and are similar to the single pulse spectra (Figure 2.3) except for the absence of the peak at -12 ppm arising from the rotor. This result indicates that the types of phosphate represented by the two peaks must occur near hydrogen, because the CP/MAS signal arises from transfer of magnetization from protons to ^{31}P nuclei over distance less than about 5 Å. To determine the relative relationship between the proton-bearing species associated with phosphate, the CP dynamics were analyzed by fitting spectra of sam6 obtained at different contact times (τ) to a consistent set of Gaussian curves, allowing only the intensities to vary. The resulting intensities are well described by the classical bi-exponential relationship

$$I(\tau) = I_0\left[1 - \frac{T_{PH}}{T_{1\rho,H}}\right]^{-1}\left[1 - \exp\left(-\frac{T_{PH}}{\tau}\right)\right]\exp\left(-\frac{T_{1\rho,H}}{\tau}\right) \qquad (1)$$

where T_{PH} is the characteristic time for $^{1}\mathrm{H}\rightarrow{}^{31}\mathrm{P}$ magnetization transfer and $T_{1\rho,\mathrm{H}}$ is the time constant for decay of the ^{1}H magnetization in the rotating frame [34]. Best fits of the variable contact time data (Figure 2.6) give the T_{PH} values of 0.42 ms and 0.34 ms and $T_{1\rho,,\mathrm{H}}$ of 3.7 and 3.1 ms, respectively for the peaks at $\delta_{\mathrm{iso,P}} = 0$ and -6 ppm. These short T_{PH} values indicate a close association of phosphate with protons, as could be expected for the hydroxylated surface of an oxyhydroxide. In the rigid limit, T_{PH} is related to the sum over the phosphate-proton distances: $T_{PH}^{-1} \propto \sum_{1}^{i}\left[d\left({}^{31}P{-}{}^{1}H_i\right)\right]^{-6}$, where $d\left({}^{31}P{-}{}^{1}H_i\right)$ is the internuclear distance between the phosphate P and the *i*th nearby proton [35]. However, motion of H and H-bearing species can modify the relationship and prevents strictly quantitative interpretation of the CP rate. The ^{1}H MAS NMR spectra of H near both types of phosphate, obtained indirectly by $^{31}\mathrm{P}\{^{1}\mathrm{H}\}$ heteronuclear correlation (data not shown), contain a narrow peak for mobile water, in addition to a very broad signal for rigid, strongly coupled H (most evident in the time-domain signal). Nonetheless, the relative T_{PH} values suggest that the peak at $\delta_{\mathrm{iso,P}} = -6$ ppm represents phosphate groups that are in closer association with protons.

Comparison of the CP dynamics and SP/MAS results for sam6 indicate that the intensity ratios in CP/MAS spectra are approximately quantitatively correct at contact times of 1-2 ms. Based on this result, we obtained CP/MAS spectra (Figure 2.7) for a series of samples prepared along the pH edge (Figure 2.1) from pH 3 to 11. CP/MAS allowed reasonably high signal-to-noise ratios at the low P coverage available at high pH. All of the spectra appear to show the same two resolved peaks, but with a systematic increase in chemical shift of about 1.6 ppm with increasing pH from 3 to 11 (Table 2.3), perhaps reflecting the reduction in surface charge. However, the local structure of the phosphate species does not appear to change appreciably over this pH range and no distinctly new peaks appear. Most of the spectral changes can be attributed to changes in intensity of the same two peaks near 0 and -6 ppm. The two peaks exhibit distinct variation with the pH, with the left peak ($\delta_{iso,P}$ = 0 ppm at pH 5) more intense at high pH whereas right peak ($\delta_{iso,P}$ = -6 ppm at pH 5) dominates at low pH (i.e. pH 3).

2.3.4. Proton environment indirectly measured by $^{31}P\{^{1}H\}$ heteronuclear correlation

2-dimensional (2-d) $^{31}P\{^{1}H\}$ heteronuclear correlation (HetCor) spectra were collected to investigate the ^{1}H species that are associated with the phosphate adsorbed on the surface. The ^{31}P dimension of the 2-d contour plots (Figure 2.8a) shows the same two signals for phosphate as shown in the CP/MAS (Figure 2.5 and Figure 2.7) and SP/MAS spectra (Figure 2.3). The HetCor sequence used here is slightly modified from CP/MAS by adding a second time variable (*t*1) before CP contact time. With *t*1 incrementing at short intervals, a series of $^{31}P\{^{1}H\}$ CP/MAS spectra were collected to indirectly build the ^{1}H free induction decay. Thus only protons strongly coupled with phosphate (through ^{1}H-^{31}P dipolar coupling) and other H connected by ^{1}H-^{1}H homonuclear dipolar coupling will be observed. Thus, the ^{1}H slices (cross sections) taken at the phosphate peak positions correspond to the ^{1}H NMR spectra of the hydrogen that are in close proximity to the phosphate.

For a sample prepared at pH 5, the HetCor ^{1}H slices are very similar for the peaks at δ_{P} = 0 and -6 ppm, showing a relative narrow peak with chemical shift at approximately δ_{H-1} = 5.2 ppm plus a weaker and broad signal associated with spinning sidebands (SBBs) (Fig. 2.9a). The narrow peak is assigned to mobile water on boehmite surface; the absence of spinning sidebands suggests motional averaging of dipolar and CSA interaction. The broad peak is centered near δ_{H-1} = 6.6 ppm fitted to its SSBs. This peak could be ascribed to more rigid water, such as surface bridging hydroxyls, structural water, or protonated phosphate. In addition, another feature (very broad) was not able to be observed in the Frequency domain due to its low signal and peak breadth, but can be evidenced by its quick decay in the first 10 μs time-domain signal, free induction decay (FID) (Figure 2.9b). Additional HetCor spectra were acquired with a mixing time (τ_{mix}) of 200 ms before the CP contact time, which allows the ^{1}H in different environments to exchange polarization with each other through the ^{1}H-^{1}H homonuclear dipolar interactions. The intensity of ^{1}H slices for both phosphate ^{1}H peaks decreases after mixing time is applied (Figure 2.8b), which indicates ^{1}H spin diffusion to mobile water which relaxes quickly.

2.3.5. $^{31}P\{^{1}H\}$-^{27}Al REAPDOR and TRAPDOR results

The $^{31}P\{^{27}Al\}$ REAPDOR NMR experiments [23, 26] were performed to measure the ^{31}P-^{27}Al heteronuclear dipolar interactions, which depend on the interatomic distances and geometries and thus can be used to distinguish phosphate coordination models for the boehmite surface. Experimentally, sets of two ^{31}P-observed NMR spectra are acquired, one (S) obtained with a heteronuclear dipolar dephasing sequence and a control spectrum (S_0) acquired under identical conditions but without irradiation at the ^{27}Al frequency. The difference in peak intensity between the dephased spectrum and the control ($\Delta S = S_0 - S$) depends on the ^{31}P-^{27}Al heteronuclear dipolar coupling and the length of the dephasing period (τ_D). The control spectrum (S_0) serves as a quantitative comparison to remove the effects of T_2 decay and pulse imperfection on the peak intensities.

The inset of Figure 2.10 shows a typical set of ^{31}P-^{27}Al REAPDOR NMR spectra acquired for a phosphate adsorbed sample prepared at pH 5 (Sam6) with 0.75 ms dephasing time (product of the number of rotor cycles and rotor period), but nearly identical results were obtained for a sample prepared at pH 9 (See Chapter 3). The difference in peak intensity between the top and bottom spectra, ΔS represents the influence of ^{31}P-^{27}Al dipolar coupling at this dephasing time. The REAPDOR fraction $\Delta S/S_0$ was measured as a function of dephasing time, yielding a REAPDOR dephasing curve (Figure 2.10) which characterizes the magnitude of ^{31}P-^{27}Al heteronuclear dipolar coupling interactions. It is evident from Figure 2.10 that the REAPDOR curves for the two distinct ^{31}P NMR peaks ($\delta_{iso,P}$ = 0 and -6 ppm) are almost identical, providing strong evidence that the two peaks arise from phosphate adsorption sites with essentially the same coordination to Al, over the range pH 5 to 9. Both peaks also gave similar dephasing curves using the TRAPDOR sequence (Figure 2.11).

Quantitatively, simulations of the REAPDOR experiment using the SIMPSON package [37] were undertaken using the distances between P and Al from models of phosphate bonded to edge-shared $Al(O)_6$ octahedra suggested by Fry et al. [38]. A bridging bidentate model used two P-Al distances, at 3.10 and 3.14 Å, and the monodentate model assumed one short distance between P and the Al to which it is linked, 3.26 Å, and two more distant Al at 4.39 and 4.62 Å. For the SIMPSON simulations we used ^{27}Al quadrupolar coupling constants of 3 MHz for the Al near phosphate, which was estimated from ^{31}P{^{27}Al} TRAPDOR NMR experiments[24] with varying ^{27}Al irradiation frequency.

The simulations (Figure 2.10) show that the bidentate coordination model yields a REAPDOR dephasing curve close to the experimental data, whereas that calculated from the monodentate model deviates significantly. This result indicates that two relatively short Al-P distances are required to explain the REAPDOR results and provides strong indication that both the ^{31}P peak at 0 ppm and that at -6 ppm arise from phosphate with bridging bidentate coordination to Al. For comparison, to fit the experimental data with a single Al near P would require an unrealistically short 2.7 Å P-Al distance.

The small difference between the calculated and measured REAPDOR curves for the bidentate model is of the order that can be attributed to the presence of additional, more distant Al on the surface, whereas the simulations used simplified 3- and 4-spin systems. Preliminary models of phosphate on common boehmite surfaces suggest that bridging bidentate configurations could have one additional Al at about 4.65-4.7 Å, which could account for much of the difference between the experimental and calculated dephasing curves. All other P-Al distances are likely to be greater than 5 Å and would have negligible effect individually, but in summation could help account for the difference.

2.3.6. The ^{31}P chemical shift anisotropy

The NMR chemical shift is a tensor property, described by the chemical shift anisotropy (CSA) and representations of the principal tensor values: δ_{ii}; $1 \leq ii \leq 3$. The peak positions of the ^{31}P NMR centerbands reported above are the isotropic chemical shifts ($\delta_{iso,P}$), equal to the average of the principal values, but the CSA provides additional information to potentially distinguish molecular environments. In particular, previous studies have noted large and systematic changes in the ^{31}P CSA with the protonation state of phosphate in crystalline compounds [39]. We determined the ^{31}P CSA's for both peaks from the spinning sideband (SSB) intensities of a ^{31}P CP/MAS spectrum collected at a spinning rate of 3.5 kHz (Figure 2.5). The integrated intensity and frequency of each isotropic resonance and its respective SSB's were obtained by fitting the spectrum to a sum of Gaussian curves, from which the CSA's were extracted by the Herzfeld-Berger method [40] via the program HBA [41].

The resulting principal values of the CSA's are shown in Table 2.2, from which it is evident that the main difference between the observed peaks lies in the δ_{22} value. This change of about -20 ppm in δ_{22} is responsible for most of the difference in the isotropic chemical shift between the two surface complexes, whereas their δ_{33} and, especially, δ_{11} values are similar. Qualitatively this shift in δ_{22} results in a reversal of the relative intensities of the +1 and -1 SSB's apparent in Figure 2.5. In terms of the shape of the chemical shift tensor, δ_{22} for the peak near 0 ppm is closer in value to δ_{11} whereas for the peak at -6 ppm it is nearer to that for δ_{33}, causing a change in the sign of the skew ($\kappa = 3(\delta_{22} - \delta_{iso})/\Omega$; where the span $\Omega = \delta_{11} - \delta_{33}$) in the IUPAC convention, and of the anisotropy ($\Delta\delta = 3(\delta_{zz} - \delta_{iso})/2$, where $z = 1$ if $\delta_{11} - \delta_{iso} > \delta_{33} - \delta_{iso}$, or $z = 3$ otherwise) in the Haeberlen representation (Table 2.2). These results provide additional evidence that the two ^{31}P NMR peaks arise from distinct adsorption complexes, and indicate that both are characterized by low-symmetry configurations. For example, a complex with C_{3v} symmetry similar to that observed by IR at high pH and phosphate coverage on hematite [42] would exhibit an axially symmetric CSA, with δ_{22} equal to either δ_{11} or δ_{33}.

Unfortunately, no phosphate coordination environment directly analogous to the inferred bridging bidentate geometry is known from crystalline aluminum phosphate phases with which to compare the observed CSA's. To investigate whether the distinct CSA's could reflect different protonation states we calculated shielding tensors for several model complexes based on a single pair of edge-shared Al-octahedra connected by hydroxyl bridges. From the $^{31}P/^{27}Al$ REAPDOR results, we limited our attention to binuclear bidentate complexes with water molecules and hydroxyl groups completing the Al coordination. Two sets of complexes were investigated, each having between $0 \leq n \leq 2$ protons bonded to the phosphate group, but differing in the number of explicit solvent water molecules; eight waters for models denoted Bi-*n*H-8 and four for Bi-*n*H-4 (Table 2.2). Geometry was optimized by minimizing the energy calculated with the B3LYP functionals using the 6-31G(d) basis set; a typical cluster is illustrated in Figure 2.12. The shielding tensor at the P position was then calculated by the GIAO method and diagonalized to yield the principal values σ_{ii}. Illustrations of tensor orientations for the Bi-*n*H-8 models are shown in Figure 2.13. To facilitate comparison with the experimental data, the absolute shielding values were converted to chemical shifts ($\delta_{ii} = -\sigma_{ii}$) and then shifted to make the average value of δ_{11} for each set of calculated complexes equal to that of the observed peaks ($\delta_{11} = 30.2$ ppm). This method was preferred over calculation of the absolute shielding of the chemical shift reference because the calculated σ_{11} values for each set of complexes are nearly the same within the uncertainty of the method and because of anticipated difficulties in capturing the ensemble of configurations needed to accurately represent dissolved phosphoric acid.

As is clear from Table 2.2, the results for the larger clusters are in excellent agreement with the experimental data in terms of the span (Ω) and anisotropy ($\Delta\delta$). Although the variations in the calculated δ_{iso} with protonation (*n*H) are probably within the error of the approximations and insufficient to suggest an assignment, the shift in δ_{22} value between the $n = 0$ or 2 and $n = 1$ complexes shows distinct similarities to the differences between the observed CSA's. Compared to the Bi-0H-8 and Bi-2H-8 models, the CSA for Bi-1H-8 complex is unique in that δ_{22} lies closer in value to δ_{33}, resulting in a reversal in the sign of the skew and anisotropy. This shift in δ_{22} closely resembles that between the observed resonances suggests assignment of peak 2 ($\delta_{iso,P} = -6$ ppm) to the model with the unique CSA, corresponding to the singly-protonated surface complex. The calculated CSA's for

Bi-2H-8 and Bi-0H-8 are similar and consistent with that observed for peak 1 ($\delta_{iso,P} = 0$ ppm). However, the increase of the relative intensity of this peak with increasing pH (Figure 2.7) suggests assignment to phosphate having fewer protons than that corresponding to the peak at $\delta_{iso} = -6$ ppm, resulting in assignment to non-protonated phosphate. In addition, an increase in isotropic chemical shift with a decrease in the number of protons bonded to the adsorbed phosphate is consistent with ^{31}P chemical shift relationships in other systems, such as aqueous orthophosphate [43].

Agreement between the calculated and experimental CSA's in terms of the span and anisotropy is poorer for the smaller clusters (Bi-*n*H-4; Table 2.2), as might be expected for models lacking sufficient explicit waters to approximate the hydrogen bonded network around the adsorbate complex. However, the general relationships among the CSA's calculated for these smaller clusters closely resemble those for the larger Bi-*n*H-8 models in that the CSA's for the $n = 0$ and 2 models are similar, but distinct from that for the $n = 1$ cluster, especially in the relative value of δ_{22} and, correspondingly, in the signs of κ and $\Delta\delta$. This result suggests that the shape of the shielding tensor is governed principally by the coordination of the phosphate oxygens and is relatively insensitive to the number of explicit water molecules, and hence to the details of the hydrogen bonding network.

2.4. Discussion

In terms of the number of peaks observed and intensity changes with pH, the present results are in good agreement with previous NMR studies of phosphate uptake by boehmite under broadly similar conditions [16, 20], but offer additional detail about the nature of the adsorbate complexes resulting from sorption of dissolved phosphate by boehmite. The ^{31}P NMR results for samples prepared along the pH 5 isotherm and across the pH edge show that two distinct surface complexes contribute to the phosphate sorption reactions under these conditions, even though the macroscopic sorption can be modeled perfectly well with a single Langmuir isotherm. Absence of ^{31}P NMR intensity in the chemical shift range previously determined for amorphous aluminophosphates presents strong evidence that the NMR signals we observe arise mainly from adsorbed phosphate. Aluminophosphate precipitates give a broad (ca. 16 ppm FWHM) ^{31}P NMR peak near -12 ppm [17, 20] which produces significant intensity in the -20 ppm region for samples prepared at higher phosphate concentration and/or longer reaction time than used for our experiments, but which is not observed here.

All of our NMR results indicate that the adsorbed phosphate is dynamically rigid, which is readily interpreted to indicate dominantly inner-sphere surface complexation. It is expected that outer-sphere phosphate (lacking a direct Al-O-P linkage) would exhibit significant mobility at the millisecond and shorter time scales. Such motions would effectively average NMR interactions, such as the CSA and the dipolar coupling. The observation of broad ^{31}P spinning sideband envelopes (Figure 2.5) and the similarity of the corresponding CSA's to those calculated for static structural models (Table 2.2) indicate no significant averaging at timescales of the order of the inverse of the spectral width (ca. 16 kHz). Similarly, the rapid intensity build-up in the CP/MAS kinetics requires a strong dipolar coupling between P and H, and the large REAPDOR/TRAPDOR dephasing indicate strong P/Al dipolar interactions, both of which would be sharply reduced or eliminated by motion of the phosphate group. Qualitatively, it could be expected for any outer-sphere phosphate to yield a relatively narrow peak, but the SP spectra contain no solution-like peak and comparison to that obtained by CP methods show them to be nearly identical. The similarities between the spectra obtained for samples that were rinsed and air-dried with those for pastes show that the rigidity of the adsorbed phosphate is not an artifact of sample preparation. Small differences in peak width between spectra of the wet and dried samples are likely due to differences in spinning rate, but could also arise from differences in diffusional mobility of the surface fluid layer.

Combining the NMR spectroscopic results with the pH dependence of the relative peak intensities provides strong evidence that the predominant surface complexes have a binuclear bidentate configuration, one mono-protonated and the other having no directly bonded protons. The REAPDOR dephasing curves for the two ^{31}P resonances shows that the difference between them does not lie in the type of coordination to Al. Furthermore, agreement with those calculated for small Al/phosphate coordination models can only be obtained with a bridging bidentate configuration having two relatively short Al-P distances, reflecting the dependence of the dipolar coupling on the sum of the inverse-cubed P-Al distances. Our assertion that the difference between the two types of surface complexes lies mainly in the protonation state was inferred from comparison of the observed and calculated CSA's as detailed in Table 2.2, and is consistent with the results of dipolar dephasing experiments reported by Bleam et al. [16] from which it was concluded that a peak near -6 ppm (peak A_0 in that study) arose from protonated phosphate. Our assignments are also consistent with the shorter T_{PH} observed for the peak at -6 ppm in the CP kinetics, indicating larger coupling to ^{1}H compared to the peak near 0 ppm. The T_{PH} values we observe are consistent with other reports for protonated and non-protonated phosphate [44], although significant variation might be expected with experimental conditions and molecular motions. That the T_{PH} values for the protonated and non-protonated complexes differ by only a factor of 1.4 is likely a consequence of relatively short P-H distances to rigid hydroxyl groups of boehmite, yielding strong P-H coupling and short T_{PH} even in the absence of H directly bonded to the phosphate group. The relative change in the adsorbate chemical shift is also consistent with that for orthophosphate in aqueous fluids, which become more positive with increasing pH [43] as the average number protons bonded to the phosphate group decreases.

The pH dependence of the NMR peak intensities also shows our assignment of the two peaks to be a reasonable one. Site-specific pH edges can be constructed by distributing the macroscopic sorption densities (Figure 2.1) between the mono-protonated and non-protonated surface phosphate according to the relative NMR intensities, obtained from least-squares fits of SP spectra taken of samples prepared in the range $5 \leq \mathrm{pH} \leq 8$ with 1mM initial phosphate concentration. Plotting in log-log space shows that the decrease of sorption density over this pH range results almost entirely from reduction in concentration of the mono-protonated complex.

Within uncertainty, the surface concentration of non-protonated phosphate remains constant over this pH range, as could be expected for a complex that cannot yield another proton. A similar conclusion was reached by Bleam et al. [16], who estimated a coverage for this pH-independent site ($0.16\ \mathrm{nm}^{-2}$) similar to that found here ($0.25\ \mathrm{nm}^{-2}$) considering our higher initial phosphate concentration (0.1 vs. 1 mM). Unfortunately, SP signal intensities were too low at $\mathrm{pH} > 8$ to accurately quantify the peak intensities, but it is likely that the sharp decrease in sorption density above pH 8.5 results from decrease of both complexes owing to increased concentration of negatively charged $\mathrm{Al\text{-}O^-}$ surface sites.

The shallow, non-integral slope of the pH dependence for the mono-protonated complex (-0.16) cautions against interpreting these results in terms of simple ligand substitution-like reactions or of Bronsted acid/base reactions at the adsorption complex. For example, adsorption of a di-protonated phosphate (dominant in the fluid at pH 5; < $\mathrm{p}K_{a2}$) leading to substitution of two terminal hydroxyls by a mono-protonated surface complex should consume one proton:

$$2(\equiv\mathrm{Al{-}OH}) + \mathrm{H_2PO_4^-} + \mathrm{H^+} \quad = \quad [\equiv\mathrm{Al{-}(HPO_4){-}Al}\equiv] + 2\mathrm{H_2O}$$

, leading to an expected slope of -1. Furthermore, one would expect a change in slope near $\mathrm{pH} = \mathrm{p}K_{a2} = 7.2$ for orthophosphate in the fluid phase, whereas the slope appears constant from pH 5 to 8. Likewise, interpreting the relative changes in NMR intensities in terms of a simple Bronsted acid/base reaction between surface phosphate complexes would predict a decrease in the concentration of the non-protonated species at pH below the apparent $\mathrm{p}K_a$ of the surface complex (ca. 6.1), which is also not apparent.

These observations suggest that the variation in the concentrations of adsorbed species arises from a number of parallel reactions, likely involving combinations of active surface sites (terminal hydroxyl and water ligands), solution phosphate speciation, and possibly side-reactions and changes in basicity at reactive oxygens adjacent to adsorption sites. In addition, it is possible for the pH dependence of adsorption to vary with different crystal faces. Among the common forms reported for boehmite [45], both {001} and {101} contain relatively high densities of paired terminal oxygens bonded to edge-shared Al octahedra with configuration suitable for forming complexes such as that shown in Figure 2.14 The picture of the phosphate adsorption complexes on boehmite as suggested by these NMR results remains incomplete in the sense that each observed peak likely represents a range of adsorption complexes in detail within each coarsely defined type, encompassing a distribution of environments, structures, and chemical properties. This conclusion is similar to that inferred from fluoride substitution on similar material [46], in which expressions derived for fluoride-promoted dissolution in terms of populations of resolved terminal and bridging substitution sites required unphysical rate orders. However, it is clear that systematic NMR experiments can provide not only some structural detail on the broadly defined types adsorption complexes, but also quantitative constraints on the relative populations of protonated and non-protonated surface complexes that should prove useful for constraining macroscopic models of phosphate uptake by Al-oxyhydroxides.

2.5. Conclusions

In this work, I employed ^{31}P solid-state NMR spectroscopy to examine the specific adsorption of phosphate to boehmite (γ-AlOOH). I show strong evidence for the presence of two bridging bidentate surfaces complexes with different protonation at pH 5. Phosphate environments show little change for samples prepared along the sorption isotherm at pH 5 and for sample along the adsorption pH curve, with two major peaks (chemical shifts of 0 and -6 ppm) observed in all the ^{31}P NMR spectra. But relative intensity of the peaks showed different dependence on pH. Both peaks could be assigned to bridging bidentate surface complexes by comparing the ^{31}P{^{27}Al} dephasing curves in rotational echo adiabatic passage double resonance (REAPDOR) experiments and theoretical dephasing curves simulated by SIMPSON. The two resolved phosphate species exhibit distinct ^{31}P chemical shift anisotropy (CSA) and intensity variations with pH, the peak near 0 ppm being dominant at pH > 7. ^{31}P CSA's from quantum chemical calculations of hydrated bidentate cluster models with varying protonation state show that the CSA for mono-protonated phosphate is unique and closely matches that for the peak at -6 ppm. The CSA for the peak at 0 ppm is consistent with both di- and non-protonated phosphate, but assignment to the latter is suggested based on the dominance of this peak in samples prepared at high pH and with trends in ^{31}P NMR chemical shifts.

References

[1] Goldberg, S.; Sposito, G., *Commun. Soil Sci. Plant Anal.* **1985,** *16*, 801-821.

[2] Brown, G. E.; Henrich, V. E.; Casey, W. H.; Clark, D. L.; Eggleston, C.; Felmy, A.; Goodman, D. W.; Gratzel, M.; Maciel, G.; McCarthy, M. I.; Nealson, K. H.; Sverjensky, D. A.; Toney, M. F.; Zachara, J. M., *Chem. Rev.* **1999,** *99*, 77-174.

[3] Rajan, S. S. S., *Nature* **1975,** *253*, 434-436.

[4] Rajan, S. S. S., *Nature* **1976,** *262*, 45-46.

[5] Khare, N.; Martin, J. D.; Hesterberg, D., *Geochim. Cosmochim. Acta* **2007,** *71*, 4405-4415.

[6] Rahnemaie, R.; Hiemstra, T.; van Riemsdijk, W. H., *Langmuir* **2007,** *23*, 3680-3689.

[7] Parfitt, R. L.; Atkinson, R. J.; Smart, R. S. C., *Soil Sci. Soc. Am. J.* **1975,** *39*, 837-841.

[8] Parfitt, R. L.; Atkinson, R. J., *Nature* **1976,** *264*, 740-742.

[9] Tejedor-Tejedor, M. I.; Anderson, M. A., *Langmuir* **1990,** *6*, 602-611.

[10] Persson, P.; Nilsson, N.; Sjoberg, S., *J. Colloid Interface Sci.* **1996,** *177*, 263-275.

[11] Arai, Y.; Sparks, D. L., *J. Colloid Interface Sci.* **2001,** *241*, 317-326.

[12] Hesterberg, D.; Zhou, W. Q.; Hutchison, K. J.; Beauchemin, S.; Sayers, D. E., *J. Synchrotron Radiat.* **1999,** *6*, 636-638.

[13] Khare, N.; Hesterberg, D.; Martin, J. D., *Environ. Sci. Technol.* **2005,** *39*, 2152-2160.

[14] Alvarez, R.; Fadley, C. S.; Silva, J. A., *Soil Sci. Soc. Am. J.* **1980,** *44*, 422-425.

[15] Kwon, K. D.; Kubicki, J. D., *Langmuir* **2004,** *20*, 9249-9254.

[16] Bleam, W. F.; Pfeffer, P. E.; Goldberg, S.; Taylor, R. W.; Dudley, R., *Langmuir*

1991, *7*, 1702-1712.

[17] Lookman, R.; Grobet, P.; Merckx, R.; Vlassak, K., *Eur. J. Soil Sci.* **1994,** *45*, 37-44.

[18] Lookman, R.; Grobet, P.; Merckx, R.; Van Riemsdijk, W. H., *Geoderma* **1997,** *80*, 369-388.

[19] Johnson, B. B.; Ivanov, A. V.; Antzutkin, O. N.; Forsling, W., *Langmuir* **2002,** *18*, 1104-1111.

[20] Kim, Y.; Kirkpatrick, R. J., *Eur. J. Soil Sci.* **2004,** *55*, 243-251.

[21] Van Emmerik, T. J.; Sandstrom, D. E.; Antzutkin, O. N.; Angove, M. J.; Johnson, B. B., *Langmuir* **2007,** *23*, 3205-3213.

[22] Nordin, J.; Persson, P.; Laiti, E.; Sjoberg, S., *Langmuir* **1997,** *13*, 4085-4093.

[23] Gullion, T., *Chem. Phys. Lett.* **1995,** *246*, 325-330.

[24] Grey, C. P.; Vega, A. J., *J. Am. Chem. Soc.* **1995,** *117*, 8232-8242.

[25] Accelrys; *Cerius^2 Modeling Evnironment*; Accelrys, Inc.: San Diego CA, 2003.

[26] Frisch, M. J.; Trucks, G. W.; Schlegel, H. B.; Scuseria, G. E.; Robb, M. A.; Cheeseman, J. R.; Montgomery, J. A., Jr. ; Vreven, T.; Kudin, K. N.; Burant, J. C.; Millam, J. M.; Iyengar, S. S.; Tomasi, J.; Barone, V.; Mennucci, B.; Cossi, M.; Scalmani, G.; Rega, N.; Petersson, G. A.; Nakatsuji, H.; M. Hada; M. Ehara; K. Toyota; Fukuda, R.; Hasegawa, J.; Ishida, M.; Nakajima, T.; Honda, Y.; Kitao, O.; Nakai, H.; Klene, M.; Li, X.; Knox, J. E.; Hratchian, H. P.; Cross, J. B.; Adamo, C.; Jaramillo, J.; Gomperts, R.; Stratmann, R. E.; Yazyev, O.; Austin, A. J.; Cammi, R.; Pomelli, C.; Ochterski, J. W.; Ayala, P. Y.; Morokuma, K.; Voth, G. A.; Salvador, P.; Dannenberg, J. J.; Zakrzewski, V. G.; Dapprich, S.; Daniels, A. D.; Strain, M. C.; Farkas, O.; Malick, D. K.; Rabuck, A. D.; Raghavachari, K.; Foresman, J. B.; Ortiz, J. V.; Cui, Q.; Baboul, A. G.; Clifford, S.; Cioslowski, J.; Stefanov, B. B.; Liu, G.; Liashenko, A.; Piskorz, P.; Komaromi, I.; Martin, R. L.; Fox, D. J.; Keith, T.; Al-Laham, M. A.; Peng, C. Y.; Nanayakkara, A.; Challacombe, M.; Gill, P. M. W.; Johnson, B.; Chen, W.; Wong, M. W.; Gonzalez, C.; Pople, J. A.; *Gaussian 03, Revision C.02*; Gaussian, Inc.: Wallingford CT, 2004.

[27] Becke, A. D., *J. Chem. Phys.* **1997,** *107*, 8554-8560.

[28] Lee, C. T.; Yang, W. T.; Parr, R. G., *Phys. Rev. B* **1988,** *37*, 785-789.

[29] Hehre, W. J.; Ditchfie, R.; Pople, J. A., *J. Chem. Phys.* **1972,** *56*, 2257-2261.

[30] Wolinski, K.; Hinton, J. F.; Pulay, P., *J. Am. Chem. Soc.* **1990,** *112*, 8251-8260.

[31] Alam, T. M. *Ab Initio Calculation of Nuclear Magnetic Resonance Chemical Shift Anisotropy Tensors I. Influence of Basis Set on the Calculations of ^{31}P Chemical Shifts*; Sandia National Laboratories: Albequerque NM, 1998.

[32] Zhang, Y.; Oldfield, E., *J. Phys. Chem. B* **2004,** *108*, 19533-19540.

[33] McLean, A. D.; Chandler, G. S., *J. Chem. Phys.* **1980,** *72*, 5639-5648.

[34] Kolodziejski, W.; Klinowski, J., *Chem. Rev.* **2002,** *102*, 613-628.

[35] Mehring, M., *Principles of High Resolution NMR in Solids*; 2nd ed.; Springer-Verlag: Berlin, 1983.

[36] Chopin, L.; Vega, S.; Gullion, T., *J. Am. Chem. Soc.* **1998,** *120*, 4406-4409.

[37] Bak, M.; Rasmussen, J. T.; Nielsen, N. C., *J. Magn. Reson.* **2000,** *147*, 296-330.

[38] Fry, R. A.; Kwon, K. D.; Komarneni, S.; Kubicki, J. D.; Mueller, K. T., *Langmuir* **2006,** *22*, 9281-9286.

[39] Hartmann, P.; Vogel, J.; Schnabel, B., *J. Magn. Reson. A* **1994,** *111*, 110-114.

[40] Herzfeld, J.; Berger, A. E., *J. Chem. Phys.* **1980,** *73*, 6021-6030.

[41] Eichele, K.; Wasylishen, R. E.; *WSOLIDS*, 2.0.18; Dalhousie University: Halifax, 2000.

[42] Elzinga, E. J.; Sparks, D. L., *J. Colloid Interface Sci.* **2007,** *308*, 53-70.

[43] Mortlock, R. F.; Bell, A. T.; Radke, C. J., *J. Phys. Chem.* **1993,** *97*, 775-782.

[44] Holland, G. P.; Sharma, R.; Agola, J. O.; Amin, S.; Solomon, V. C.; Singh, P.; Buttry, D. A.; Yarger, J. L., *Chem. Mat.* **2007,** *19*, 2519-2526.

[45] Chiche, D.; Digne, M.; Revel, R.; Chaneac, C.; Jolivet, J. P., *J. Phys. Chem. C* **2008,** *112*, 8524-8533.

[46] Nordin, J. P.; Sullivan, D. J.; Phillips, B. L.; Casey, W. H., *Geochim. Cosmochim. Acta* **1999,** *63*, 3513-3524.

Tables and figures

Table 2.1 Quantitative integrated intensities of the three peaks observed in ^{31}P MAS/NMR spectra for P/boehmite sorption samples along the pH = 5 isotherm.

Sample	**mass**[1] (mg)	**C$_0$**[2] (μM)	**sorption density** (P nm^{-2})	**integrated ^{31}P NMR intensity** (arb. units) rotor ($\delta_{iso,P}$ = -12)	peak 1 ($\delta_{iso,P}$ = 0)	peak 2 ($\delta_{iso,P}$ = -6)
Sam1	44.6	100	0.071	34.3	101.0	58.9
Sam2	32.3	200	0.160	47.8	148.5	52.0
Sam3	34.3	400	0.324	41.9	205.2	203.6
Sam4	31.0	600	0.456	48.9	253.6	376.7
Sam5	33.0	800	0.550	44.2	373.7	372.1
Sam6	33.4	1000	0.629	48.5	420.8	507.2

[1] Amount of sample in rotor. [2] Initial phosphate concentration.

Table 2.2 Comparison of ^{31}P chemical shift tensor values for phosphate adsorbed on boehmite at pH 5 and calculated for phosphate bridging hydroxyl-linked Al octahedra. Calculated clusters are denoted Bi-*n*H-*m*, which are bridging bidentate with *n* protons on the phosphate group and *m* explicit solvent waters. For comparison with observed data, calculated shieldings for all clusters were offset by -335.8 (Bi-*n*H-8) and -312.2 ppm (Bi-*n*H-4), such that the average observed and calculated δ_{11} values were the same for each set.

	$\delta_{iso,P}$ (ppm)	principal tensor values[1]			span (Ω)	skew (κ)	anisotropy ($\Delta\delta$)	asymmetry (η)
		δ_{11}	δ_{22}	δ_{33}				
peak 1	0	31	10	-41	72	0.39	-61	0.5
peak 2	-6	29	-11	-36	65	-0.21	52	0.7
Bi-0H-8	-2.3	29.9	2.5	-39.4	69	0.21	-55.7	0.74
Bi-1H-8	-4.7	29.2	-10.3	-33.0	62	-0.27	50.9	0.67
Bi-2H-8	-4.2	31.3	0.4	-44.4	76	0.18	-60.3	0.77
Bi-0H-4	-28.2	33.6	-3.6	-114.6	148	0.50	-130	0.43
Bi-1H-4	-24.8	27.0	-28.8	-72.7	100	-0.12	78	0.85
Bi-2H-4	-27.1	29.8	-5.5	-105.6	135	0.47	-118	0.45

[1] estimated uncertainty ±1 ppm for experimental data

Table 2.3 Observed peak parameters from least-squares fits of the ^{31}P CP/MAS spectra of phosphate/boehmite sorption samples prepared at different pH (Fig. 7).

Sample	**Chemical shift** (ppm)	**FWHM**[1] (ppm)	**relative intensity** (%)
pH3	-0.30	3.0	23
	-6.39	8.0	77
pH5	0	3.5	42
	-6	6.5	58
pH7	0.51	3.3	57
	-5.58	6.0	43
pH9	0.92	2.6	80
	-5.17	5.5	20
pH11	1.32	3.8	73
	-4.77	5.6	27

[1] full width at half maximum

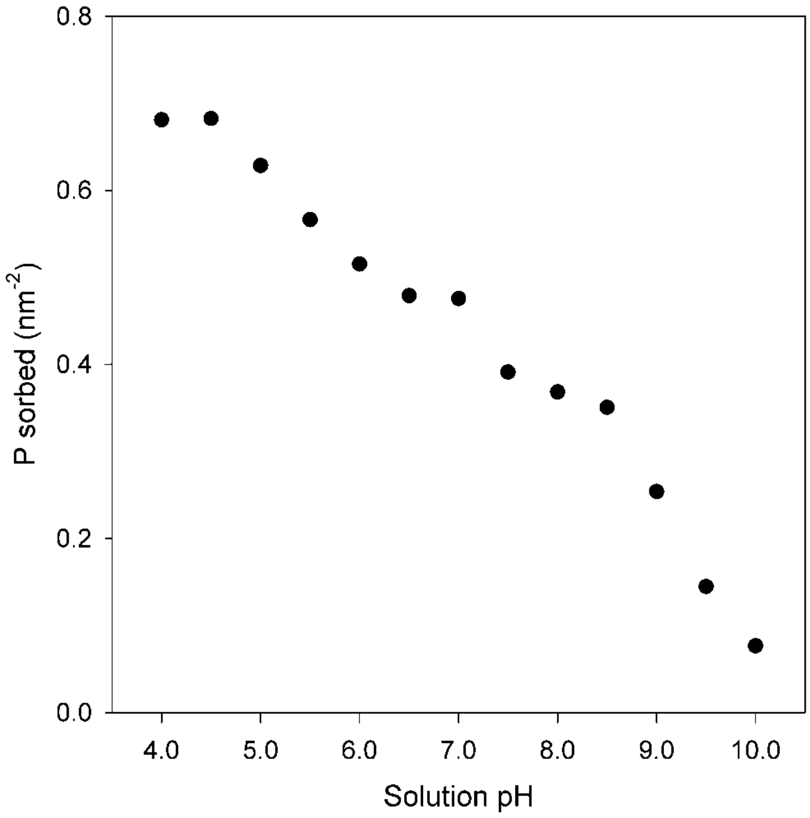

Figure 2.1 Phosphate uptake by boehmite at different pH values with 1 mM initial phosphate concentration, 10 mM NaCl background electrolyte, and 15 minute reaction time at room temperature.

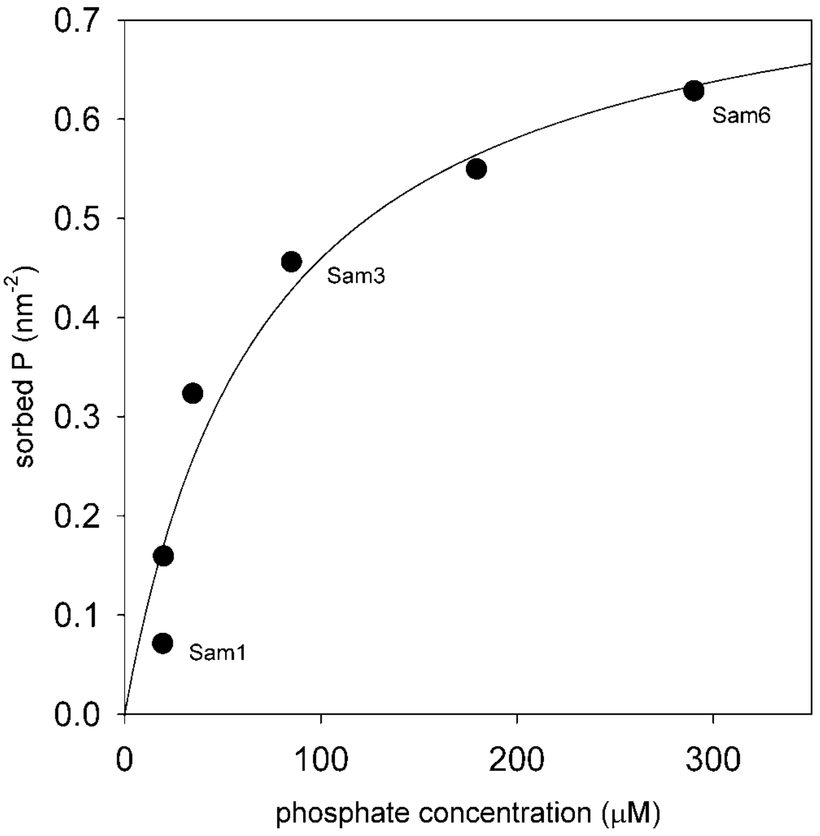

Figure 2.2 Variation of phosphate uptake by boehmite at pH 5 in 0.01 M NaCl with final solution concentration, normalized to the BET specific surface area. The data for each point are the average value of duplicate experiments. 10 mM NaCl background electrolyte, and 15 minute reaction time at room temperature.

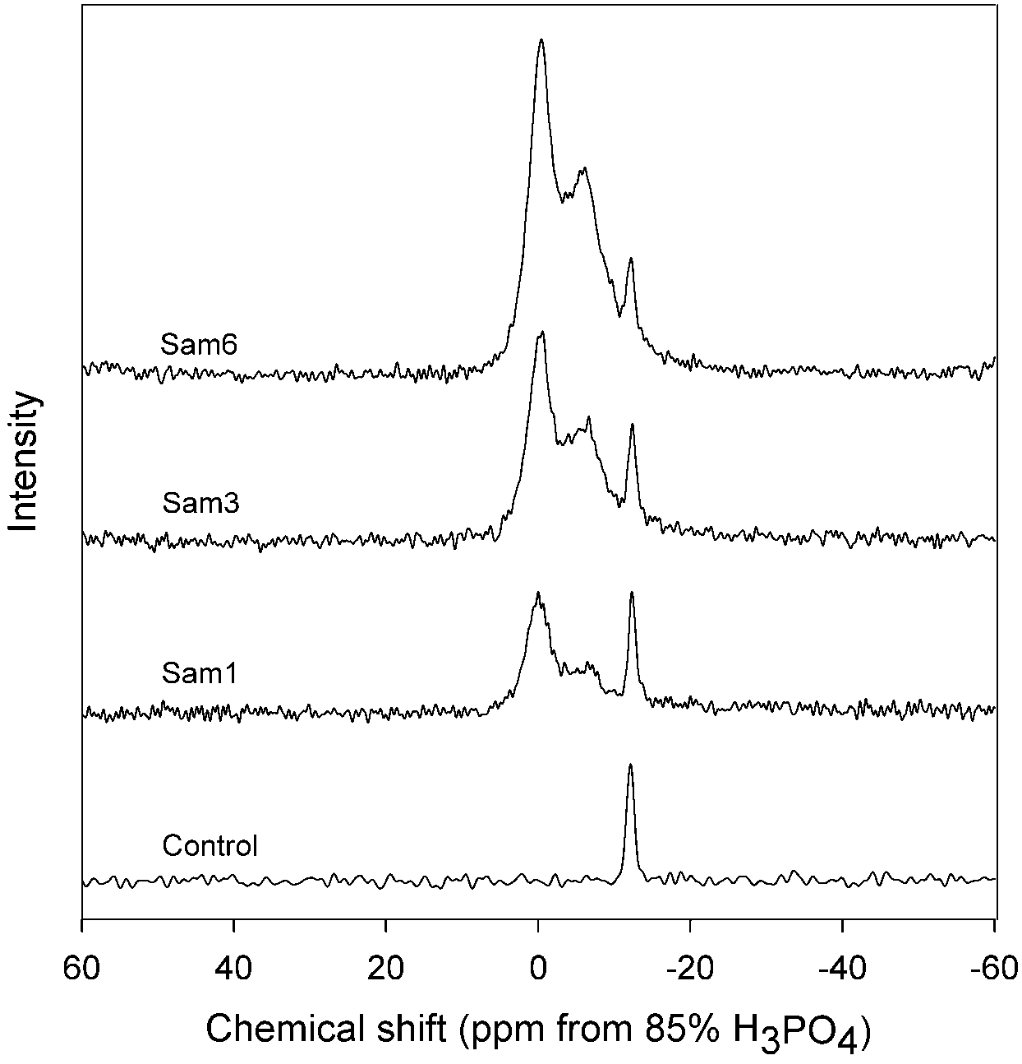

Figure 2.3 ^{31}P SP/MAS NMR spectra for P adsorbed boehmite samples with different surface phosphate loading on the isotherm at pH 5 (see Fig. 2). "Control" denotes spectrum for an empty rotor. Spectra scaled by constant integrated intensity for the peak at -12 ppm.

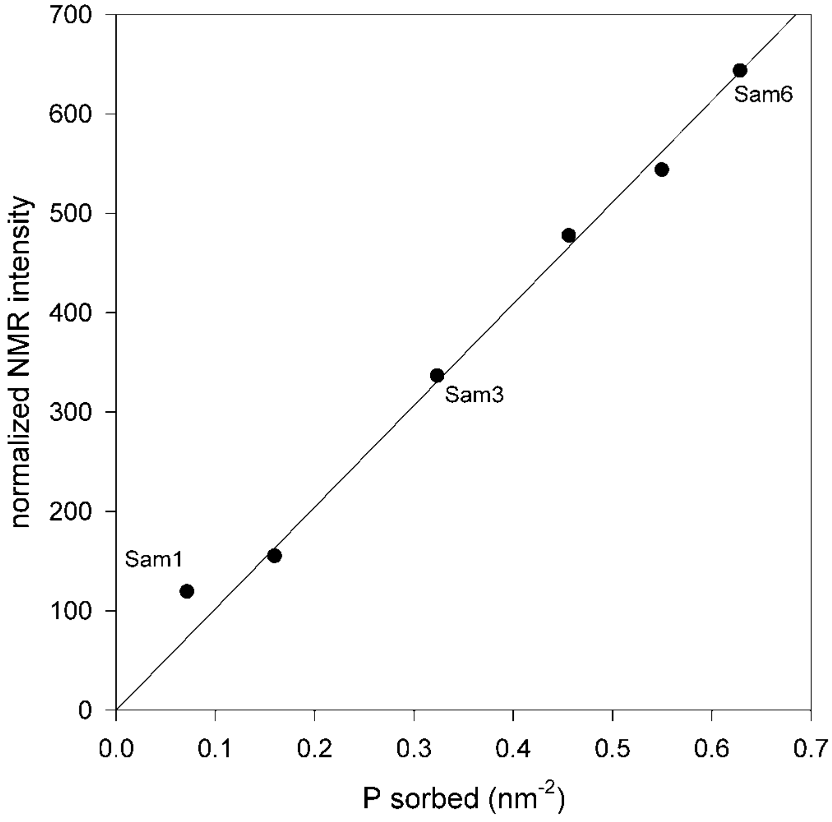

Figure 2.4 Relationship between macroscopic surface phosphate coverage and the sum of the integrated intensities of ^{31}P SP/MAS NMR peaks assigned to adsorbed phosphate ($\delta_{iso,P}$ = 0 and -6 ppm). Integrated NMR peak intensities were normalized between samples by dividing by the intensity of the peak at $\delta_{iso,P}$ = -12 ppm arising from the rotor.

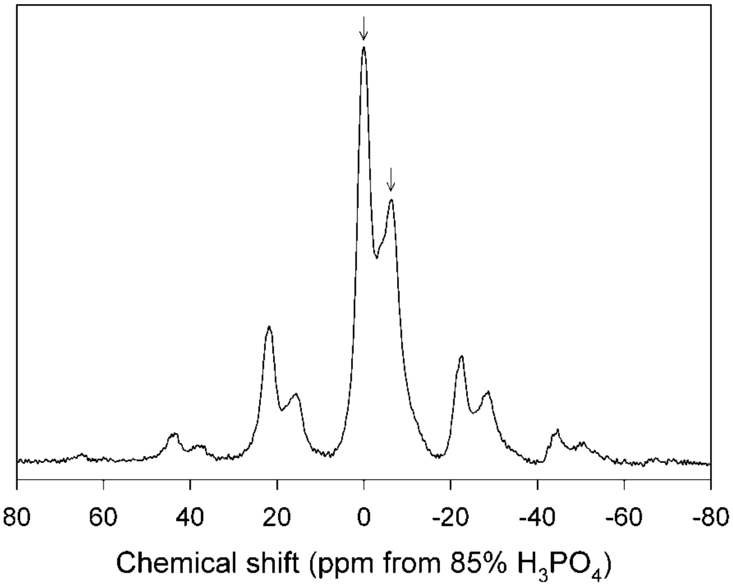

Figure 2.5 Full $^{31}P\{^1H\}$ CP/MAS spectrum (1 ms contact time) of phosphate adsorbed on boehmite (Sam6) at a spinning rate of 3.5 kHz from which the CSA tensor parameters were extracted via the Herzfeld-Berger method. Arrows denote isotropic peaks, all others are spinning sidebands.

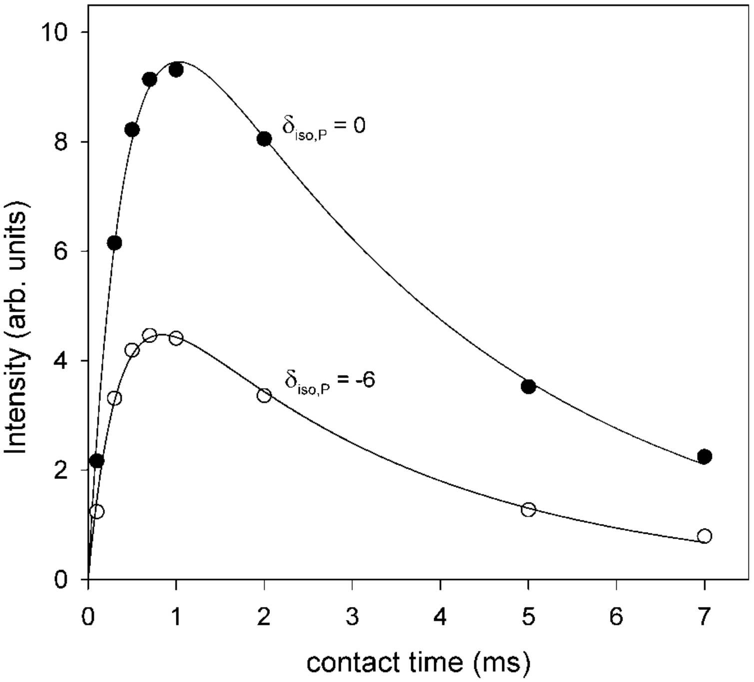

Figure 2.6 $^{31}P\{^{1}H\}$ CP/MAS kinetics for phosphate adsorbed on boehmite, sample Sam6.

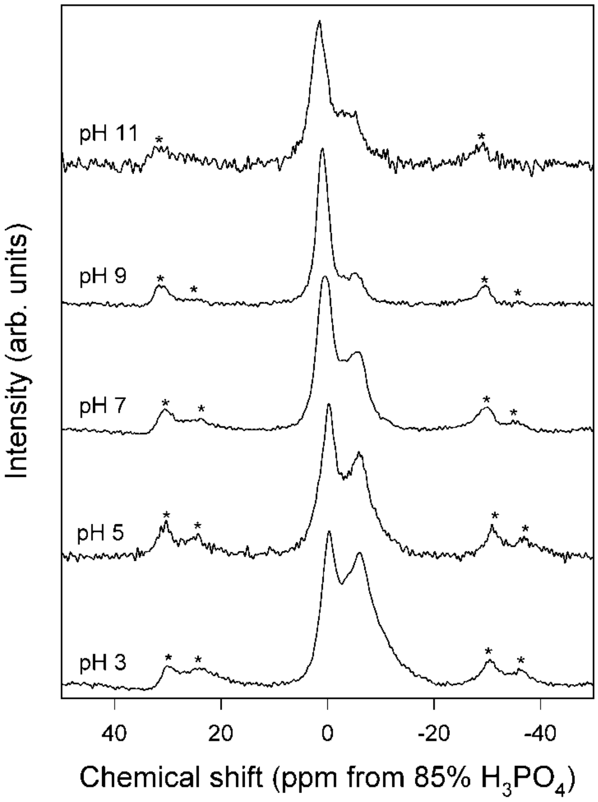

Figure 2.7 $^{31}P\{^1H\}$ CP/MAS NMR spectra for phosphate adsorbed on boehmite prepared at different pH values with 1mM initial phosphate concentration. Spectra acquired with 1 ms contact time, 2 s repetition delay at the spinning rate of 5 kHz, and scaled by constant maximum height. Asterisks denote spinning sidebands.

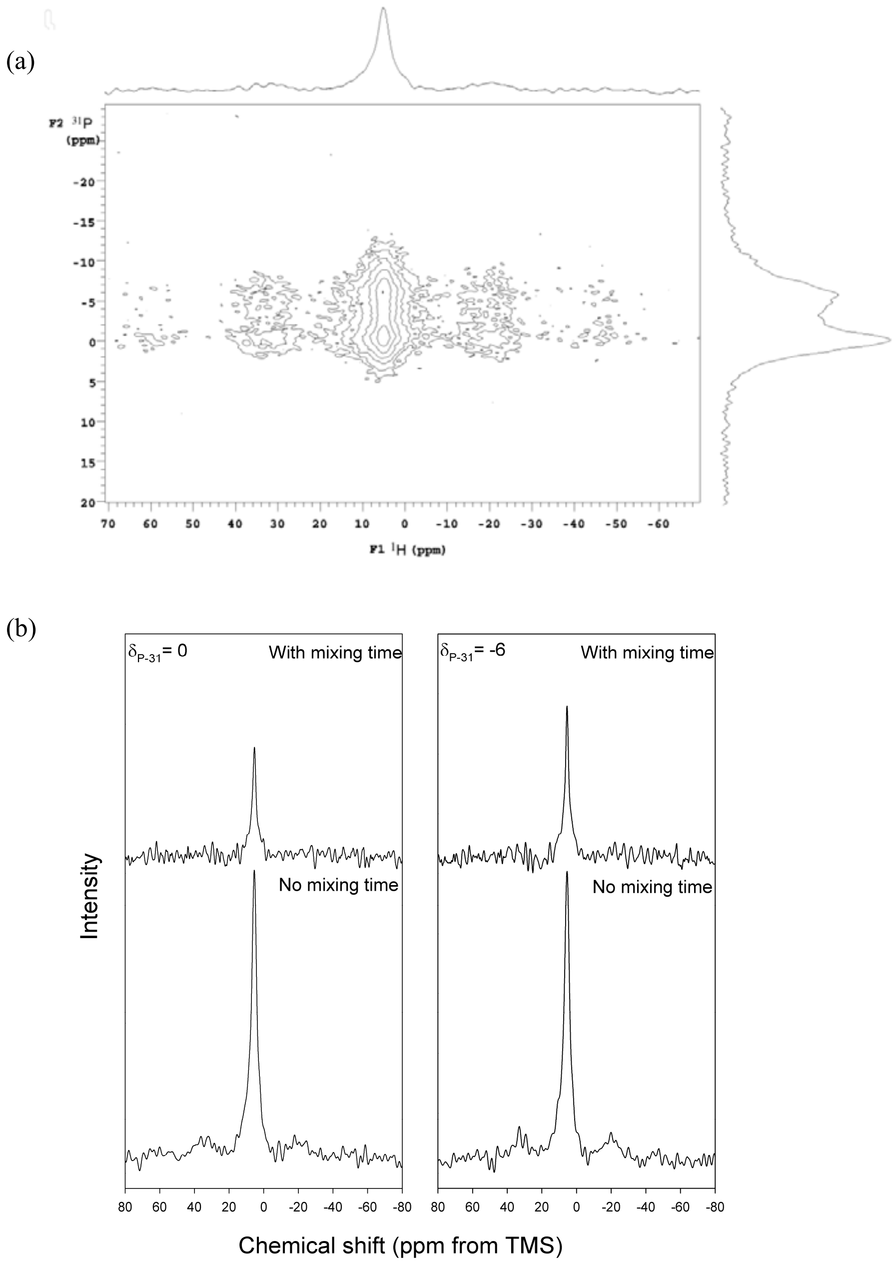

Figure 2.8 $^{31}P\{^{1}H\}$ HetCor spectra for phosphate/boehmite sorption sample at pH 5 at 1 mM initial concentration. **a)** Typical 2-d contour plot (1 ms contact time); top is slice at $\delta_{iso,P} = 0$ ppm, right is a summed projection. **b)** ^{1}H slices (*F*1) at the indicated ^{31}P positions, acquired with a 1 ms contact time with (top) and without (bottom) a 200 ms mixing time for ^{1}H-^{1}H spin diffusion. Narrow ^{1}H peak near 5 ppm arises from mobile water and dominates the spectra at long equilibration times indicating abundance at the surface.

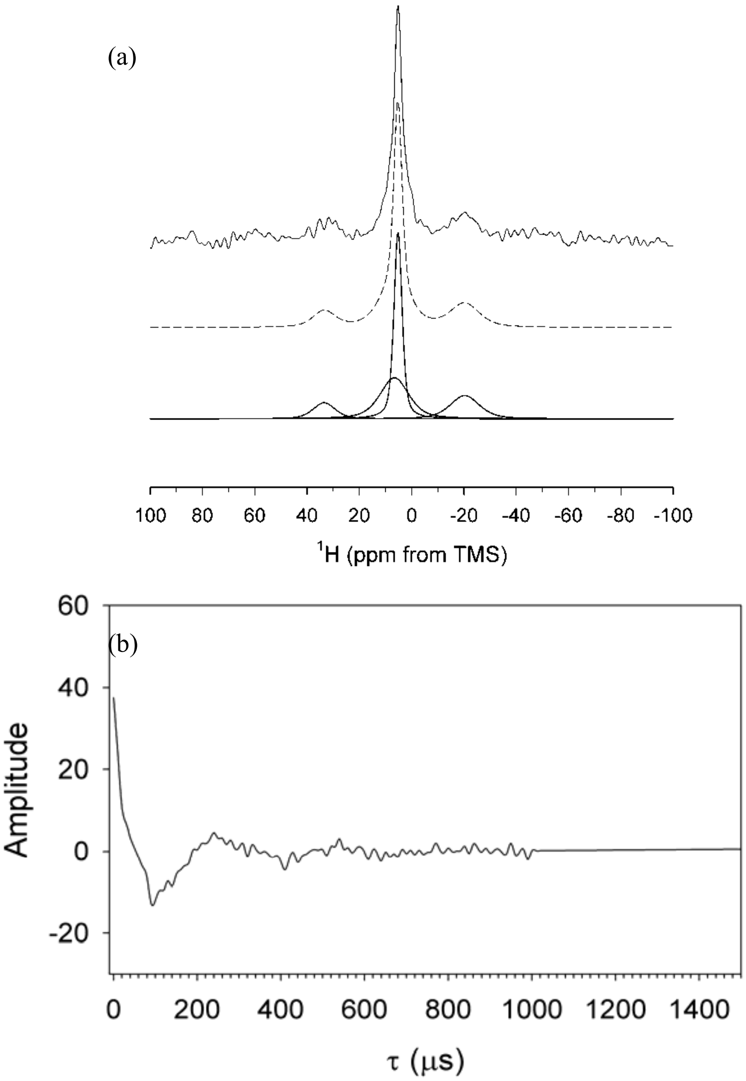

Figure 2.9 a) Simulation of ^{1}H projection in Figure 2.8a. b) Time-domain ^{1}H free induction decay (FID) in *t1*, showing a rapid initial decay that corresponds to a broad signal that is not apparent in the frequency spectra (Figure 2.9a). Data were obtained as the *t*1 slice at the ^{31}P peak at -6 ppm, after 1-d Fourier transformation of $t2 \rightarrow F2$

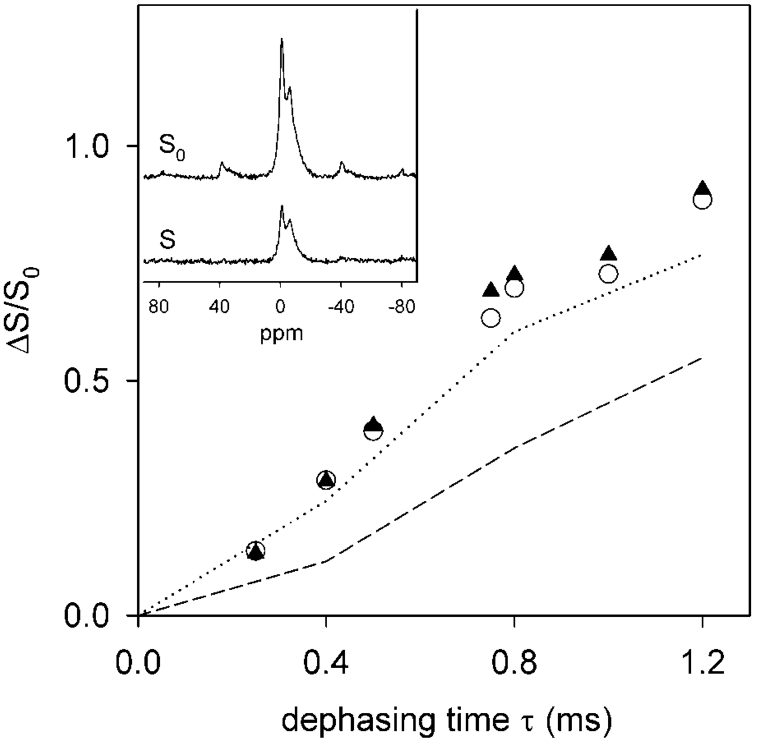

Figure 2.10 $^{31}P\{^1H\}/^{27}Al$ CP-REAPDOR NMR dephasing curves for ^{31}P peaks at $\delta_{iso,P} = 0$ ppm (▲) and at -6 ppm (○). The SIMPSON simulations were obtained for both bidentate (dotted line) and monodentate models (dashed line) suggested in ref. [38]. Inset shows typical control (S_0) and ^{27}Al-dephased (S) spectra acquired with 10 kHz spinning rate, 2 s repetition delay, 1 ms CP contact time, 6 rotor cycles and 11588 scans.

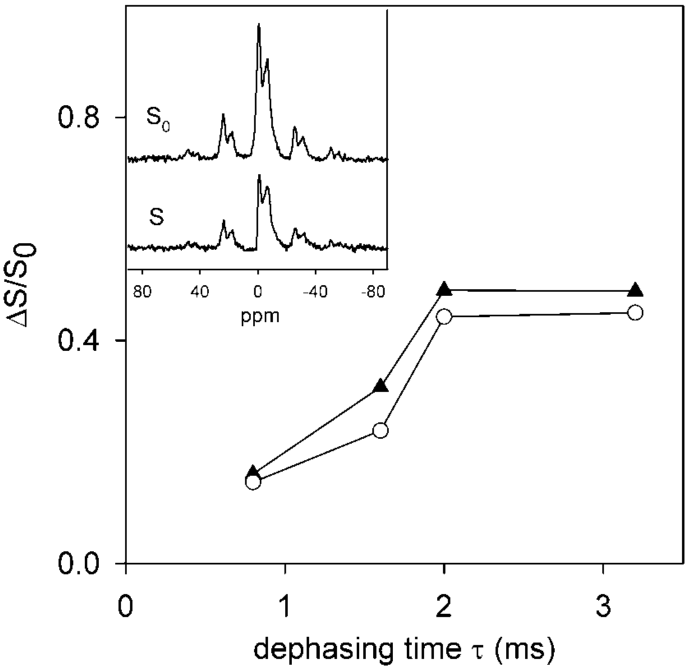

Figure 2.11 $^{31}P\{^1H\}/^{27}Al$ CP-TRAPDOR NMR data for ^{31}P peaks at 0 ppm (▲) and at -6 ppm (○) of Sam6. The inset shows the control (S_0) and TRAPDOR (S) NMR spectra acquired with 5 kHz spinning rate, 2 s repetition delay, 1 ms CP contact time, 10 rotor cycles and14764 scans.

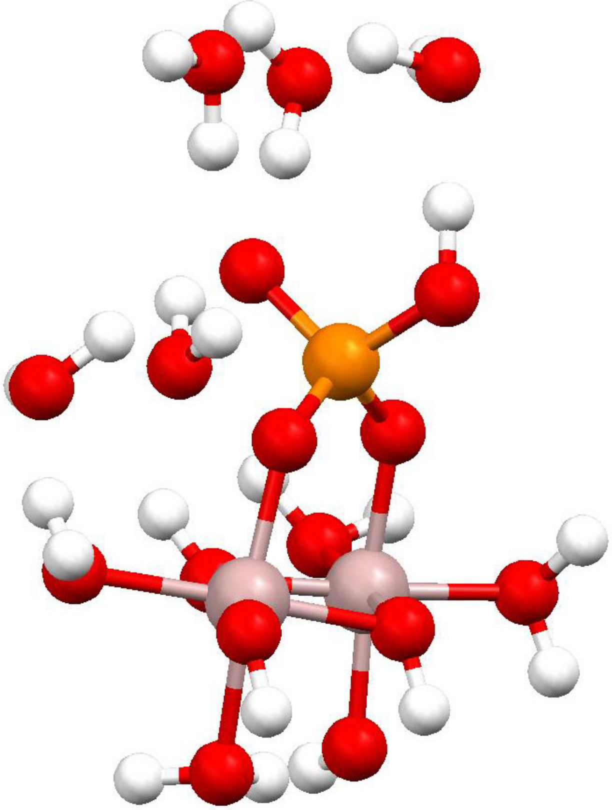

Figure 2.12 Representative cluster model (Bi-1H-8) used to calculate ^{31}P CSA tensor values (Table 2). Atoms are O(red), Al(pink), P (gold), H(white). Three solvent water molecules have been omitted for clarity.

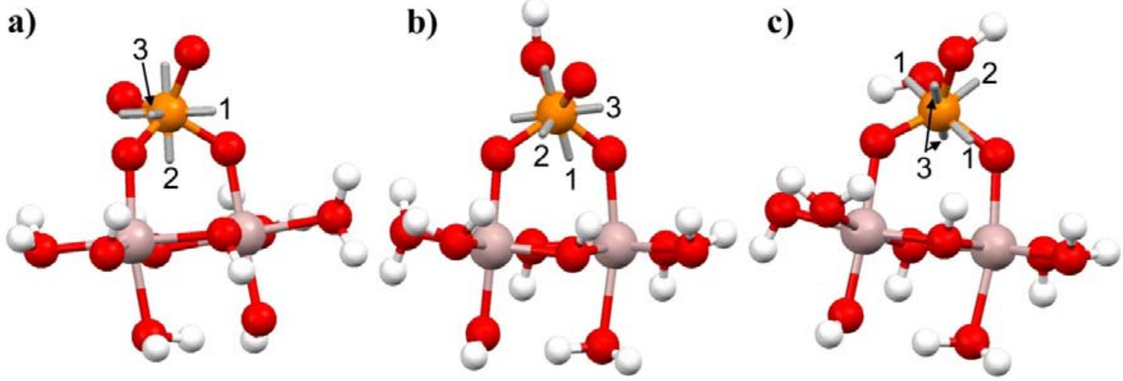

Figure 2.13 CSA principal axis orientations (gray lines) calculated for the cluster models Bi-*n*H-8 for $n = 0$ **(a)**, $n = 1$ **(b)**, and $n = 2$ **(c)**. Numerical axis labels correspond to the value of x for the principal axis with chemical shift δ_{xx}. Atoms are O (red), Al (pink), P (gold), and H (white). All solvent waters have been omitted for clarity.

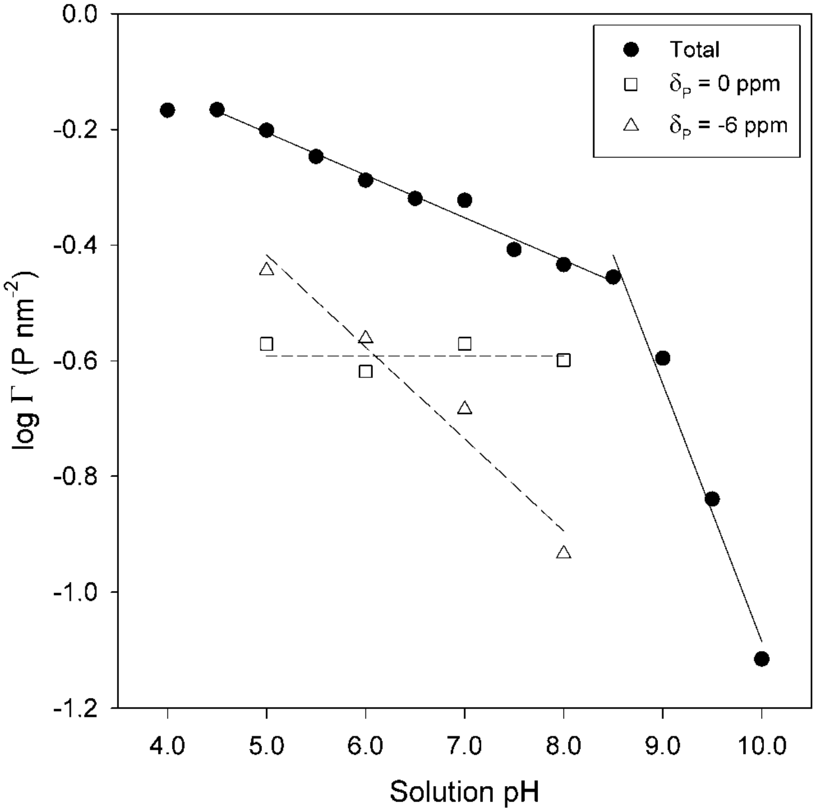

Figure 2.14 Site-specific adsorption of phosphate on boehmite at different pH values, 1 mM initial phosphate concentration and 10 mM NaCl electrolyte. Solid circles represent total phosphate uptake measured macroscopically, and open symbols the distribution of total adsorbed phosphate according the relative intensity of the corresponding NMR peaks.

Chapter 3

^{31}P solid state NMR investigation of phosphate sorption on aluminum (hydr)oxides

Abstract

In this work, ^{31}P solid-state NMR spectroscopy was employed to examine the phosphate adsorbed samples prepared at different concentration, pH, moisture and ionic strength, in order to systematically assess the impact of environmental factors on phosphate environments. The results revealed that the phosphate environment tended on boehmite (γ-AlOOH) surface tended to remain unchanged with respect to different environment, as evidenced by the presence of the similar two peaks at chemical shift of $\delta_P = 0$ and -6 ppm in all the spectra. The major differences among these samples were the relative population of the two peaks.

Careful examination of the a dry sample prepared at pH 9 by ^{31}P{^{27}Al} rotational echo adiabatic passage double resonance (REAPDOR) revealed a bidentate phosphate/Al coordination. This is almost identical to the phosphate bonding structure at pH 5, which indicates bridging bidentate surface complexes predominate in a wide pH range. In the presence of surface moisture, an additional peak at $\delta_P =$ -3 ppm but with very small amount could be observed in the REAPDOR spectra for a wet paste sample prepared at pH 5. This peak was further assigned to mobile monodentate mononuclear inner-sphere complexes by analysis of its ^{31}P{^{27}Al} REAPDOR curve. In addition, phosphate adsorbed at different Al (hydr)oxides yield significantly distinct NMR spectra, which indirectly implies the impact of the mineral surface on phosphate adsorption.

Key words: NMR; phosphate; adsorption; Al hydroxide; boehmite

3.1. Introduction

Phosphate interaction with minerals is important to the global phosphorus cycle and phosphate mineralization. Extensive studies have reported that phosphate ions are strongly sorbed by metal (hydr)oxides and the sorption loading depends on phosphate concentration, pH, ionic strength and the presence of competing ions (i.e. CO_3^{2-},SO_4^{2-} etc.) [1-10]. These studies have provided large amount of information about the macroscopic behavior of phosphate interaction with minerals, however, the reaction mechanism at mineral/water interface is poorly understood at the molecular level. One particular question is what the molecular structure of phosphate adsorbed on mineral surface is. And does this type of interfacial species show special dynamical property compared to free anions in bulk solution or/and phosphate-bearing minerals? Furthermore, what is the underlying relation between mineral crystal structure and phosphate adsorption complexes? Satisfied answers of these questions could provide deep insight into aqueous geochemical reactions such as natural-occurring water-rock interaction and mineral dissolution.

Determining the molecular structure of phosphate adsorbed on mineral surface relies on spectroscopic techniques. Information provided by infrared (IR), X-ray absorption spectroscopy (XAS) and nuclear magnetic resonance (NMR) revealed that the phosphate sorption mechanism involves both surface complexation and surface precipitation. In the surface complexation process, phosphate replaces the surface hydroxyl groups (e.g. ≡MeOH) and form bidentate surface complexes $[(\equiv MeO)_2\text{-}PO_2]$ or monodentate surface complexes $[(\equiv MeO)\text{-}PO_3]$. Surface precipitation refers to the formation of a new phase with multilayer structure of phosphate and metal ions or solid solution [1]. It is presumed that surface precipitates are formed when surface adsorbed phosphate continues reacting with dissolved cation released from mineral dissolution and/or phosphate/cation ion pairs.

Extensive studies using structurally well-defined iron (hydr)oxides [1-3, 5] as adsorbent indicated the bridging bidentate surface complexes were the dominant speices for phosphate uptake by goethite (α-FeOOH) at acid condition and mononuclear monodentate surface complexes predominated at alkaline condition [1-2,4]. Considering the chemical and structural similarities of Fe(III) and Al(III) oxyhydroxides, it is very interesting to know whether the results obtained from the studies of Fe oxyhydroxides can be applied to Al oxyhydroxides. Besides, compared to the studies using iron oxyhydroxide, fewer studies provided direct spectroscopic evidence for bridging bidentate or monodentate monouclear surface complexes for phosphate adsorbed on Al oxyhydroxides.

Previous studies suggest that ^{31}P NMR can be used to detect the local environment of phosphorus at the aluminum (hydr)oxide/water interface, and provide molecular-level information for interpreting phosphate sorption mechanism. Bleam et al. (1991) [6] combined the constant capacitance surface complexation model (CCM) with ^{31}P solid state NMR to investigated phosphate adsorption on boehmite (γ-AlOOH). They reported that the phosphate is adsorbed as protonated inner-sphere complexes from pH 3 to pH 9. Lookman et al. (1994) [7] studied phosphate uptake by synthetic amorphous $Al(OH)_3$ by ^{31}P and ^{27}Al magic angle spinning NMR, and concluded that phosphate is bound to surface octahedral aluminum as inner sphere complexes by comparing two synthetic aluminum phosphates that contain octahedral and tetrahedral Al respectively. They further applied NMR spectroscopy to study the phosphate speciation in fertilized soils using NMR spectroscopy [8, 9], which allows distinguishing between calcium phosphates (Ca-P) and aluminum phosphates (Al-P). Combining batch uptake experiments and NMR spectroscopy, Johnson et al (2002) [10] further investigated organic phosphate adsorption on γ-Al_2O_3. They suggest that phenyl phosphate forms both inner-sphere and outer-sphere complexes on the surface of γ-Al_2O_3. Recently, similar studies have been reported on activated carbon [11], boehmite and γ-Al_2O_3 [12] and gibbsite and kaolinate [13]. However, although these studies suggest that outer-sphere complexes, inner-sphere complexes and surface precipitates could be distinguished by NMR spectroscopy, more detailed information on the structural configurations such as monodentate and bidentate P/Al coordination have not been determined. With the aid of quantum chemical calculation, Fry et al (2006) [14] could distinguish between bidentate and monodentate phosphate/Al coordination by NMR spectroscopy. By comparing the chemical shift anisotropy (CSA) observed with those calculated by density function theory (DFT) based on theoretical models for bidentate and monodentate complexes, these authors suggest the structure of mononucleotide 2'-deoxyadenosine 5'-monophosphate (dAMP) adsorbed on mesophorous alumina is monodentate. More recently, in Chapter 1 [15], I used rotational echo adiabatic passage double resonance (REAPDOR) NMR technique to estimate the ^{31}P-^{27}Al dipolar coupling, and identified the P-O-Al local structure of phosphate adsorbed on boehmite at pH 5 as bidentate binuclear surface complexes.

On the basis of chapter 1, in this chapter I aim to comprehensively investigate the phosphate binding environment on boehmite at different experimental conditions and on several other Al (hydr)oxides by solid state NMR spectroscopy. In particular, several specific objectives are intended: 1) to compare the phosphate coordination environment on boehmite surfaces at different pH; 2) to test the impacts of ionic strength and higher P concentration on the adsorption mechanism; 3) to examine the effect of moisture on the observed surface complexes; 4) to investigate how different mineral surface structures influence phosphate adsorption.

3.2. Materials and methods

3.2.1. Materials

Boehmite was acquired from CONDEA Chemie GmbH and contained no impurity phases detectable by Scintag powder XRD analysis. The solid has a specific surface area (SSA) of 136 m^2g^{-1} as measured by the BET method, and point of zero charge (pH_{pzc}) of 9.1 [15]. IR spectrum of boehmite was obtained with a Nicolet 6700 FTIR with a deuterated triglycine sulfate (DTGS) detector. ^{27}Al MAS NMR spectrum was collected by a 400 MHz Varian Inova spectrometer (9.4 T) to check the possible impurity of γ-alumina.

3.2.2. Phosphate sorption

Phosphate adsorption experiments were conducted using a pH-stat method. A 0.25 g aliquot of dry boehmite powder was added to 50 ml of solution at the desired pH with a 0.01M NaCl background electrolyte. One titrator (Metrohm STAT 718) was used to automatically maintain constant pH by adding increments of 0.1M HCl. A second titrator was used to add a small amount of 50 mM phosphate solution into the reaction vessel to reach the desired total phosphate concentration. After reaction, the samples were centrifuged to separate the solid and solution. The supernatant solutions were filtered by a 0.2μm-filter and then analyzed for phosphorus by the Direct Coupled Plasma-Atomic Emission Spectroscopy (DCP-AES). The solid samples were quickly rinsed with a small volume of deionized water and then air-dried for NMR measurement, except for one sample which was maintained as a wet paste for NMR measurement.

The sorption pH edge was measured with the initial phosphate concentration of 1 mM at pH values ranging from 4 to 10, for 15 minutes. A few samples at pH 5 with the initial concentration ranging from 1 mM to 10 mM and ionic strength from 0.001 M to 0.5 M with 15 minute reaction times were prepared. Several samples using gibbsite, bayerite and corundum as the adsorbent were prepared with initial phosphate concentration of 1 mM, pH 5 and 15 minutes reaction, to compare different mineral surfaces.

3.2.3. NMR data collection

Solid-state ^{31}P single-pulse (SP) and ^{31}P{^{1}H} cross-polarization (CP) MAS NMR spectra were collected on a 400 MHz Varian Inova spectrometer (9.4 T), at operating frequencies of 161.8 MHz and 399.8 MHz for ^{31}P and ^{1}H, respectively. Spectra were collected using a Varian/Chemagnetics T3-type probe with samples contained in 3.2 mm (o.d.) thin wall ZrO_2 rotors. The ^{31}P chemical shifts ($\delta_{iso,P}$) are reported relative to external 85% H_3PO_4 solution, using hydroxylapatite as a secondary reference set to $\delta_{iso,P}$ = 2.65 ppm.

The ^{31}P SP/MAS spectra were obtained with an excitation 90° pulse of 6 μs, using a 120 s relaxation delay, based on spectra obtained with varying relaxation delay that indicate essentially complete relaxation by 120 s for quantitatively accurate intensities. Spectra taken for some samples at a longer delay showed no further increase in absolute intensity. With single-pulse excitation, the standard ZrO_2-based rotor sleeves give ^{31}P signals in the spectral region for orthophosphate groups with a chemical shift at -12 ppm.

The ^{31}P{^{1}H} CP/MAS spectra were obtained at spinning rates of from 3 to 5 kHz and contact times that varied from 0.1 to 7 ms, using a probe assembly configured for 7.5 mm (o.d.) rotors. CP kinetics curves were measured at a spinning rate of 3 kHz with continuous wave (CW) irradiation at the n = -1 sideband match condition. For other CP/MAS spectra the transverse ^{1}H field ($\gamma B_{1,H}$) was ramped over approximately

5 kHz, centered near the first sideband match with a 42 kHz ^{31}P field. Proton decoupling (CW) was employed during acquisition of all $^{31}P\{^1H\}$ CP/MAS spectra.

$^{31}P\{^1H\}/^{27}Al$ REAPDOR [16, 17] NMR spectra were obtained on a 500 MHz Varian Infinity plus spectrometer (11.7 T) using a 3-channel Varian/Chemagnetics 'T3' probe assembly configured for 4 mm (o.d.) rotors. These pulse sequences employed excitation of the ^{31}P signal through $^{31}P\{^1H\}$ cross-polarization with a linear ramp of the ^1H B_1 field during the contact time to flatten the match condition. The length of 90°pulse for ^1H was 6 μs, the optimized contact time 1 ms, and the relaxation delay 1 s. For REAPDOR NMR experiments, the ^{31}P 180° pulse-length was 12 μs and the duration and strength of ^{27}Al pulse in the middle of the dephasing pulse train are 1/5 of the rotor period and 75 kHz, respectively.

3.3. Results and discussion

3.3.1. Characterization of boehmite

Figure 3.1a shows a typical powder x-ray diffraction pattern for the boehmite used in this work. The XRD pattern contains four major sharp peaks at 2θ values of 14.4°, 28.2°, 38.3°, and 49.1°, which can be indexed to the (200), (210), (301) and (501) reflections of crystalline boehmite. The full width at half maximum (FWHM) for the four major peaks is similar (about 0.8°), which is slightly broader than that for well-crystalline boehmite. An average crystallite size can be estimated to be ~ 11 nm from the Scherrer equation using $k = 1$ and $\lambda = 0.154$ nm (Cu K_α), where the Scherrer is described as $D_{Scherrer} = k \cdot \lambda \cdot 57.3 / [FWHM \cdot \cos(\theta)]$ [18]. The estimated average crystal size is consistent with the TEM images in Figure 3.2. SEM and TEM were employed to observe the particle morphology of boehmite. With a 100000×magnification, the SEM image (Figure 3.2a) indicates that the particles are homogenously distributed and that the particle size is under 100 nm. The TEM image (Figure 3.2b) shows the morphology of boehmite particle as plates approximately 20-40 nm in diameter.

FTIR was performed to check for possible impurity of pseudo-boehmite, a common byproduct when synthesizing aluminum hydroxides. No strong IR signal was observed in the range of 1500-1600 cm^{-1}, a region in which pseudo-boehmite may have IR absorption due to bound water (IR and XRD data for pseudo-boehmite not shown). The typical ^{27}Al NMR spectrum of boehmite (Figure 3.1c) shows only one peak at δ_{Al} = 9 ppm representative of octahedral aluminum plus its spinning sidebands. Careful inspection of the chemical shift range of 20 to 80 ppm indicates no detectable tetrahedral or 5-coordination aluminum, suggesting absence of γ-Al_2O_3 impurity.

3.3.2. NMR spectra for phosphate adsorption at different concentration, ionic strength and pH

Figure 3.3 shows ^{31}P{^{1}H} CP/MAS and ^{31}P SP/MAS spectra of phosphate adsorbed on boehmite at different initial phosphate concentrations. Figure 3.3a is reproduced here from Figure 2.3 in chapter 2 for comparison. In Figure 3.3b, the SP/MAS spectra of three samples prepared at pH 5 with initial phosphate concentration of 2, 5 and 10 mM yield the three peaks, at δ_P = 0, -6 and -12 ppm, which are in the same position as those samples prepared at lower concentration (Figure 3.3a). In chapter 2, the two peaks, at δ_P = 0, and -6 ppm, were assigned to deprontated bridging bidentate and singly-protonated bridging bidentate respectively, and the peak at δ_P = -12 ppm to background signal that arises from the rotor. The similarity of chemical shifts observed for the six samples prepared over phosphate concentrations ranging from 0.1 to 10 mM suggest phosphate adsorption environments are independent of initial phosphate concentration. However, the relative population of the two peak differs among those samples.

Figure 3.3c shows ^{31}P{^{1}H} CP/MAS spectra for the same samples as in Figure 3.2b, in which only the two peaks for adsorbed phosphate at δ_P = 0 and -6 ppm are observed, lacking the background peak at δ_P = -12 ppm. These ^{31}P{^{1}H} CP/MAS spectra were collected for ca. 2 hours, but have much better signal-to-noise ratio than their corresponding SP/MAS spectra that were collected for roughly 24 hours each. The mechanism for signal enhancement lies in the polarization transfer from abundant ^{1}H nuclei to ^{31}P nuclei through ^{1}H-^{31}P dipolar coupling. This process allows rapid repetition delay rate in cross-polarization owing to fast ^{1}H relaxation compared to that for ^{31}P nuclei, whereas single pulse experiment require a pulse delay that allow the full recovery of ^{31}P magnetization.

Figure 3.4 shows the $^{31}P\{^{1}H\}$ CP/MAS spectra for four samples prepared at pH 5 with 1 mM P concentration and varying ionic strength from 0.001 M to 0.5 M. There are no significant differences discerned among these spectra, suggesting that the chemical environment for the phosphate adsorbed on boehmite is independent on ionic strength. Also, according the chemical shift values, it is concluded the surface adsorbed phosphate at different ionic strength are inner-sphere complexes.

Figure 3.5a presents a series of CP/MAS spectra collected for samples prepared with 1mM initial phosphate concentration from pH 4-10 (Figure 3.5b). All the spectra show only two resolved peaks at chemical shifts around 0 and -6 ppm. The chemical shifts of the two peaks changed slightly to the lower field as pH increases (Figure 3.6). The left peak shifts from $\delta_P = -0.15$ ppm at pH 4 to $\delta_P = 1.1$ ppm at pH 10 whereas the right peak shifts from -6.24 ppm to -5.12 ppm. Similar pH-dependence of chemical shift has been reported in previous studies [6, 12, 15], and was interpreted as arising from the decrease of the boehmite surface charge. This interpretation is supported by the pH-dependent chemical shift for aqueous $H_xPO_4^{3-x}$ species in solution [18]. In Figure 3.6, the ^{31}P chemical shift for aqueous phosphate remains constant at $\delta_P = 4$ ppm from pH 3 to pH 6 due to predominance of the $H_2PO_4^-$ species; it drifts gradually from $\delta_P = 4$ ppm to 6 ppm from pH 6 to pH 9, because of the transformation of $H_2PO_4^-$ to HPO_4^{2-} over this range ($pK_{a2} = 7.2$), and remains constant again at 6 ppm since HPO_4^{2-} species dominate in the solution from pH 9 to pH 11. It is worth mentioning that in solution only a single NMR peak would be observed at any given pH due to the rapid chemical exchange among the aqueous phosphate species. The chemical shift changes for aqueous $H_xPO_4^{3-x}$ is unlike that of surface adsorbed phosphate from pH 3 to pH 11, which changes very steadily at less than 0.2 ppm per pH unit. This is reasonably ascribed to the gradual decrease of the boehmite surface charge over increase of pH. However, since the full widths at half maximum (FWHM) of the two peaks are about 3 and 8 ppm, an average change of 0.2 ppm per pH unit is almost negligible. The small change does not reflect a change of phosphate/Al coordination from bidentate to monodentate surface complexes, which would cause a strong deshielding due to fewer P-O-Al bonds. The only change is the relative population of the two peaks over the wide pH range, suggesting a different protonation state between the two phosphate environments. The left peak is predominant from pH 8 to pH 10, and indicates a non-protontated environment; in contrast, the significant pH-dependence of the right peaks suggests it is a protonated phosphate.

3.3.3. Phosphate bonding structure at pH 9

In order to compare the bonding structure of phosphate adsorbed on the boehmite surface between acid and alkaline conditions, $^{31}P\{^{27}Al\}$ REAPDOR NMR experiments were performed one a sample prepared at pH 9. Experimentally, sets of two ^{31}P-observed NMR spectra are acquired, one (S) obtained with a heteronuclear dipolar dephasing sequence, and a second control spectrum (S_0) acquired under identical conditions but without irradiation at the ^{27}Al frequency. The difference in peak intensity between the dephased spectrum and the control ($\Delta S=S_0-S$) depends on the ^{31}P-^{27}Al heteronuclear dipolar coupling and the length of the dephasing sequence (τ). The inset of Figure 3.7 shows a typical set of the ^{31}P-^{27}Al REAPDOR NMR spectra acquired for phosphate adsorbed on boehmite at pH 9 with 0.75 ms dephasing time, which is the product of number of rotor cycles and rotor period. The REAPDOR fraction $\Delta S/S_0$ was measured as a function of dephasing time, yielding a REAPDOR dephasing curve (Figure 3.7) to characterize the magnitude of ^{31}P-^{27}Al heteronuclear dipolar coupling. The REAPDOR curves for the two distinct ^{31}P NMR peaks (δ_P = 0.9 ppm and δ_P = -5.2 ppm) are almost identical, indicating similar coordination to Al. In addition, the READDOR curves at pH 9 are the same within uncertainty as those for the two peaks observed for an earlier sample prepared at pH 5, suggesting the phosphate/Al coordination at pH 9 is also bidentate as was determined at pH 5 in Chapter 2.

Quantitatively, SIMPSON simulations [19] were performed to calculate two simulated REAPDOR curves for models of monodentate and bidentate phosphate bonding to edge-sharing Al octahedra with geometry suggested by Fry et al. (2006)

[14]. The bidentate model constrains two P-Al distances of 3.10 and 3.14 Å, whereas the monodentate inputs one short P-Al distance of 3.26 Å and two longer P-Al distances of 4.39 and 4.62 Å. We used ^{27}Al quadrupolar coupling constants of 3 MHz for the Al bonded to phosphate, which was estimated from the TRAPDOR frequency offset effect as described in Chapter 2. The simulated REAPDOR curve for the bidentate model shows a much larger slope than that for monodenate model, reflecting a stronger ^{31}P-^{27}Al dipolar coupling in the bidnetate model as expected from its shorter P-Al distances. The experimental REAPDOR curves for both peaks are very close to the simulated curve for bidentate model, but deviate significantly from that for monodentate model, consistent with assignment of both ^{31}P peaks at pH 9 to bidentate surface complexes. The small difference between the calculated and measured REAPDOR curves can be attributed to the presence of additional more distant Al on the surface, whereas the simulations only considered the two closest Al. Conceptually, more Al could be taken into account in the SIMPSON simulation, but the computational time is subject to geometric growth. Direct comparison of REAPDOR results from the samples prepared at pH 5 and pH 9 confirms that the P/Al coordination structure for phosphate adsorbed on boehmite surface remains unchanged over a wide pH range occurring in most natural water and soil solution.

Figure 3.8 shows the CP kinetic curves (intensity a function of contact time) for the two peaks observed for the sample prepared at pH 9. The CP kinetic curves were analyzed by fitting the ^{31}P{^{1}H} CP/MAS spectra obtained at different contact times (τ) to a consistent set of Gaussian curves, allowing only the intensities to vary. The intensities are well fitted by the classical bi-exponential relationship

$$I(\tau) = I_0\left[1 - \frac{T_{PH}}{T_{1\rho,H}}\right]^{-1}\left[1 - \exp\left(-\frac{T_{PH}}{\tau}\right)\right]\exp\left(-\frac{T_{1\rho,H}}{\tau}\right) \quad (1)$$

where T_{PH} is the characteristic time for $^{1}\mathrm{H}\rightarrow{}^{31}\mathrm{P}$ magnetization transfer and $T_{1\rho,\mathrm{H}}$ is the time constant for decay of the ^{1}H magnetization in the rotating frame [20]. Least square fits of the variable contact time data (Figure 3.8) give the T_{PH} values of 0.59 ms and 0.59 ms and $T_{1\rho,,\mathrm{H}}$ of 4.7 and 2.9 ms, respectively for the peaks at $\delta_{\mathrm{P}} = 0.9$ and -5.2 ppm. In the rigid limit, T_{PH} is related to the sum over the phosphorus-proton distances: $T_{PH}^{-1} \propto \sum_{1}^{i} \left[d\left(^{31}P{-}^{1}H_i \right) \right]^{-6}$, where $d\left(^{31}P{-}^{1}H_i \right)$ is the internuclear distance between the phosphate P and the i^{th} nearby proton [21]. However, motion of H and H-bearing species can modify the relationship and prevents strictly quantitative interpretation of the CP rate. Nonetheless, these T_{PH} values for the sample prepared at pH 9 is larger than those for the two peak at $\delta_{\text{P}} = 0$ and -6 ppm for the sample at pH 5 (0.42 and 0.34 ms respectively). The result indicates small ^{31}P-^{1}H dipolar couplings at pH 9, corresponding to fewer rigid H atoms near adsorbed phosphate either by increased motion of H or depronation of the surface hydroxyl group on boehmite.

We determined the ^{31}P CSA's for both peaks at pH 9 from the spinning sideband (SSB) intensities of a ^{31}P{^{1}H} CP/MAS spectrum collected at a spinning rate of 3.5 kHz (Figure 3.9), for comparison with that observed for the sample at pH 5 and discussed in Chapter 2. The NMR chemical shift is a tensor property, described by the chemical shift anisotropy (CSA) and representations of the principal tensor values: δ_{ii}; $1 \leq ii \leq 3$. As an average of the three principal values, the isotropic chemical shifts ($\delta_{\text{iso,P}}$) contains less structural information than CSA. In chapter 2, direct comparison of the experimentally measured ^{31}P CSA with those calculated based on P/Al bidentate clusters with different protonation state allows assignment of the peak at -6 ppm for the sample at pH 5 to singly-protonated bidentate surface complexes and the peak at 0 ppm to depronated bidentate surface complexes. Analysis of the integrated intensity and frequency of each isotropic peak and its respective SSB's for the sample at pH 9 by the Herzfeld-Berger method [22] via the program HBA [23], yield principal tensors of the CSA's , δ_{11}, δ_{22}, and $\delta_{33,}$ of 34.4, 6.1 and -40.4 ppm for the peak at $\delta_{\text{P}} = 0.9$ ppm. For the peak at the $\delta_{\text{P}} = 0.9$ ppm, its anisotropy ($\Delta\delta = 3(\delta_{zz} - \delta_{\text{iso}})/2$, where $z = 1$ if $\delta_{11} - \delta_{\text{iso}} > \delta_{33} - \delta_{\text{iso}}$, or $z = 3$ otherwise) in the Haeberlen representation this is -61 ppm, and the asymmetry parameter is 0.70. These values are similar to those for the peak at 0 ppm for the pH 5 sample, indicating a depronated environment. The CSA values for the peak at $\delta_{\text{P}} = -5.2$ ppm were not analyzed due to the presence of fewer spinning sidebands, which could lead to large error.

3.3.4. Effect of surface moisture

Figure 3.10 compares ^{31}P SP/MAS spectra of phosphate adsorbed on boehmite obtained as a wet paste and dried in air both prepared at pH 5 with the 1 mM initial phosphate concentration. The spectrum for the air-dried sample is almost identical to those shown in Figure 3.3a. For the paste, there are two resolved peaks at δ_P = 0.1 and -5.5 ppm (the peak at -12 ppm arises from the rotor), which are shifted with slightly to downfield relative to the air-dried sample. This small change in chemical shift is likely to be caused by hydration water. Figure 3.11 shows that the REAPDOR dephasing curves for the peaks at δ_P = 0.1 and -5.5 ppm for the wet paste sample are similar to those for the air-dried sample, which have been assigned to bidentate P/Al coordination as discussed in chapter 2. A third peak at δ_P = -3 ppm becomes apparent in the spin echo spectrum (S_0) of the REAPDOR data sets (Figure 3.11, inset) for this wet paste sample, suggesting a relative longer T2 than the other two peaks. The peak at δ_P = -3 ppm yields dephasing curve that indicates very weak P-Al dipolar interaction. Considering its significantly low REAPDOR fraction, this peak could be representative of either outer-sphere P surface complexes or motional monodentate mononuclear surface complexes. In a wet condition, the P-O-Al bonds would reasonably experience a stretching or bending, leading to a reduced P-Al dipolar interaction and reduced REAPDOR effect. The mobile nature is consistent with its long T2.

3.3.5 Phosphate reaction with different Al (hydr)oxides

Figure 3.12 compares ^{31}P{1H} CP/MAS spectra for phosphate adsorbed on different Al (hydr)oxides prepared at pH 5 and 1 mM initial phosphate concentration. For corundum, only a single broad and slightly asymmetric peak centered near δ_P = -3 ppm with a FWHM of 8 ppm (Figure 3.12a) is observed. For gibbsite (α-$Al(OH)_3$), there are three well resolved peaks at δ_P = -3, -8, and -13 ppm plus a shoulder at 0 ppm. Bayerite (γ-$Al(OH)_3$) yields three resolved peaks at -2.5, -8 and -13 ppm, similar to those of gibbsite but the peak at 0 ppm is not observed. It is not surprising that phosphate adsorbed on gibbsite and on bayerite yield similar peaks, given that gibbsite and bayerite have the same chemical composition and similar layered structures of sheets of Al octahedra. These NMR results definitely show that different mineral surfaces would generate different phosphate environment. However, more detailed studies are needed to assign those peaks and to understand the relationship between mineral structure and properties such as sorption and reactivity.

3.4. Conclusion

In this work, we have systematically examined the phosphate adsorption in terms of concentration, pH, moisture and ionic strength by ^{31}P solid-state NMR spectroscopy. The phosphate bonding structure on the boehmite surface is independent of surface phosphate loading, pH and ionic strength, but the ratio between two species may vary. This result indicates that surface complexation models must take into account multiple species even though uptake curves can be fit with single-site adsorption models. The spectrum for the wet paste sample is almost identical to the air-dried sample, except that an additional peak that exhibits significant mobility. ^{31}P{^{27}Al} rotational echo adiabatic passage double resonance (REAPDOR) experiments on a dry sample prepared at pH 9, confirms the formation of bridging bidentate phosphate surface complexes at this pH condition.

This work shows that ^{31}P{^{1}H} CP/MAS technique has great advantage in signal enhancement and proton structural determination, and that REAPDOR provide fine details of structural information for understanding the phosphate bonding structure at mineral/water interface. We also found that ^{31}P NMR spectra are sensitive to adsorbent, that adsorbed phosphate on corundum, boehmite, gibbsite and bayerite shows different features, implying that ^{31}P nuclei could be used as a molecular probe to mineral surface.

Reference

[1] Khare, N.; Hesterberg, D. L.; Martin, J. D., *Environmental Science and Technology* **2005,** 39, 2152-2160.

[2] Tejedor-Tejedor, M. I.; Anderson, M. A., *Langmuir* **1990,** 6, 602-611.

[3] Persson, P.; Nilsson, N.; Sjöberg, S., *Journal of Colloid and Interface Science* **1996,** 177, 263–275.

[4] Kwon, K. D.; Kubicki, J. D., *Langmuir* **2004,** 20, 9249-9254.

[5] Rahnemaie, R.; Hiemstra, T.; van Riemsdijk, W. H., *Langmuir* **2007,** 23, 3680-3689.

[6] Bleam, W. F.; Pfeffer, P. E.; Goldberg, S.; Taylor, R. W.; Dudley, R., *Langmuir* **1991,** *7*, 1702-1712.

[7] Lookman, R.; Grobet, P.; Merckx, R.; Vlassak, K., *Eur. J. Soil Sci.* **1994,** *45*, 37-44.

[8] Lookman, R., Geerts, H., Grobet, P., Merckx, R., and Vlassak, K., *European Journal of Soil Science* **1996,** 47, 125-130.

[9] Lookman, R.; Grobet, P.; Merckx, R.; Van Riemsdijk, W. H., *Geoderma* **1997,** *80*, 369-388.

[10] Johnson, B. B.; Ivanov, A. V.; Antzutkin, O. N.; Forsling, W., *Langmuir* **2002,** *18*, 1104-1111.

[11] Harris, R. K.; Thompsona, T. V.; Normanb P. R.; Pottageb C., *Carbon* **1999,** 37, 1425-1430.

[12] Kim, Y.; Kirkpatrick, R. J., *Eur. J. Soil Sci.* **2004,** *55*, 243-251.

[13] Van Emmerik, T. J.; Sandstrom, D. E.; Antzutkin, O. N.; Angove, M. J.; Johnson, B. B., *Langmuir* **2007,** *23*, 3205-3213.

[14] Fry, R. A.; Kwon, K. D.; Komarneni, S.; Kubicki, J. D.; Mueller, K. T., *Langmuir* **2006,** 22, 9281-9286.

[15] Li, W.; Feng, J.; Kwon, K. D.; Kubicki, J. D.; Phillips, B. L., *Langmuir* **2010,** 26, 4753-4761.

[16] Gullion, T., *Chem. Phys. Lett.* **1995,** 246, 325-330.

[17] Chopin, L.; Vega, S.; Gullion, T., *J. Am. Chem. Soc.* **1998,** 120, 4406-4409.

[18] Mortlock, R. F.; Bell, A. T.; Radke, C. J., *J. Phys. Chem.* **1993,** 97, 775-782.

[19] Bak, M.; Rasmussen, J. T.; Nielsen, N. C., *J. Magn. Reson.* **2000,** 147, 296-330.

[20] Kolodziejski, W.; Klinowski, J., *Chem. Rev.* **2002,** *102*, 613-628.

[21] Mehring, M., *Principles of High Resolution NMR in Solids*; 2nd ed.; Springer-Verlag: Berlin, 1983

[22] Herzfeld, J.; Berger, A. E., *J. Chem. Phys.* **1980,** *73*, 6021-6030.

[23] Eichele, K.; Wasylishen, R. E.; *WSOLIDS*, 2.0.18; Dalhousie University: Halifax, 2000.

Tables and figures

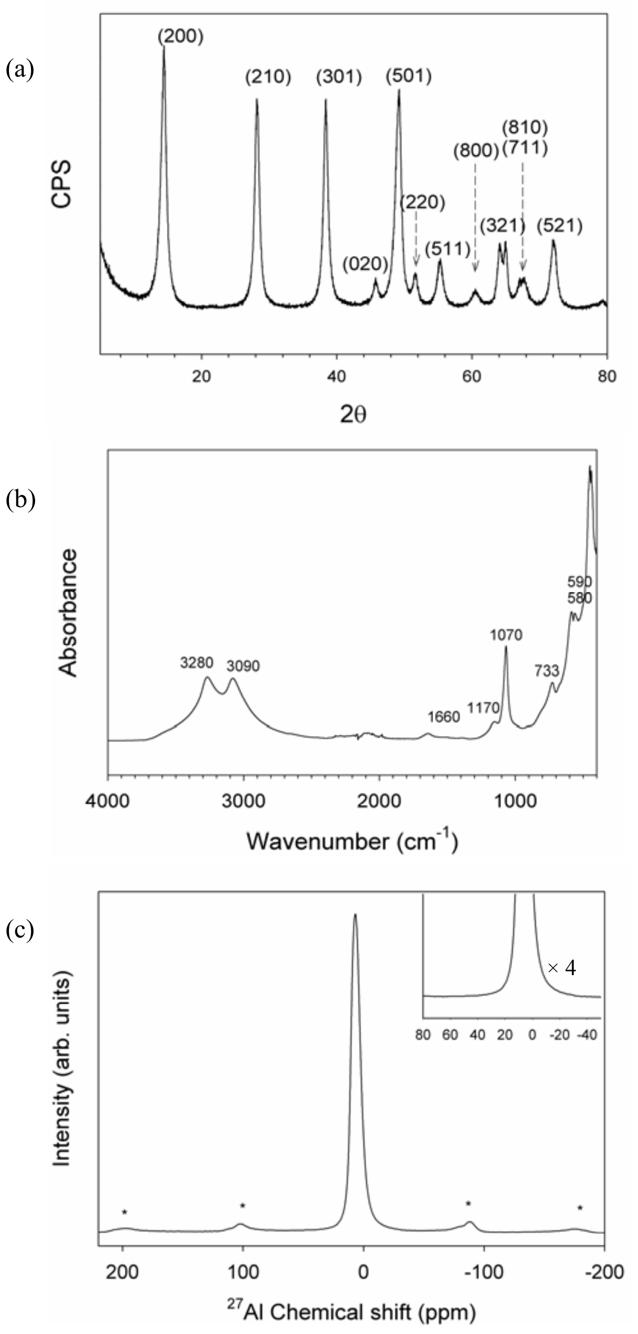

Figure 3.1 Characterization of boehmite particles by XRD (a), IR spectroscopy (b) and ^{27}Al NMR spectroscopy (c). The NMR spectrum was acquired in a single pulse/ magic angle spinning mode, with 1 μs excitation pulse (90° pulse for solution standard is 6 μs), spinning rate of 16 kHz, pulse delay of 1 s and ca. 300 scans.

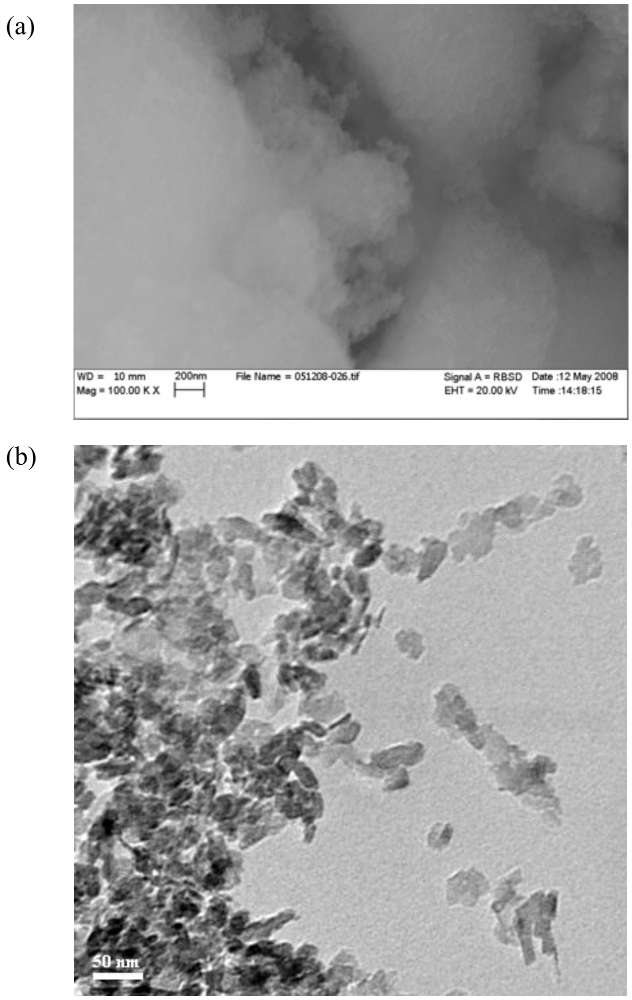

Figure 3.2 Images of boehmite particle obtained by scanning electron microscopy (SEM) (a) and transmission electron microscopy (TEM) (b).

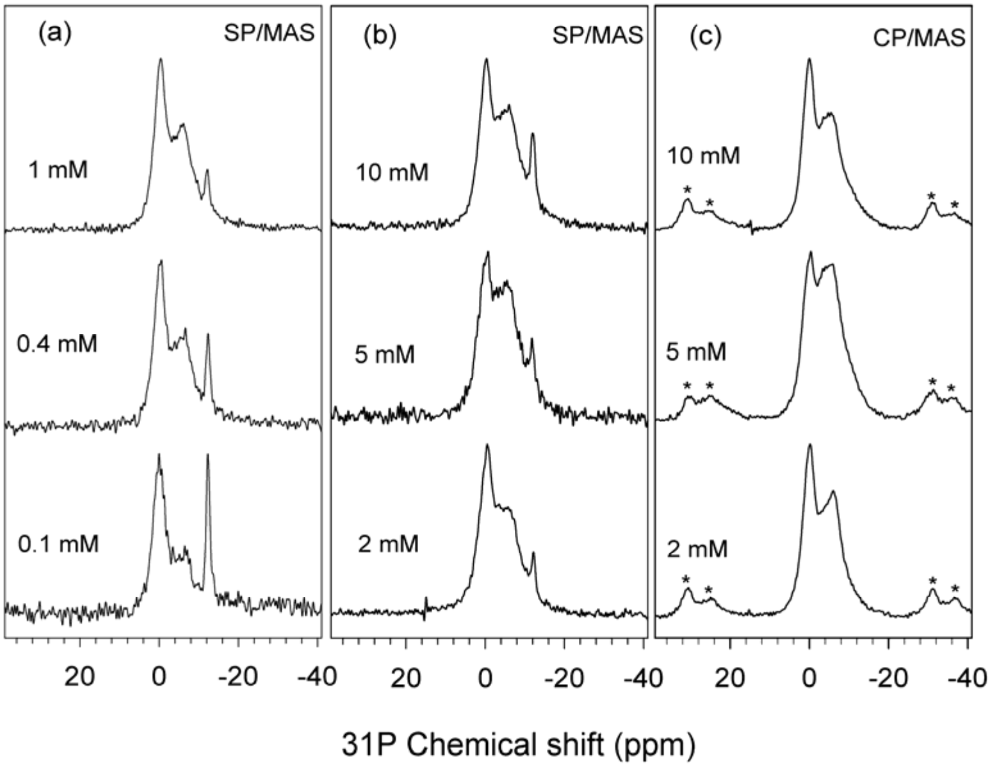

Figure 3.3 ^{31}P NMR spectra of phosphate adsorbed on boehmite at pH 5 at indicated initial P concentration, collected with ^{31}P SP/MAS (a, b) and ^{31}P{^{1}H} CP/MAS (c). For SP/MAS, the spinning rate is 10 kHz and pulse delay is 120 s; the CP/MAS experiments used a spinning rate is 5 kHz, CP contact time of 1 ms and pulse delay of 2 s. Asterisks denote spinning sidebands. NMR peaks in the ^{31}P SP/MAS spectra (a, b) at -12 ppm arise from rotor background.

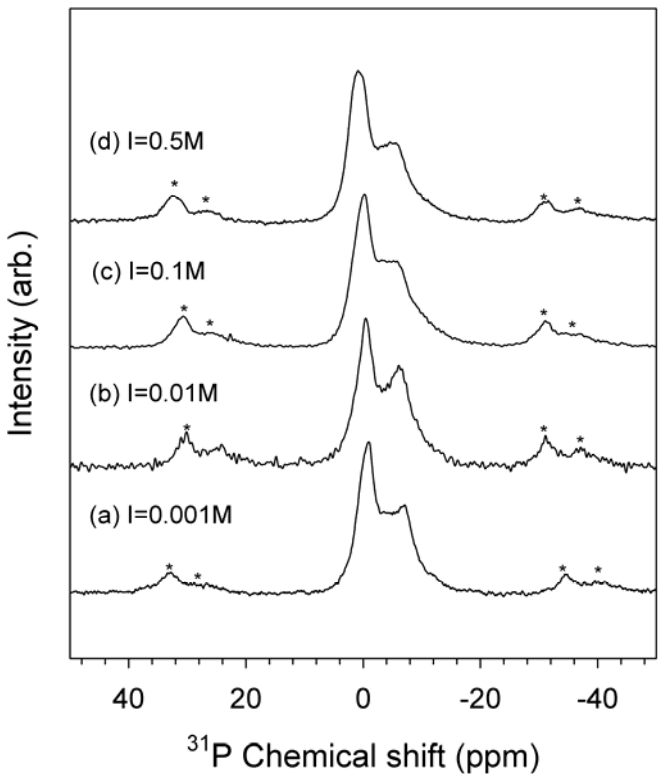

Figure 3.4 $^{31}P\{^{1}H\}$ CP/MAS spectra of phosphate adsorbed on boehmite prepared at pH 5 and 1 mM initial phosphate concentration but at different ionic strengths. CP/MAS experiments were conduced at a spinning rate is 5 kHz, CP contact time of 1 ms and pulse delay of 2 s. Asterisks denote spinning sidebands.

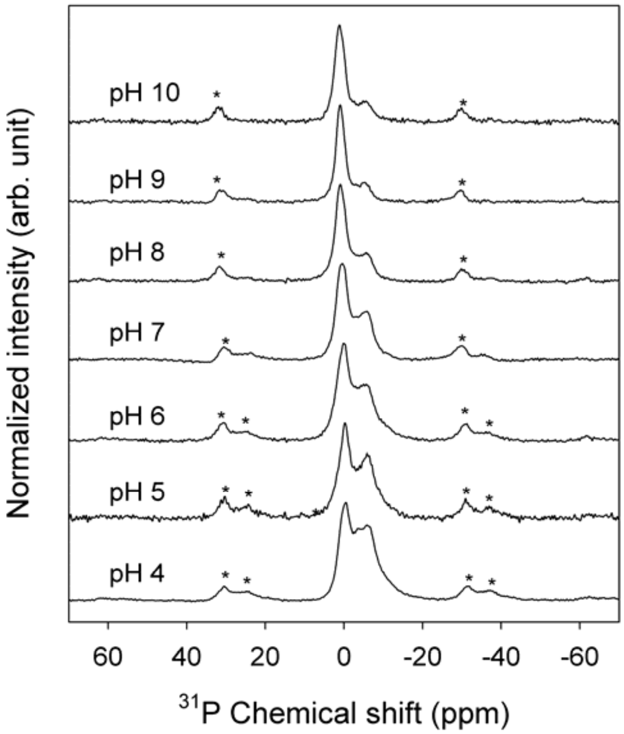

Figure 3.5 $^{31}P\{^{1}H\}$ CP/MAS spectra for phosphate adsorbed on boehmite at indicated pH. CP/MAS experiments were conduced at a spinning rate is 5 kHz, CP contact time of 1 ms and pulse delay of 2 s. Asterisks denote spinning sidebands

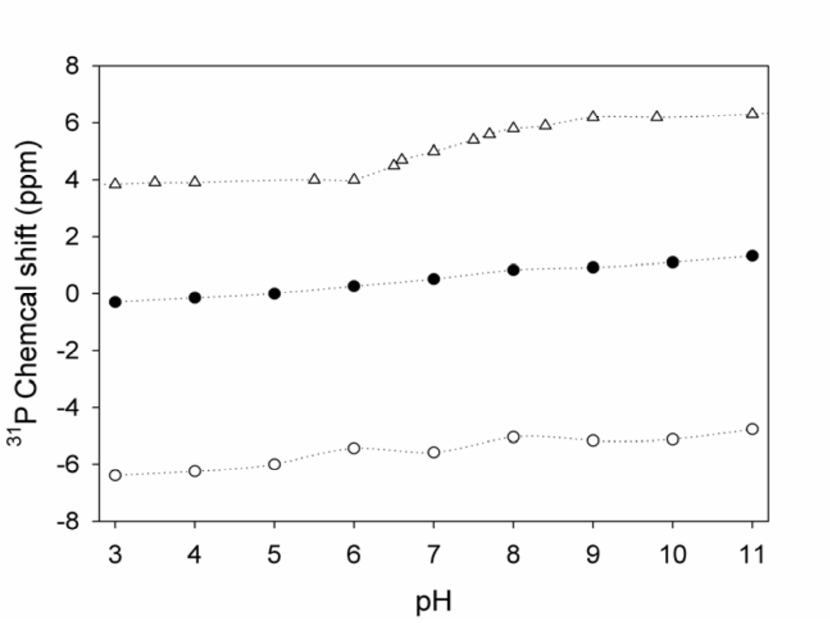

Figure 3.6 ^{31}P NMR chemical shift values as a function of pH, for the left (●)and right peaks (○) observed in NMR spectra of surface adsorbed phosphate on boehmite. Open triangles (Δ) indicate the chemical shifts for aqueous phosphate ($H_xPO_4^{3-x}$) in solution for comparison, obtained from Mortlock et al. [19].

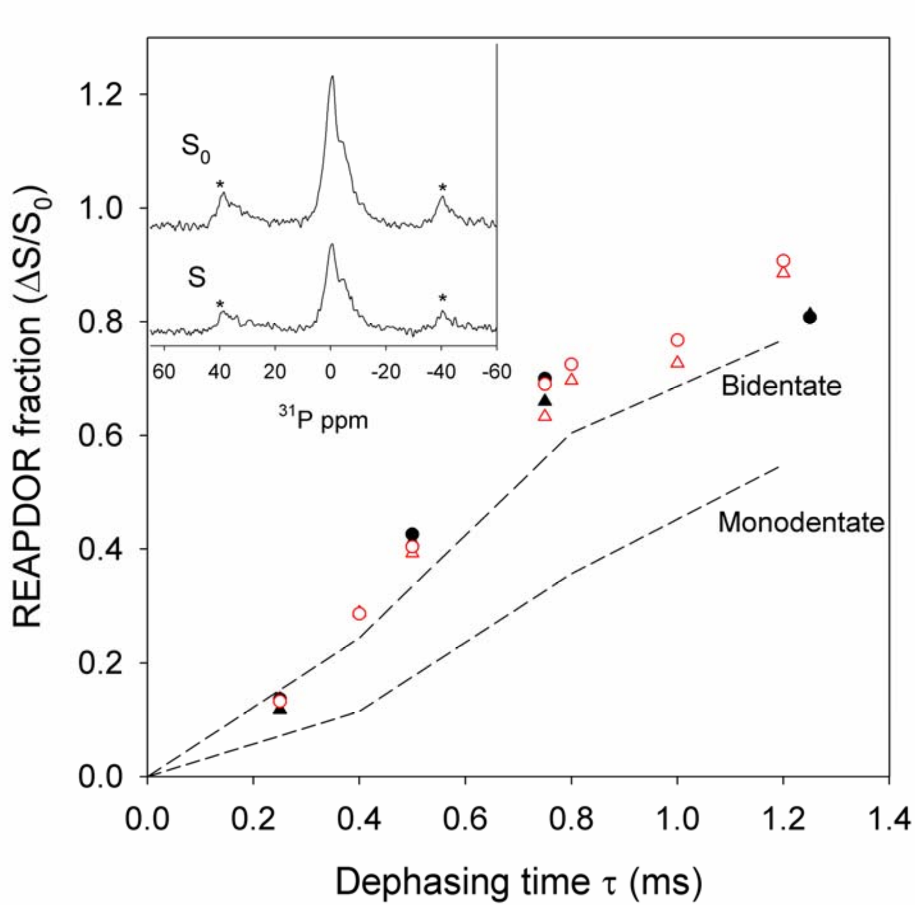

Figure 3.7 $^{31}P\{^{1}H\}/^{27}Al$ CP-REAPDOR NMR dephasing curves for ^{31}P peaks at $\delta_{iso,P} = 0.9$ ppm (●) and at -5.2 ppm (▲) for phosphate adsorbed on boehmite at pH 9. The dephasing curves for ^{31}P peaks $\delta_{iso,P} = 0$ ppm (○) and -6 ppm (Δ) for the adsorption sample prepared at pH 5 are plotted for comparison. The SIMPSON simulations were obtained for both bidentate (dotted line) and monodentate models (dashed line). Inset shows typical control (S_0) and ^{27}Al-dephased (S) spectra acquired with 8 kHz spinning rate, 0.5 s repetition delay, 1 ms CP contact time, 6 rotor cycles (τ = 0.75 ms) and 76572 scans.

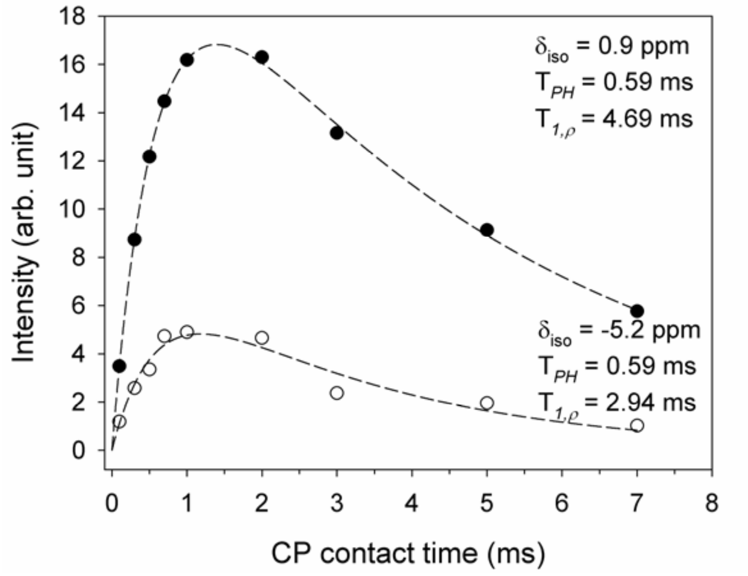

Figure 3.8 $^{31}P\{^{1}H\}$ CP/MAS kinetics for phosphate adsorbed on boehmite at pH 9. Spectra were collected with a continuous wave (CW) CP mode with a spinning rate of 3 KHz, pulse delay of 2 s and 1 ms contact time.

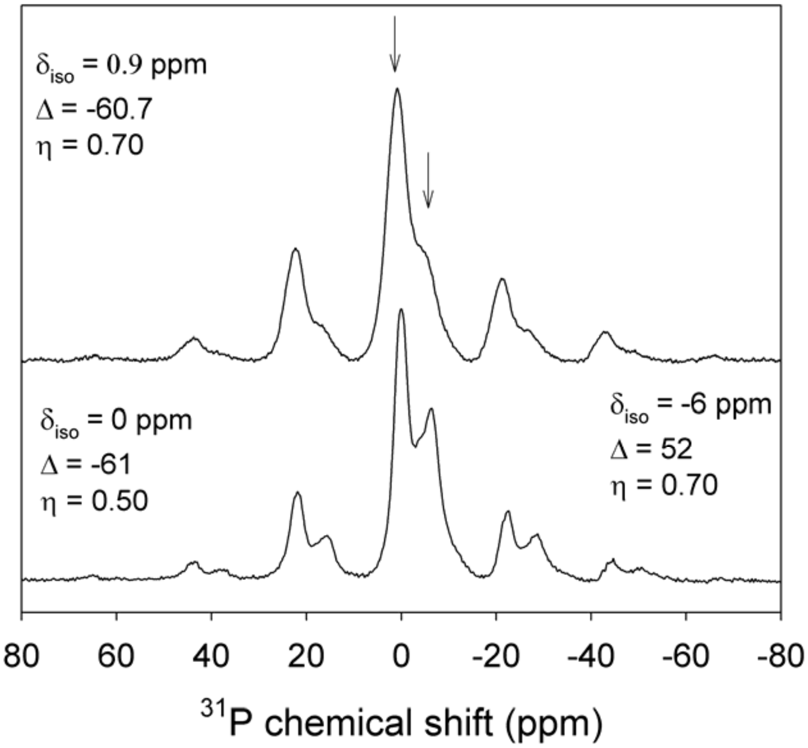

Figure 3.9 Full $^{31}P\{^{1}H\}$ CP/MAS spectra (1 ms contact time) of phosphate adsorbed on boehmite at pH 5 (bottom) and pH 9 (top). Spectra collected at a spinning rate of 3.5 kHz from which the CSA tensor parameters were extracted via the Herzfeld-Berger method. Arrows denote isotropic peaks, all others are spinning sidebands.

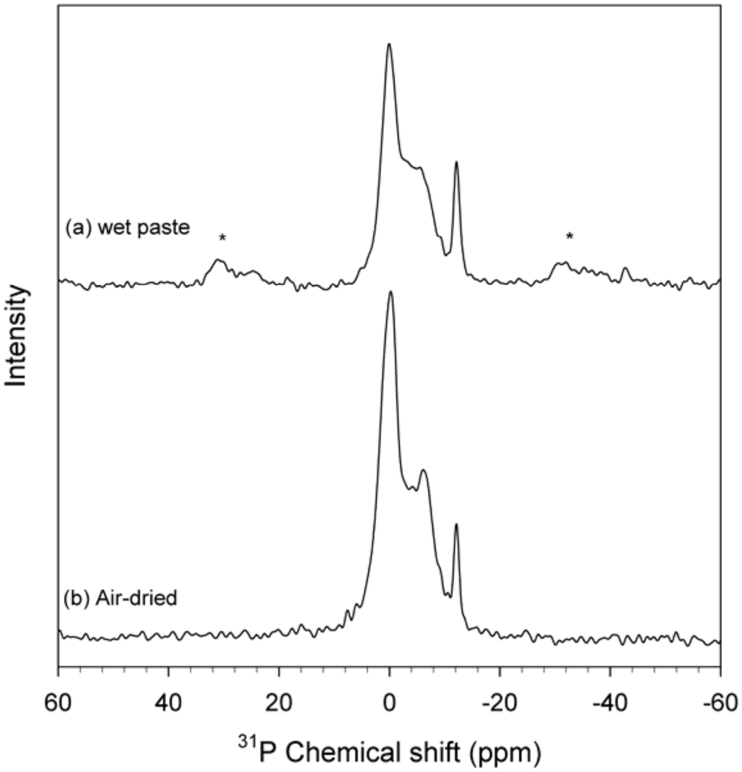

Figure 3.10 Comparison of ^{31}P SP/MAS NMR spectra for wet paste (a) and air-dried (b) samples for phosphate adsorbed on boehmite at pH 5 and 1 mM initial concentration. The spinning rate is 5 kHz for the wet paste and 10 kHz the air-dried sample. Asterisks denote spinning sidebands.

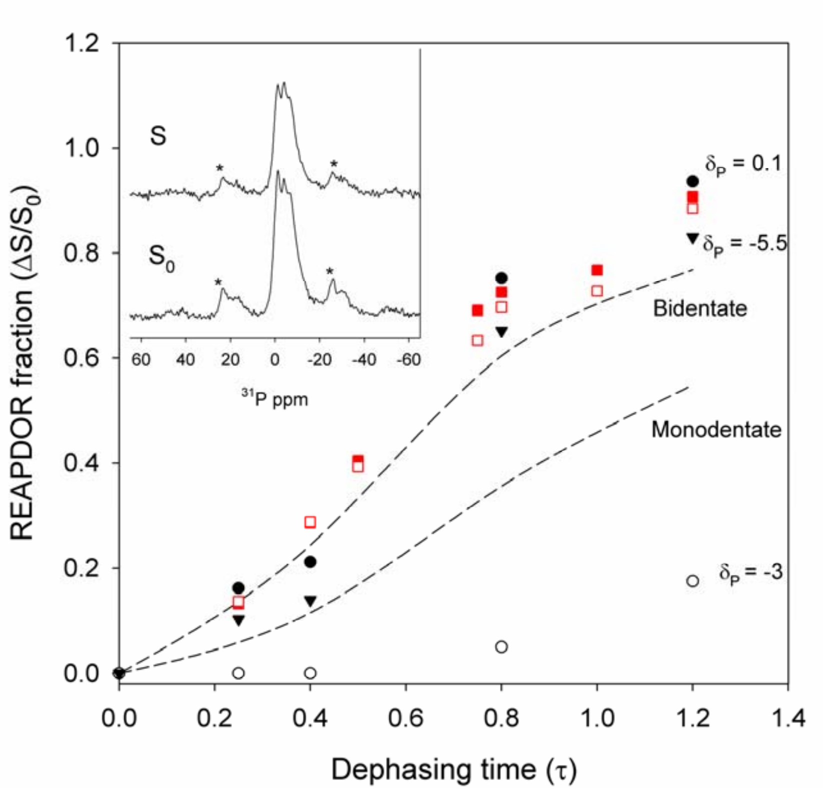

Figure 3.11 $^{31}P\{^1H\}/^{27}Al$ CP-REAPDOR NMR dephasing curves for ^{31}P peaks at $\delta_{iso,P} = 0.1$ ppm (●), -3 ppm (○) and at -5.5 ppm (▼) for the wet paste sample prepared at pH 5. Red filled (■) and open squares (□) indicate the REAPDOR curve for the peaks at $\delta_{iso,P} = 0$ ppm and -6 ppm shown in the corresponding dry sample at pH 5. Dashed lines are obtained from the SIMPSON simulations for both rigid bidentate and monodentate models.

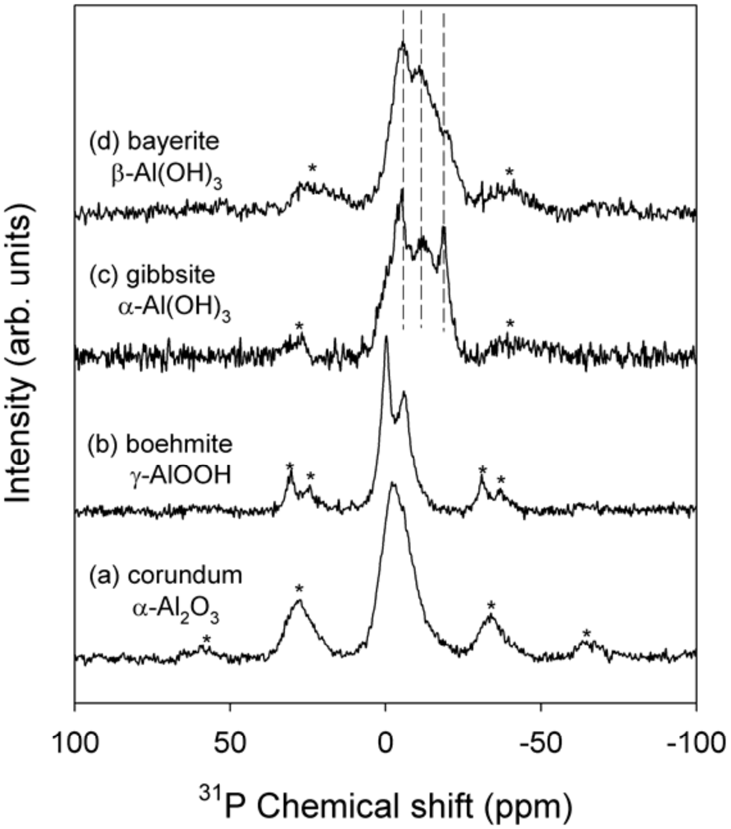

Figure 3.12 $^{31}P\{^{1}H\}$ CP/MAS of phosphate adsorbed corundum (a), boehmite (b), gibbsite (c) and bayerite (d). Samples are prepared at pH 5 with total phosphate concentration of 1 mM in 15 minutes of reaction. Spectra were collected at a spinning rate of 5 kHz, CP contact time of 1 ms, pulse delay of 2 s.

Chapter 4

Phosphate sorption on corundum (α-Al_2O_3) as studied by solid state NMR, ATR-FTIR and quantum chemical calculation*

---

* This is a collaborative research. Prof. Daniel Strongin at Temple University and his student Andro-Marc Pierre-Louis conducted the FTIR study; Prof. James Kubicki conducted the quantum chemical calculation.

Abstract

Sorption of phosphate by corundum (α-Al_2O_3) was investigated as a function of phosphate concentration and pH by ^{31}P solid state NMR spectroscopy, ATR-FTIR and quantum chemical calculation. The ^{31}P NMR spectra indicate that phosphate adsorbs on corundum mainly as inner-sphere complexes, with small amount aluminum phosphate surface precipitate as evidenced by the NMR signal observed in the chemical shift region of -12 to -20 ppm. At pH 5, the NMR signal is dominated by a peak at -2.6 ppm with full width at half maximum (FWHM) of 9.2 ppm. Comparison of the observed $^{31}P\{^{27}Al\}$ rotational echo adiabatic passage double resonance (REAPDOR) curve and SIMPSON simulations for a series of bidentate and monodentate structural models with geometry-optimized by density function theory (DFT) calculation indicates the bridging bidentate P/Al coordination. Comparison of the observed IR spectra with vibration frequencies calculated from structural models suggests a mixture of non-protonated bidentate and mono-protonated bidentate surface complexes at pH 5. At pH 9, the formation of singly-protonated phosphate inner-sphere complexes is suggested.

Key words: NMR, FTIR, phosphate, adsorption, corundum, density function theory

4.1. Introduction

The interaction of phosphate with metal oxide surfaces is of fundamental importance in many fields, including soil fertilization [1], global phosphorus cycling [2], and mineral surface reactivity [3]. Extensive studies have focused on iron (hydr)oxides, especially goethite, as the adsorbent to explore the uptake mechanism with surface complexation modeling and in-situ spectroscopies. Aluminum (hydr)oxides have received considerably less attention.

In natural environments, aluminum (hydr)oxides are abundant and can exist in the form of corundum (α-Al_2O_3), gibbsite (α-$Al(OH)_3$), boehmite (γ-AlOOH) and bayerite (γ-$Al(OH)_3$). The structural motifs found in these materials are common among other soil minerals such as dioctahedral clays, which might expose similar surface structures. Corundum is of particular interest in interfacial chemistry due to its simple chemical formula, well-known bulk structure and well-defined surface structure [4, 5]. Because it does not contain structural H, corundum has the lowest infrared (IR) background in the range from 1000 cm^{-1} to 1800 cm^{-1} of all other aluminum (hydr)oxides, yielding no interference with the phosphate IR bands.

One of the earliest Fourier transform infrared (FTIR) studies of phosphate adsorption on mineral surfaces was performed by Parfitt et al [6], who provided evidence for a ligand exchange-type mechanism and also suggested a binuclear bidentate phosphate bonding structure on goethite [7]. Using a cylindrical internal reflectance (CIR) accessory, Tejedor-Tejedor and Anderson conducted the first in-situ CIR-FTIR study on phosphate adsorbed on goethite [8]. The results suggested monodentate mononuclear complexes occurring at high pH and low surface loading and bidentate binuclear surface complexes dominating at low pH and high surface loading. Recently, similar studies have been reported on ferrihydrite [9], hematite [10] and corundum [5] with attenuated total reflectance (ATR) FTIR.

IR spectroscopy is very sensitive to phosphate coordination environment and molecular symmetry. For instance, in solution, PO_4^{3-} anions exhibit T_d symmetry and yield a single IR peak at 1007 cm^{-1}. As pH decreases, this band splits to two major vibration peaks at 1078 and 990 cm^{-1} and another minor peak at 850 cm^{-1} due to the lower symmetry of the aqueous HPO_4^{2-} (C_{3v}), and to four peaks at 1159, 1077, 940 and 875 cm^{-1} (a minor peak) for the C_{2v} symmetry of more protonated aqueous $H_2PO_4^-$ species. However, symmetry analysis has limitations in interpreting the IR features of phosphate/metal (hydr)oxide surface complexes, because proton and metal atom are considered equivalently in IR symmetry methods resulting in small difference in IR frequencies (e.g. between deprotonated bridging bidentate and singly protonated monodentate). To resolve this problem, molecular orbital/density functional theory (MO/DFT) have been employed to aid to interpretation of IR spectra [11].

In addition to IR spectroscopy, ^{31}P solid state NMR spectroscopy is a useful technique for determining phosphate chemical environment adsorbed on minerals surface. Traditional single-pulse NMR techniques rely on the chemical shift to infer structural information, which allows the inner-sphere, outer-sphere complexes and surface precipitates to be distinguished by comparison to the NMR spectra for crystalline model compounds such as alkali-phosphates and aluminum phosphates [12-17]. The chemical shift originates from the magnetic shielding of the electrons so that phosphate with different neighboring atoms will show different chemical shifts. But the bidentate and monodentate surface complexes are not necessarily distinguished unequivocally from the chemical shift alone. One problem is that there are no directly suitable structural analogues among crystalline model compounds for these types of bonding environments. Recently, quantum chemical calculations were employed to help interpret NMR data, providing proper structural models for distinguishing between bidentate and monodentate P/Al coordination [18]. More recently, I used an advanced NMR experimental technique, rotational echo adiabatic passage double resonance (REAPDOR) to assess the strength of ^{31}P-^{27}Al dipolar coupling for phosphate adsorbed on boehmite at pH 5, from which the bridging bidentate P/Al coordination on boehmite was successfully identified [19].

In this work, ^{31}P solid state NMR, ATR-FTIR and quantum chemical calculations are combined to study the phosphate bonding environment on corundum (α-Al_2O_3) surfaces. Molecular level information from three techniques would lead to a comprehensive understanding of phosphate complexation with Al oxides and Al-bearing clay minerals.

4.2. Material and methods

4.2.1. Materials

The corundum used in this study was purchased from Alfa Aesar as α-phase Al_2O_3 crystallites. No impurity phase was detected by either powder XRD, IR or ^{27}Al NMR. The solid has a specific surface area (SSA) of 7.6 m^2g^{-1} as measured by the BET method. The point of zero charge (pH_{pzc}) is 8.1 based on the electrophoresis mobility (EM) method [5]. TEM images suggest the particles are sub-micron in size.

4.2.2. Phosphate sorption

Adsorption samples were prepared using a batch technique. Simply, a 0.25 g aliquot of dry corundum powder was added to 50 ml of solution at the desired pH with a 0.01 M NaCl background electrolyte. One titrator (Metrohm STAT 718) was used to automatically maintain constant pH by adding increments of 0.1 M HCl. A second titrator was used to slowly add a small amount of 50 mM phosphate solution into the reaction vessel to reach the desired total phosphate concentration. After reaction, the samples were centrifuged to separate the solid and solution. The supernatant solutions were filtered by a 0.2μm-filter and then analyzed for phosphorus concentration by Direct Coupled Plasma-Atomic Emission Spectroscopy (DCP-AES). The solid was directly air-dried to room humidity for NMR measurements.

The sorption isotherm was measured at pH 5 with initial phosphate concentration ranging from 0.1 mM (3.1 ppm) to 1 mM (31 ppm) and 15 minute reaction times. The sorption pH curve was measured with the initial phosphate concentration at 1 mM at pH values ranging from 3 to 11, for 15 minutes of reaction. Such short reaction time was chosen to minimize the dissolution of corundum.

4.2.3. NMR data collection

Solid-state $^{31}P\{^1H\}$ cross-polarization magic angle spinning (CP/MAS) NMR spectra were collected on a 400 MHz Varian Inova spectrometer (9.4 T), at operating frequencies of 161.8 MHz and 399.8 MHz for ^{31}P and ^1H, respectively. A Varian/Chemagnetics T3-type probe configured for 7.5 mm (o.d.) ZrO_2 rotors was used. The ^{31}P chemical shifts ($\delta_{iso,P}$) are reported relative to external 85% H_3PO_4 solution, using hydroxylapatite as a secondary reference set to $\delta_{iso,P} = 2.65$ ppm.

The $^{31}P\{^1H\}$ CP/MAS spectra were obtained at spinning rates of from 3 to 5 kHz and contact times that varied from 0.1 to 7 ms. CP kinetics curves were measured at a spinning rate of 3 kHz with continuous wave (CW) irradiation at the $n = -1$ sideband match condition. For other CP/MAS spectra the transverse ^1H field ($\gamma B_{1,H}$) was ramped over approximately 5 kHz, centered near the first sideband match with a 42 kHz ^{31}P field. 32 kHz proton decoupling (CW) was employed during acquisition of all $^{31}P\{^1H\}$ CP/MAS spectra.

$^{31}P\{^1H\}/^{27}Al$ REAPDOR [20] NMR spectra were obtained on a 500 MHz Varian Infinity plus spectrometer (11.7 T) using a 3-channel Varian/Chemagnetics ‘T3’ probe assembly configured for 4 mm (o.d.) rotors. The pulse sequences employed excitation of the ^{31}P signal through $^{31}P\{^1H\}$ cross-polarization with a linear ramp of the ^1H B_1 field during the contact time to flatten the match condition. The ^1H 90° pulse length was 6 μs, the optimized contact time 1 ms, and the relaxation delay 0.5 s. For REAPDOR NMR experiments, the ^{31}P 180° pulse-length was 12 μs and the duration and strength of ^{27}Al pulse in the middle of the dephasing pulse train are 1/5 of the rotor period and 75 kHz, respectively.

4.2.4. ATR-FTIR Analysis

A Nicolet 6700 FTIR spectrometer with a deuterated triglycine sulfate (DTGS) detector and equipped with a Smart Orbit ATR attachment with a N_2 purge gas generator was used for data collection. Diamond crystal was used for the blank corundum samples and phosphate adsorption samples. A total of two hundred continuous scans at a resolution of 4 cm^{-1} were averaged to obtain each spectrum. Since phosphate vibration modes occur in the mid-infrared, data were collected in the 1200-960 cm^{-1} region. All spectra were reprocessed against the spectra of the diamond window (blank). For example, the spectra of the slurry of phosphate/corundum adsorption sample were subtracted from that of the slurry of corundum at the same pH to obtain the final IR spectra for surface adsorbed phosphate. All spectra were normalized with respect to the aluminum oxide modes ($\approx$ 800-500 cm^{-1}) and manually baseline-corrected for each final spectrum.

4.2.5. Molecular orbital/Density function theory calculation

Quantum chemical calculations were performed using Gaussian 03 [21] for optimizing the structure of orthophosphate/aluminum clusters ($PO_4Al_2(OH)_6(H_2O)_4$), which were energy minimized without any constraints. The model phosphate surface complexes were hydrated by 8 H_2O molecules to account for adsorbed H_2O in the experiments from ambient water vapor. The IR frequencies based on the geometry-optimized structures were calculated using B3LYP functionals [22, 23] and the 6-31G(d) basis set [24]. A factor of 0.9614 [25] was multiplied on the frequencies to correct for systematic errors, such as the neglect of anharmonicity and approximation of electron correlation. MOLDEN (version 4.0) was used to calculate atomic movements and the corresponding frequencies [26].

4.3. Results and discussion

4.3.1. Macroscopic sorption

Figure 4.1 shows the sorption isotherm of phosphate uptake by corundum with initial phosphate concentration from 0.1 M to 1 mM. Over this range, the surface coverage increases from 8.5 µmole g^{-1} (1.12 µmole m^{-2} or 0.67 P nm^{-2}) to 37.0 µmole g^{-1} (4.88 µmole m^{-2} or 2.94 P nm^{-2}). The sorption isotherm is well fitted by a one-site Langmuir equation, $Q = \frac{Q_m KC}{1 + KC}$, where Q is the amount of adsorbed phosphate (µmole g^{-1}), C is the equilibrium concentration (µM), Q_m is the maximum adsorption amount and K is the equilibrium constant for the sorption reaction. A least-square fit yields the Q_m as 50.9 µmole g^{-1} and K 4600 L mol^{-1}. This model provides a good fit to the experimental data ($R^2 = 0.96$), suggesting that adsorption reactions can account for the uptake of phosphate by corundum. The surface coverage along the isotherm is much lower than the Q_m, which reduces the likelihood of surface precipitates. Also, it is noticed that the Q_m for corundum is much smaller than that for similarly prepared bohemite (178.5 µmole g^{-1}) [19], owing to the larger particle size of corundum (~200 µm) over boehmite (~20 nm). However, if normalizing by specific surface area, the density of surface P loading on corundum is about 5 times of that on boehmite.

At a 1 mM initial concentration, sorption of phosphate by corundum follows a trend typical of oxyanion ligands, in which the sorption amount decreases with increasing pH (Figure 4.1, inset). At this concentration, the phosphate coverage decreases from 47.5 µmole g^{-1} (3.74 P nm^{-2}) at pH 3 to 4.24 µmole g^{-1} (0.34 P nm^{-2}) at pH 11. These results are similar to those reported previously for phosphate on other metal oxyhydroxides, such as ferrihydrite [1].

4.3.2. $^{31}P\{^1H\}$ CP/MAS spectra

Three samples prepared at different concentrations along the isotherm at pH 5 were examined by $^{31}P\{^1H\}$ CP/MAS NMR spectroscopy (Figure 4.2). The NMR spectra for the three samples are very similar in peak position, line shape and spinning sideband envelope, indicating similar phosphorus environments. For all three samples, the spectral profile is asymmetric and broad, with one obvious peak centered at about δ_P = -2.8 ppm with full with at half maximum (FWHM) of 9 ppm and a small shoulder in the region of δ_P from -12 to -20 ppm as marked by arrows (Figure 4.2). Although the center band can be reasonably well fitted by two Gaussian curves, at δ_P = -2.8 ppm with 9 ppm FWHM and -11.6 ppm with 8.9 ppm, the asymmetry of the profile requires addition of a third peak to fit some spectra, which is more apparent at an expanded scale (Figure 4.3). For example, the spectrum at 1mM intial phosphate and pH 5 can be fit by a main peak at -2.6 ppm with FWHM of 9.2 ppm (78%), a second peak at -8.6 ppm with 6 ppm FWHM (6%) and a shoulder at -13.2 ppm with 9.5 ppm FWHM (16%). Although this fit is not unique and poorly constrained, a similar combination of resonance can fit all other spectra (Table 4.1). The proportion of the resonance near -9 ppm is only significant at pH 3 and pH 5, and accounts for about 10% of the total signal intensity for these samples. Peaks for samples prepared > pH 7 are more symmetrical, but noisier. The spectra could fit with two Gaussian components, near -2 and -12 ppm. The shoulder near -12 ppm accounts for 5 to 23% of the total phosphate, and that the proportion tends to decreases with surface loading densities at pH 5 and with increasing pH at constant initial phosphate concentration (Table 4.1). Single pulse magic angle spinning experiments were attempted but did not yield sufficient signal owing to the low total P-content in these samples.

The major peak at δ_P = ~ -2.6 ppm with ~9 ppm FWHM in all spectra can be reasonably assigned to inner-sphere surface complexes. ^{31}P NMR chemical shifts for solid alkaline phosphates [16] and solution $H_xPO_4^{3-}$ species are in the range of +3 to +10 ppm according to previous literature [27]. Aluminum phosphates yield a more negative chemical shift due to the shielding of the Al-O-P bonds. For instance, brazilianite ($NaAl_3(OH)_4(PO_4)_2$) yields a peak at δ_P = -10.2 ppm, wavellite ($Al_3(OH)_3(PO_4)_2$) -11 ppm, metavarisite ($AlPO_4•2H_2O$) -13.2 ppm and variscite ($AlPO_4•2H_2O$) -19 ppm [28]. In addition, previous NMR studies of phosphate adsorption reported peaks at 0 and -6 ppm on boehmite [19], -3 ppm on γ-alumina [15], -6 ppm on amorphous $Al(OH)_3$ [13]. Taken together, NMR peaks in the range of 0 to -6 ppm appear to be typical for inner-sphere phosphate complexes on aluminum (hydr)oxides surface. The strong cross-polarization signal and significant spinning sideband intensity indicates a rigid phosphate environment, which is also a strong evidence for inner-sphere complexation. The shoulder at ~ -12 ppm denoted with arrow in Figure 4.3 that accounts for intenisties the chemical shift range from -10 ppm to -20 ppm could arise from a minor component of surface precipitates, considering the chemical shift of crystalline Al-phosphates listed above. In addition, Lookman et al [13] has reported that synthetic octahedral aluminum phosphate yields a peak at δ_P = -10 ppm and tetrahedral aluminum phosphate -27 ppm. This assignment is consistent with the higher intensity at lower pH which would promote dissolution of high energy surface Al sites, leading to the formation of Al-P surface precipitates.

The similarity of the three spectra for samples prepared at pH 5 in terms of chemical shift and line width suggests different initial concentration does not greatly affect the phosphorus environment on the corundum surface. This observation is similar to that found with phosphate adsorption on boehmite at pH 5 [19], and hematite at pH 9 [10], but differs from the results for goethite [8], from which phosphate bonding structure is dependent on surface loading. This difference may owe to different concentration range and different minerals used as adsorbent in each work.

Figure 4.3 shows the $^{31}P\{^1H\}$ CP/MAS spectra for phosphate adsorbed samples prepared from pH 3 to pH 11 at initial phosphate concentration of 1 mM. These intensity-normalized spectra all show broad and asymmetric resonance lineshapes, similar to those shown in Figure 4.2. There are slight variations that peak position changed from -3.0 ppm at pH 3 to -0.4 ppm at pH 11. A similar increase in chemical shift with increasing pH has been observed in previous work on boehmite [19]. Possible reasons could be the change of surface charge on corundum as a function of pH, deprotonation of surface adsorbed phosphate, or changes in hydrogen bonding environment. Deprotonation as pH increases can cause variation of chemical shift moving to the upfield (more positive) as evidenced in both solids for $Na_xH_{3-x}PO_4$ [15, 16] and solution for $H_xPO_4^{3-x}$ species over a wide pH range [27], because of the shielding of proton (electron of proton) on ^{31}P nuclei. This process is more complicated at solid/water interface, because the presence of mineral surface may alter the arrangement of interfacial water molecule and the H-bonding environment around surface adsorbed phosphate and thus influence the chemical shielding to ^{31}P nuclei [29].

To determine the relationship between surface adsorbed phosphate and the associating proton environment, the CP dynamics were analyzed by fitting the major peak at -2.6 ppm in the spectra for the sample prepared at pH 5 and 1mM. These spectra are obtained at different contact times (τ) and carefully fitted to a consistent set of Gaussian curves with fixed position and width, allowing only the intensities to vary. The resulting intensities are well-described by the classical bi-exponential relationship

$$I(\tau) = I_0\left[1-\frac{T_{PH}}{T_{1\rho,H}}\right]^{-1}\left[1-\exp\left(-\frac{T_{PH}}{\tau}\right)\right]\exp\left(-\frac{T_{1\rho,H}}{\tau}\right) \quad .\ (1)$$

Where T_{PH} is the characteristic time for $^1H \rightarrow {}^{31}P$ magnetization transfer and $T_{1\rho,H}$ is the time constant for decay of the ^1H magnetization in the rotating frame [30]. A least square fit of the variable contact time data (Figure 4.4) gives the T_{PH} value of 0.31 ms and $T_{1\rho,H}$ of 2.7 ms, respectively for the peak at $\delta_P = -2.6$ ppm. In the rigid limit, T_{PH} is related to the sum over the phosphate-proton distances: $T_{PH}^{-1} \propto \sum_i^1 \left[d\left({}^{31}P{-}{}^1H_i\right)\right]^{-6}$, where $d\left({}^{31}P{-}{}^1H_i\right)$ is the internuclear distance between the phosphate P and the *i*th nearby proton [31]. However, motion of H and H-bearing species can modify the relationship between T_{PH} and $d\left({}^{31}P{-}{}^1H_i\right)$, and prevent strictly quantitative interpretation of the CP rate. Nevertheless, the short T_{PH}

here is very similar to that for the protonated phosphate on bohemite [19], indicating a close association of phosphate with rigid H, as could be expected for the hydroxylated surface of corundum at pH 5. CP dynamics analysis was not performed on the peaks at δ_P = -8.6 and ~ -13.2 ppm, because the intensities of these two peaks could not be measured accurately at short and long contact times.

4.3.3. ^{31}P{^{27}Al} REAPDOR

The ^{31}P{^{27}Al} REAPDOR NMR experiments [20] were carried out to measure the ^{31}P–^{27}Al heteronuclear dipolar coupling which depends on the interatomic distances and geometry [19]. Such structural information can help constrain the range of possible structural configurations, for example whether bidendate or monodentate surface complexes predominate. Experimentally, sets of two ^{31}P-observed NMR spectra are acquired, one (S) obtained with a heteronuclear dipolar dephasing sequence and a second control spectrum (S_0) acquired under identical conditions but without irradiation at the ^{27}Al frequency. The inset of Figure 4.5 shows a typical set of ^{31}P–^{27}Al REAPDOR NMR spectra acquired for phosphate adsorbed on corundum prepared at pH 5, with a 0.25 ms dephasing time (product of the number of rotor cycles and rotor period). The bottom spectrum (S) shows a signal loss compared to the top spectrum (S_0), indicating a strong dipolar coupling between phosphate (P) and surface aluminum. Because dipolar coupling has an inverse cubic relationship with interatomic distance and is reduced or averaged by molecular motion, such strong coupling indicates a rigid structure for phosphate sorption products and short P-Al distances (less than 5 Å).

To quantitatively characterize the strength of ^{31}P–^{27}Al heteronuclear dipolar coupling, the REAPDOR experiment was repeated, changing the dephasing time (τ) to build a curve of the REAPDOR fraction, $(S_0 - S)/S_0$, with dephasing time, τ (Figure 4.5). Because of the poor signal-to-noise ratio, REAPDOR curve only for the major peak at -2.6 ppm were analyzed. The SIMPSON package [32] was used to simulate the theoretical REAPDOR curves for possible structural models with geometry optimized by DFT calculations (Figure 4.6). These models are illustrated in Figure 4.6 as the binuclear bidentate non-protonated phosphate [$\equiv Al_2PO_4^{3-}$

(BB-H0)] (a), binuclear mono-protonated phosphate [$\equiv Al_2HPO^{2-}_4$ ($BB-H_1$)] (b), binuclear monodentate bi-protonated phosphate [$\equiv Al_2H_2PO^{-}_4$ ($BB-H_2$)] (c), monodentate non-protonated [$AlPO^{3-}_4$ ($MM-H_0$)] (d), and monodentate mono-protonated phosphate [$\equiv AlHPO^{2-}_4$ ($MM-H_1$)] (e). All the bridging bidentate models contain two P-O-Al linkages with two close $d_{(P-Al)}$, at 3.09(1) and 3.08(1) Å, and the monodentate models [19] assume one P-O-Al linkage with $d_{(P-Al)}$ at 3.13(2) Å and an other long $d_{(P-Al)}$ at 4.35(1) Å not connected by an oxygen. Addition of a second longer distance (ca. 4.3 Å) does not significantly alter the dephasing curve, which relects dominantly the influence of the shorter distance (ca. 3.1 Å). The SIMPSON simulations also require the ^{27}Al quadrupolar coupling constants (QCC) for the aluminum associated with phosphate. We are unable to measure the QCC directly by $^{31}P\{^{27}Al\}$ TRAPDOR experiments as was possible for boehmite [19], because of insufficient signal intensity resulting from the much lower phosphate content compared with boehmite. A QCC of 3 MHz, equal to that measured for Al bound to phosphate on boehmite was assumed, but varying QCC values from 1 to 6 MHz does not significantly affect the SIMPSON simulations results.

The simulations (Figure 4.5a-f) show that the three bridging bidentate models yield very similar calculated REAPDOR curves that agree well with the experimental data. The calculated curves for the monodentate models significantly differ from the experimental data. This result indicates two short P-Al distances are needed to model the observed REAPDOR dephasing curve and provides strong evidence that the ^{31}P peak at −3 ppm arises from phosphate with bridging bidentate coordination to Al. We note that the SIMPSON simulations used simplified 3- and 4-spin systems with more distant Al on the surface not considered. This simplification may cause the small difference between the experimental and calculated REAPDOR curves for the bidentate model. The difference caused by this simplication is much smaller than that between the bidentate and monodentate models, because all other P−Al distances that are not considered are likely close to or greater than 5 Å and have negligible effect owing to the inverse cubic relationship of dipolar coupling to interatomic distance.

The significant difference between bidentate and monodentate models in their corresponding SIMPSON simulations demonstrate the utility of dipolar coupling identifying phosphate bonding structure. The $1/r^3$ dependence of dipolar interactions makes it more sensitive to coordination type than measurements of distance only. For example, it has been argued that with distance only it is not possible to distinguish bidentate and monodentate structure for As adsorbed on goethite by traditional extended X-ray absorption fine structure spectroscopy (EXAFS). Loring et al. [33] found that the EXAFS spectra for As adsorbed on goethite was almost identical to that for a monodentate mononuclear model compound ($As(NH_3)_5Co$), in which structure the As-O-Co linkage is bent to accommodate hydrogen bonding to make the As-Co distance (3.25 Å) as short as the value in traditional bidenate binuclear model (typical 3.20 -3.30 Å) [34]. To test the sensitivity of REAPDOR technique to such a monodentate model for phosphate adsorbed on corundum, we calculated a REAPDOR curve using one P-Al distance of 3.07 Å and the other one 4.36 Å (labeled as modified monodentate model, Figure 4.5f), shorter than the P-Al distances in the bidentate models. This calculated curve has steeper slope than those for other monodentate models\, but is still significantly different from the experimental REAPDOR curve for phosphate adsorbed on corundum.

4.3.4. ATR-FTIR spectra

IR frequencies of the clusters shown in Figure 4.6 were calculated with the B3LYP functional and the 6-31G(d) basis set (Table 4.2). With the same method, we calculated theoretical IR frequencies for aqueous $H_2PO_4^-$ and HPO_4^{2-}, in which 18 explicit water molecules were used to model the H-environment at pH 5 and pH 9 in solution. The calculated frequencies for $H_2PO_4^-$ (aq) are 892, 1006, 1080 and 1160 cm^{-1}, and those for HPO_4^{2-} (aq) are 873, 998, 1051 cm^{-1}. These calculated frequencies match well the earlier experimental values (Figure 4.7a) [8, 9].

The ATR-FTIR spectra of phosphate adsorbed on corundum prepared at pH 5 and pH 9 are shown in Figure 4.7 for the region 960 to 1200 cm^{-1}. Frequencies lower than 960 cm^{-1} are not considered due to overlap with the IR background of corundum and complicated stretching-bending coupling. Although both spectra show poorly resolved broad features, the spectrum for the sample at pH 5 clearly differs from that at pH 9 in peak intensity and main peak position. Relative to the sample at pH 5, the pH 9 sample has a narrower peak and less intensity, due to the lower phosphate loading. These differences are similar to the results for phosphate adsorbed on hematite at different pH [9]. This pH effect may arise from the different H-bonding network around phosphate at different pH conditions, deprotonation of surface adsorbed phosphate, or different coordination of phosphate to surface Al. Centered at ~1100 cm^{-1}, the IR feature at pH 5 differs significantly from those for aqueous $H_2PO_4^-$, the predominant species in solution at this pH, suggesting that the spectral feature arises from the formation of inner sphere P complexes on the corundum surface. A similar conclusion can be drawn from the data at pH 9 by comparing the IR frequencies of aqueous HPO_4^{2-} species in solution and those observed from adsorption samples.

The IR spectra of the phosphate adsorbed on the corundum surface are interpreted by comparing the experimental data with frequencies calculated for the structural models (Table 4.2). The calculated bidentate non-protonate structure (BB-H_0) yields the widest distribution of frequencies with IR vibration frequency at 1003, 1021, 1095, 1115 and 1195 cm^{-1} (Figure 4.7b), and the mono-protonated monodentate nodel (MM-H_1) yields the narrowest range, with frequencies of 1009, 1020, 1093 and 1130 cm^{-1}. Results for these two models differ from the experimental observations markedly; with the highest wavenumber band BB-H_0 falling outside the observed bands and the region 1100-1180 cm^{-1} not covered by the MM-H_1 model.

The remaining three models yield very similar frequency ranges, all of which are consistent with the experimental spectra at pH 5 and pH 9. As a result, it seems unlikely that the IR data alone are sufficient to distinguish among them. The similarities of the calculated frequency ranges suggest that the differences between observed IR spectra at pH 5 and pH 9, lies on primarily in the 1110 – 1190 cm^{-1} range, likely arise from intensity changes among adsorption complexes, which cannot be determined with the computational methods here. Of these models with compatible IR frequencies, the most probable phosphate bonding configuration at pH 9 seems to be the bidentate mono-protonated (BB-H_1) structure since the calculated frequency at 1072 cm^{-1} matches the center of experimental IR spectra well. The calculated frequencies for bidentate bi-protonated (BB-H_2) seem to match the observed IR feature at pH 9 also, but at such alkaline condition the fully protonated species (BB-H_2) is not expected to predominate. The frequencies for monodentate non-protonated structure (MM-H_0) fall within the range of the two experimental IR spectra, such surface adsorbed phosphate is possible at pH 9, but at pH 5 it is unlikely to form the completely non-protonated species and is not consistent with the NMR results from P/Al REAPDOR experiments. At pH 5, two species might exist simultaneously as BB-H_1 and BB-H_2 phosphate complexes, which are evidenced by the difference spectrum produced by subtraction of the spectrum for pH 9 from that for pH 5. The difference spectrum could be explained as the contribution from BB-H_2 phosphate complexes if intensities for the higher frequency bands are high.

Unfortunately, more specific and detailed structural interpretation could not be obtained to distinguish between those species because of the poor resolulotion of the IR bands. In this case it appears that analysis of phosphate bonding on aluminum (hydr)oxides is much more difficult than characterizing phosphate structure on iron (hydr)oxides, for which well separated IR peaks can be observed. Compared to the IR studies of phosphate on goethite [8] and/or hematite [10], the analytical region is smaller in this work due to the background IR absorption of corundum and the IR features are much broader and severely overlaping.

4.4. Conclusion

^{31}P solid state NMR spectroscopy, together with ATR-FTIR and quantum chemical calculations were employed to study the uptake of phosphate by corundum (α-Al_2O_3) as a function of initial phosphate concentration (100 - 1000 μM) and pH (3.0 – 11.0). The macroscopic sorption isotherm and pH curve indicate the uptake of phosphate on corundum follows a trend typical for oxyanion adsorption on metal (hydr)oxides, with uptake decreasing with increasing pH. The results of ^{31}P NMR experiments indicate that under most conditions a mixture of phosphate environments exist on the corundum surface, with a majority of inner-sphere surface complexes and a small amount of surface precipitates. Analysis of $^{31}P\{^{27}Al\}$ rotational echo adiabatic passage double resonance experiments, the majority inner-sphere complexes occurring at pH 5 have bidentate ate phosphate/Al coordination. This assignment is in good agreement with ATR-FTIR spectra, which suggest the formation of both mono-protonated ($\equiv Al_2PO_4$) and non-protonated bridging bidentate surface complexes ($\equiv Al_2PO_4H$) at pH 5. At pH 9, the detailed structure cannot be accurately determined due to the limitations of NMR and IR techniques.

Reference

[1] Arai, Y.; Sparks, D. L., *Adv. Agron.* **2007,** 94, 135-179.

[2] Paytan, A.; McLaughlin K., *Chem. Rev.* **2007,** 107, 563–576.

[3] Strongin, D. R.; Grey, C. P.; Parise, J. B.; Kubicki, J. D., *Surf. Sci.* **2010,** 604, 1065-1071.

[4] Catalano, J. G.; Park, C.; Zhang, Z.; Fenter, P., *Langmuir* **2006**, 22, 4668-4673.

[5] Nero, M, D.; Galindo, C.; Barillon, R.; Halter, E.; Madé, B., *J. Colloid Interface Sci.* 342, 437-444.

[6] Atkinson, R. J.; Parfitt, R. L.; Smart, R. S. C., *J. Chem. Soc. Faraday Trans. I* **1974**, 70, 1472–1479.

[7] Parfitt, R. L.; Atkinson, R. J., *Nature* **1976**, 264, 740−742

[8] Tejedor-Tejedor, M. I.; Anderson, M. A., *Langmuir* **1990**, 6, 602-611.

[9] Arai, Y.; Sparks, D. L., *J. Colloid Interface Sci.* **2001**, *241*, 317-326

[10] Elzinga, E. J.; Sparks, D. L., *J. Colloid Interface Sci.* **2007**, *308*, 53-70.

[11] Kwon, K. D**.;** Kubicki, J. D., *Langmuir* **2004**, 20, 9249-9254.

[12] Bleam, W. F.; Pfeffer, P. E.; Goldberg, S.; Taylor, R. W.; Dudley, R., *Langmuir* **1991,** *7*, 1702-1712.

[13] Lookman, R.; Grobet, P.; Merckx, R.; Vlassak, K., *Eur. J. Soil Sci.* **1994,** *45*, 37-44.

[14] Lookman, R.; Grobet, P.; Merckx, R.; Van Riemsdijk, W. H., *Geoderma* **1997,** *80*, 369-388.

[15] Johnson, B. B.; Ivanov, A. V.; Antzutkin, O. N.; Forsling, W., *Langmuir* **2002,** *18*, 1104-1111.

[16] Kim, Y.; Kirkpatrick, R. J., *Eur. J. Soil Sci.* **2004,** *55*, 243-251.

[17] Van Emmerik, T. J.; Sandstrom, D. E.; Antzutkin, O. N.; Angove, M. J.; Johnson, B. B., *Langmuir* **2007,** *23*, 3205-3213.

[18] Fry, R. A.; Kwon, K. D.; Komarneni, S.; Kubicki, J. D.; Mueller, K. T., *Langmuir* **2006**, *22*, 9281-9286.

[19] Li, W.; Feng, J.; won, K. D.; Kubicki, J. D.; Phillips, B. L., *Langmuir* **2010**, *26*, 4753-4761.

[20] Gullion, T., *Chem. Phys. Lett.* **1995**, 246, 325-330.

[21] Frisch, M. J.; Trucks, G. W.; Schlegel, H. B.; Scuseria, G. E.; Robb, M. A.; Cheeseman, J. R.; Montgomery, J. A., Jr. ; Vreven, T.; Kudin, K. N.; Burant, J. C.; Millam, J. M.; Iyengar, S. S.; Tomasi, J.; Barone, V.; Mennucci, B.; Cossi, M.; Scalmani, G.; Rega, N.; Petersson, G. A.; Nakatsuji, H.; M. Hada; M. Ehara; K. Toyota; Fukuda, R.; Hasegawa, J.; Ishida, M.; Nakajima, T.; Honda, Y.; Kitao, O.; Nakai, H.; Klene, M.; Li, X.; Knox, J. E.; Hratchian, H. P.; Cross, J. B.; Adamo, C.; Jaramillo, J.; Gomperts, R.; Stratmann, R. E.; Yazyev, O.; Austin, A. J.; Cammi, R.; Pomelli, C.; Ochterski, J. W.; Ayala, P. Y.; Morokuma, K.; Voth, G. A.; Salvador, P.; Dannenberg, J. J.; Zakrzewski, V. G.; Dapprich, S.; Daniels, A. D.; Strain, M. C.; Farkas, O.; Malick, D. K.; Rabuck, A. D.; Raghavachari, K.; Foresman, J. B.; Ortiz, J. V.; Cui, Q.; Baboul, A. G.; Clifford, S.; Cioslowski, J.; Stefanov, B. B.; Liu, G.; Liashenko, A.; Piskorz, P.; Komaromi, I.; Martin, R. L.; Fox, D. J.; Keith, T.; Al-Laham, M. A.; Peng, C. Y.; Nanayakkara, A.; Challacombe, M.; Gill, P. M. W.; Johnson, B.; Chen, W.; Wong, M. W.; Gonzalez, C.; Pople, J. A.; *Gaussian 03, Revision C.02*; Gaussian, Inc.: Wallingford CT, 2004.

[22] Becke, A. D., *J. Chem. Phys.* **1997**, 107, 8554-8560.

[23] Lee, C. T.; Yang, W. T.; Parr, R. G., *Phys. Rev. B* **1988**, 37, 785-789.

[24] Hehre, W. J.; Ditchfie, R.; Pople, J. A., *J. Chem. Phys.* **1972**, 56, 2257-2261.

[25] Scott, A. P.; Radom, L., *J. Phys. Chem.* **1996**, 100, 16502-16513.

[26] Schaftenaar, G.; Noordik, J. H., *J. Comput. Aided Mol. Design* **2000**, 14, 123-134.

[27] Mortlock, R. F.; Bell, A. T.; Radke, C. J., *J. Phys. Chem.* **1993**, 97, 775-782.

[28] Cade-Menun, B.J. *Talanta* **2005**, 66, 359-371.

[29] Conte, P.; Šmejkalová, D.; Piccolo, A.; Spaccini, R., *Eur. J. Soil Sci.* **2008**, 59, 584 – 591.

[30] Kolodziejski, W.; Klinowski, J., *Chem. Rev.* **2002**, 102, 613-628.

[31] Mehring, M., *Principles of High Resolution NMR in Solids;* 2nd ed.; Springer-Verlag: Berlin, 1983.

[32] Bak, M.; Rasmussen, J. T.; Nielsen, N. C., *J. Magn. Reson.* **2000**, 147, 296-330.

[33] Loring, J. S.; Sandstrom, M. H.; Noren, K.; Persson, P., *Chem. Eur. J.* **2009**, 15, 5063-5072.

[34] Sherman, D. M.; Randall, S. R., *Geochim. Cosmochim. Acta* **2003**, 67, 4223-4230.

Tables and figures

Table 4.1 Results of least-square fits of Gaussian curves to the of the $^{31}P\{^{1}H\}$ CP/MAS spectra of phosphate adsorbed on corundum at different pH and concentration

Sample (concentration, pH)	Chemical shift (ppm)	FWHM (ppm)	Relative intensity (%)
0.1 mM, pH 5	-2.8	9	91
	-11.6	8.9	9
0.4 mM, pH 5	-2.8	9.0	70
	-7.5	6	7
	-10.5	12.7	23
1 mM, pH 5	-2.6	9.2	78
	-8.6	5.9	6
	-13.2	9.5	16
1 mM, pH 3	-3.2	9	72
	-9.2	5.5	11
	-13.3	11.2	17
1 mM, pH 7	-2.2	10.3	84
	-11.8	8.9	16
1 mM, pH 9	-2.2	10	96
	-12.1	8	4
1 mM, pH 11	-0.4	9.3	93
	-12	12	7

Table 4.2 Experimental IR frequencies of aqueous phosphate and calculated frequencies of phosphate (aq) and phosphate/Al complexes from DFT

Experimental[1]		Calculated frequencies (cm^{-1})						
$H_2PO_4^-$	HPO_4^{2-}	$H_2PO_4^-$	HPO_4^{2-}	BB-H_0	BB-H_1	BB-H_2	MM-H_0	MM-H_1
870	850	892	873	1003	1013	1013	1009	1006
940	989	1006	998	1021	1036	1036	1020	1031
1074	1077	1080	1051	1095	1072	1054	1093	1041
1160		1160		1115	1119	1103	1130	1066
				1195		1134		1070

[1] The experimental values are from Tejedor-Tejedor and Anderson [8].

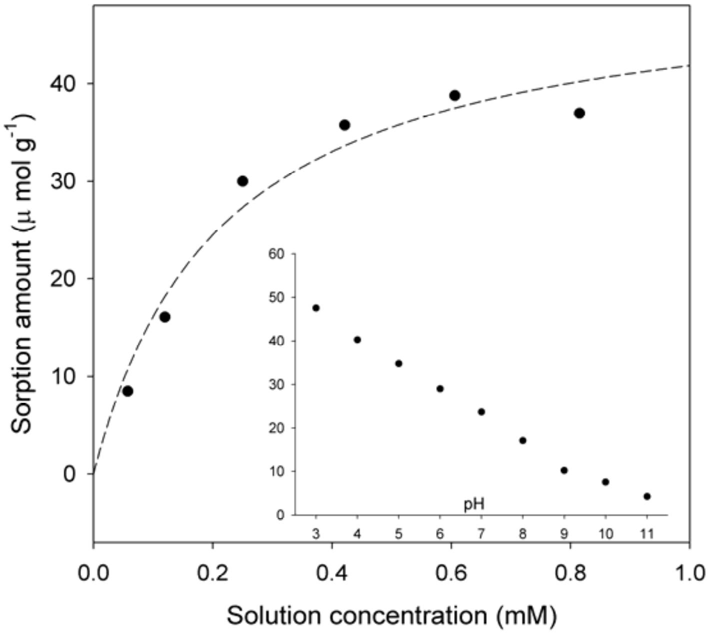

Figure 4.1 Adsorption isotherm of phosphate on corundum at pH 5. Inset shows the pH-dependence of phosphate uptake by corundum at initial concentration of 1mM. The inset has the same unit as that for adsorption isotherm.

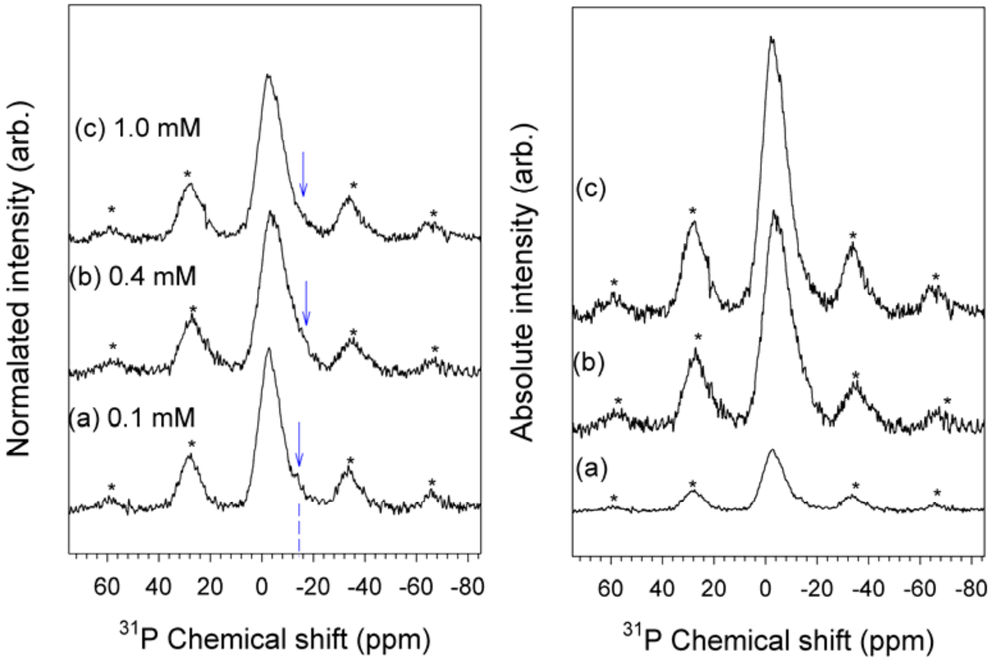

Figure 4.2 ^{31}P{^{1}H} CP/MAS spectra of phosphate adsorbed on corundum at pH 5 with indicated P concentration. The left is the spectra with intensity normalized and the right with absolute intensity for the same samples. Spectra were collected at a spinning rate of 5 kHz, 1 ms CP contact time, 1 s pulse delay. Each spectrum was acquired with 203808 scans (a), 80656 scans (b) and 72832 scans (c).

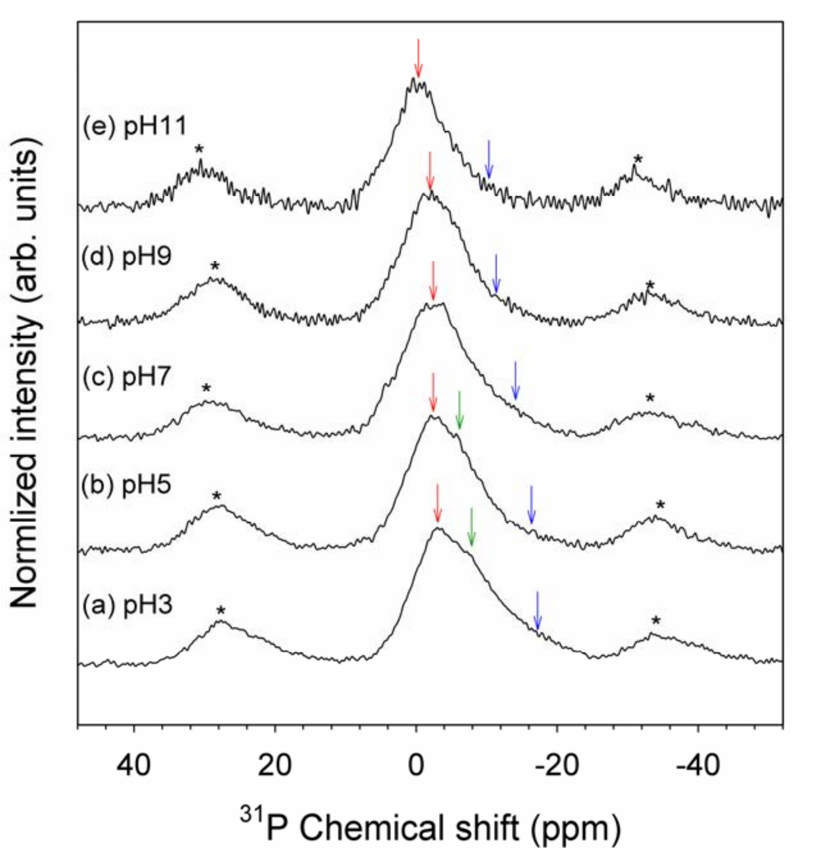

Figure 4.3 ^{31}P{^{1}H} CP/MAS spectra of phosphate adsorbed on corundum at indiated pH. Samples were prepared at indicated pH with 1 mM initial phosphate concentration. Spectra were collected at a spinning rate of 5 kHz, 1 ms CP contact time, 1 s pulse delay. Each spectrum was acquired with 90304 scans (a), 72832 scans (b), 81920 scans (c), 133224 scans (d) and 166528 scans (e).

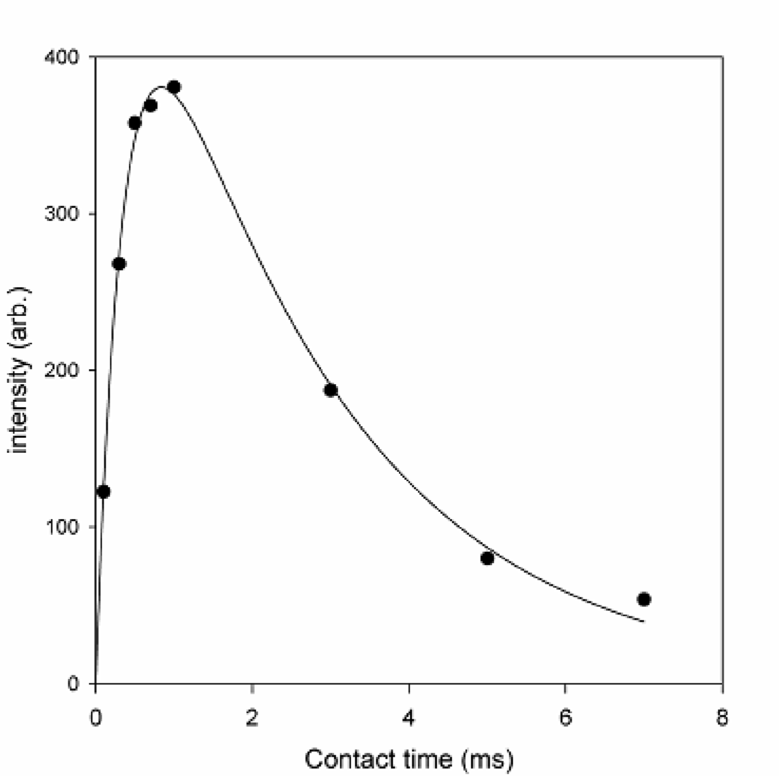

Figure 4.4 $^{31}P\{^{1}H\}$ CP/MAS kinetics for phosphate adsorbed on corundum at pH 5.

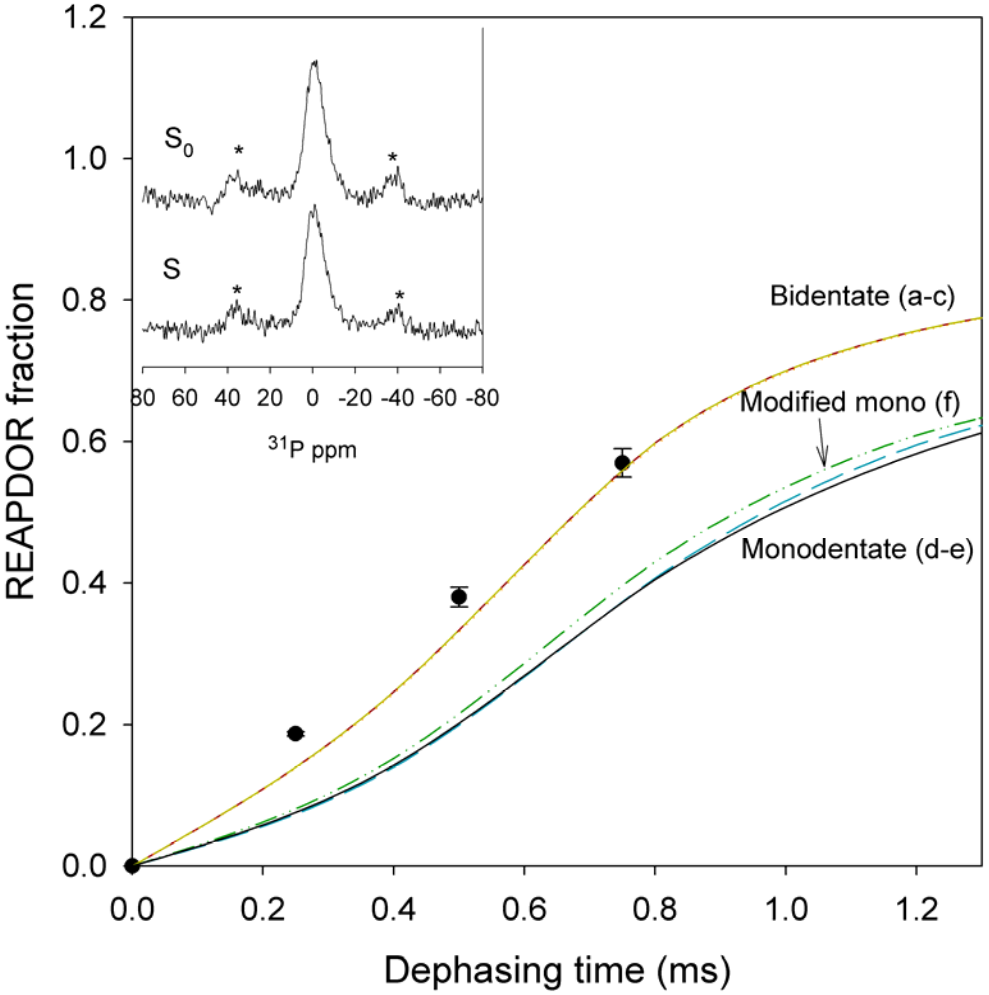

Figure 4.5 $^{31}P\{^{1}H\}/^{27}Al$ CP-REAPDOR data for the peak at δ_P = -2.6 ppm (●) in spectra of the sample at pH 5. Dash lines are calculated curves based on bidentate binuclear non protonated (BB-H_0) (a), bidentate binuclear mono-protonated phosphate (BB-H_1) (b), bidentate binuclear bi-protonated (BB-H_2) (c), monodentate mononuclear deprotonated [≡$AlPO_4$ (MM-H_0)] (d), and monodentate mononuclear mono-protonated (MM-H_1) (e), and a modified monodentate (f) structural models. Models (a-f) are from Figure 4.6 and model (f) is described in text section 3.3. Inset shows typical control (S_0) and ^{27}Al-dephased (S) spectra acquired with 8 kHz spinning rate, 0.5 s repetition delay, 1 ms CP contact time, 2 rotor cycles, and 101 588 scans.

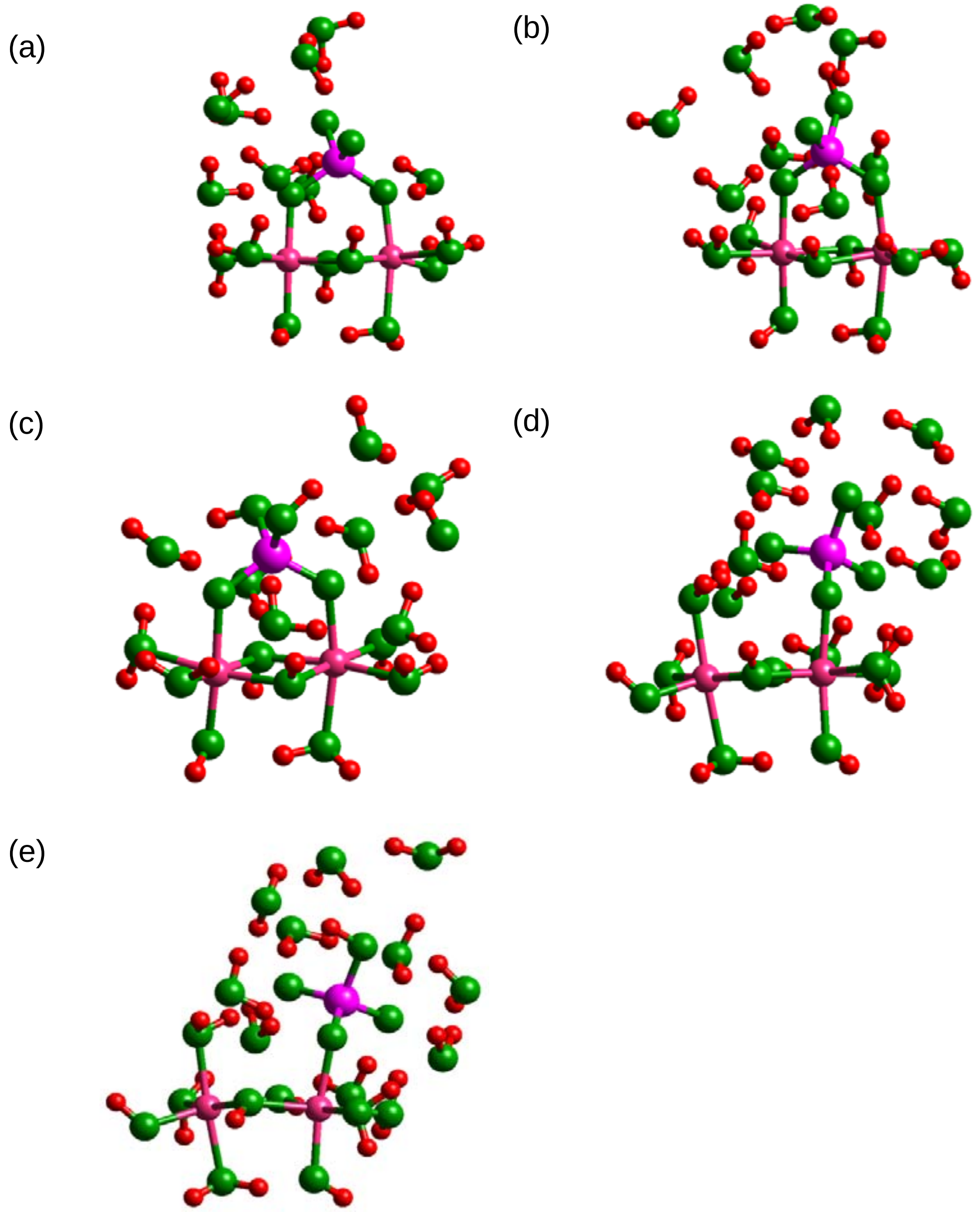

Figure 4.6 DFT minimized structures for five cluster models optimized at 6-31+Gd level theory. Atoms of P, Al, O and H are labeled as purple, pink, green and red balls respectively. The cluster models are bidentate binuclear non-protonated phosphate [$\equiv Al_2PO_4$ (BB-H_0)] (a), bidentate binuclear mono-protonated phosphate [$\equiv Al_2HPO_4$ (BB-H_1)] (b), bidentate binuclear bi-protonated phosphate [$\equiv Al_2H_2PO_4$ (BB-H_2)] (c), monodentate mononuclear non-protonated [$\equiv AlPO_4$ (MM-H_0)] (d), and monodentate mononuclear mono-protonated phosphate [$\equiv AlHPO_4$ (MM-H_1)] (e) molecular species.

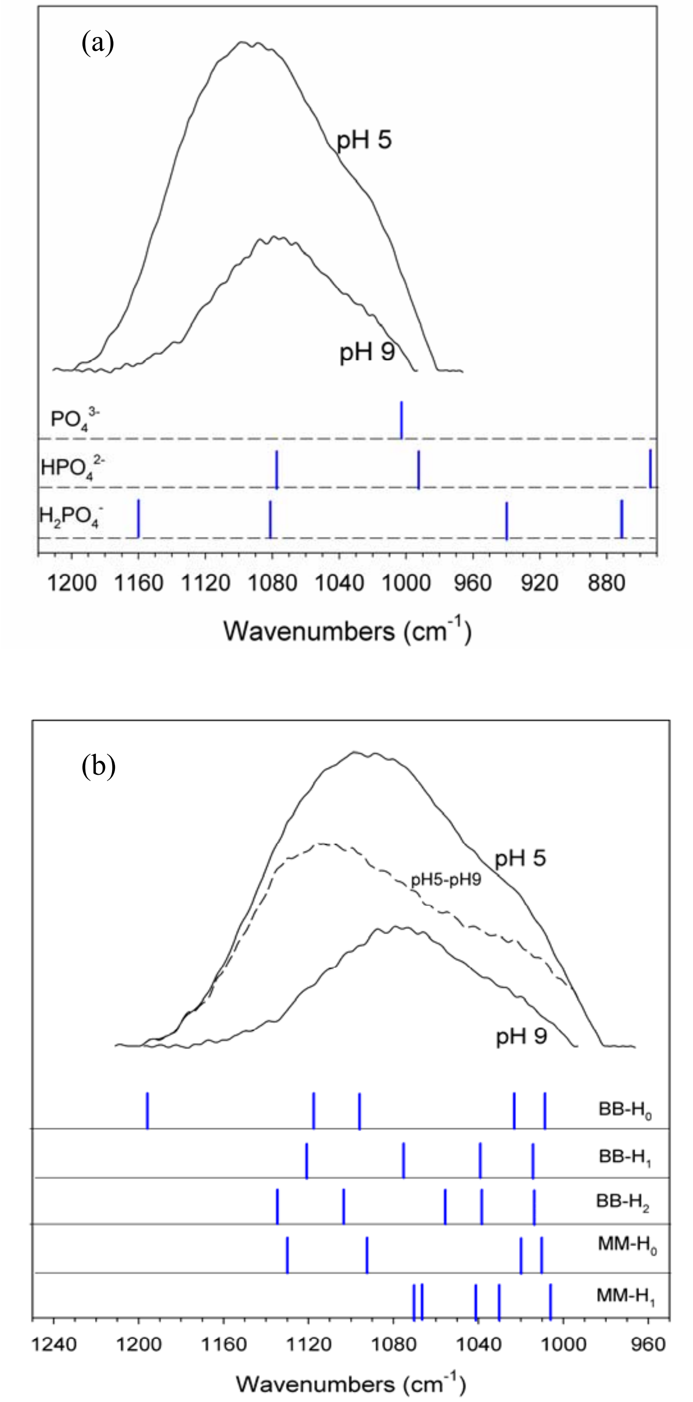

Figure 4.7 Phosphate stretching region of in-situ ATR-FTIR baseline-corrected difference spectra for phosphate absorbed on corundum at pH 5 and pH 9. (a) Comparison of observed spectra with frequencies observed for aqueous phosphate species [8]. (b) Comparison of observed spectra with stretching frequencies calculated for the adsorption surface complex models illustrated in Figure 4.6.

Chapter 5

Formation of hydroxylapatite during co-adsorption of calcium and phosphate on boehmite[*]

---

[*] This chapter has been submitted to the journal *Geochimica et Cosmochimica Acta*, and now is in revision. In this work, the X-ray diffraction experiment and data analysis were conducted by Wenqian Xu in Prof. John Parise's group.

Abstract

Calcium/phosphate interaction at mineral/water interface is of importance to both P sequestration and Ca-P mineralization. We investigated the effect of pH on calcium/phosphate co-adsorption on boehmite by batch studies, ^{31}P solid state NMR, powder XRD and SEM/EDX analysis. The results indicate precipitation of hydroxylapatite from pH 7 to pH 9. At pH 6, two major NMR peaks are observed at chemical shifts of 0 and -6 ppm, suggesting the presence of bidentate binuclear surface complexes with different protonation. At higher pH, an additional peak at 2.65 ppm is observed, indicative of the formation of hydroxylapatite. This is further supported by 2-d ^{31}P{^{1}H} heteronuclear correlation (HetCor) experiements with a ^{1}H resonance peak at 0.2 ppm that correlates to the ^{31}P peak at 2.65 ppm in the ^{31}P dimension. In powder X-ray diffraction patterns, XRD peaks at 2θ of 27° and 32° were observed, which match the two major XRD patterns of commercial hydroxylapatite. Nonetheless, hydroxylapatite single crystals are not observed in the SEM images, in agreement with its broad XRD peaks. Energy Dispersive X-ray spectroscopy reveal the Ca/P distribution on boehmite surface is inhomogeneous. Small amount of flocs was produced after the mixture of dissolved calcium and phosphate in the absence of boehmite, which was believed to be the precursor of the hydroxylapatite surface precipitates observed. The amorphous nature of these flocs indicates that boehmite surface has promoted their nucleation and crystallization.

Key words: NMR; phosphate; calcium, hydroxylapatite; adsorption; precipitation; Al oxyhydroxide; boehmite

5.1. Introduction

It has been extensively reported that presence of dissolved calcium facilitates the sequestration of phosphate in soil environments and control the phosphorus availability in alkaline settings [1-4]. At high calcium concentration, precipitation of calcium phosphates is an important mechanism for phosphorus immobilization [5].

However, there are very few studies of the precipitation process at the mineral water interface. Conceptually, detection and quantification of surface precipitates is difficult, largely as a result of low volume fraction and their disordered structures. In the phosphate/calcium co-adsorption system, crystallization of calcium phosphates from a supersaturated solution is very slow at room temperature [6], making it a challenge to predict phosphorus mobility. A more complicated situation results when common soil mineral substrates (i.e. metal oxides) are introduced. On the one hand, mineral surfaces could adsorb phosphate and calcium readily, thus reducing the ion activity products (IAP) of possible precipitates; and on the other hand, the mineral surface could serve as a substrate that reduces the nucleation barrier, favoring precipitation and crystal growth. The two opposing effects make it extremely difficult to predict the final products after mineral/fluid reaction. Will mineral precipitates form? If so, when and which mineral phases? To answer these fundamental questions, molecular level assessments of the surface speciation are necessary.

In principle, spectroscopic methods could provide molecular scale information for characterizing phosphorus speciation in environmental samples and allow direct identification of precipitates. Using attenuated total reflectance Fourier transform infrared (ATR-FTIR), Ronson and McQuilan (2002) [7] observed brushite ($CaHPO_4•2H_2O$) crystallization in the co-adsorption of calcium and phosphate on TiO_2 at pH 6.5. With ^{31}P NMR, Hunger and co-workers (2004) [8] identified the phosphorus speciation in alum-amended poultry litter**;** Cade-Menun et al. (2006) [9] characterized aquatic phosphorus in both dissolved and particulate states. X-ray absorption fine structure (XAFS) has been employed to examine the structure of Fe-phosphate, Al-phosphate minerals and mineral surface adsorbed phosphate [10], natural poultry litter [11] and manure amended soils [12, 13]. In addition, X-ray photoelectron spectroscopy (XPS) was used to study the nucleation of calcium phosphates on metal oxide thin films [14, 15]. Of these spectroscopic methods, NMR seems to be well-suited to investigate calcium/phosphate co-adsorption on boehmite, owing to its ability to resolve distinct chemical environments in heterogeneous samples [16-21] and calcium phosphates minerals [22-28].

Calcium orthophosphates exhibits similar chemical shifts and relatively broad line shapes; so that severe peak overlap is anticipated for heterogeneous systems in conventional one dimensional (1-D) ^{31}P NMR spectra. To overcome this challenge, both two-dimensional (2-D) and double resonance NMR techniques can be employed. These two techniques allow the detection of spatial connections between phosphate and protons and between phosphate and aluminum atoms. To determine the structure of phosphate adsorption surface complexes on boehmite [20], rotational echo adiabatic passage double resonance (REAPDOR) has been successfully used to identify P/Al monodentate coordination (Al-PO_4) and P/Al bidentate coordination (Al-PO_4-Al). 2-d ^{31}P{^{1}H} Heteronuclear Correlation (HetCor) was successfully applied to study the biomineralization of calcium phosphates, allowing identification from octacalcium phosphate (OCP) to hydroxylapatite (Hap) [28]**.** In another study, the detection of hydroxyl ion in bone mineral by 2-d ^{31}P{^{1}H} HetCor resolved a long-standing debate on the relationship between bone mineral and Hap [29]**.** The merit of 2-d HetCor techniques over direct observation of ^{1}H NMR is that the ^{1}H dimension of a 2-d spectrum is largely free of signal of surface and occluded waters and other H-bearing P-free compounds in the sample.

Here we apply those methods to the identify phosphate speciation on boehmite suspended in 10 mM $CaCl_2$ and 1 mM NaH_2PO_4 for 30 days in the range of pH 6-9. We found the co-existence of precipitates as hydroxylapatite and adsorbed phosphate bidentate binuclear surface complexes.

5.2. Materials and methods

5.2.1. Materials and reagent

Boehmite was purchased from CONDEA Chemie GmbH, and has a BET specific surface area of 136 m^2g^{-1} and pH_{PZC} of 9.1, as described in our previous work (Li et al., 2010). Stock solutions of 50 mM NaH_2PO_4 and 10mM $CaCl_2$ were prepared from ACS grade NaH_2PO_4 (Fisher) and $CaCl_2$ (Baker).

5.2.2. Sample preparation

A 0.25 g aliquot of dry boehmite powder was added to vigorously stirring 50 ml solution containing a 0.01 M $CaCl_2$ background electrolyte. An appropriate amount of 50 mM phosphate solution was added into the reaction vessel to reach 1mM total phosphorus concentration. Adsorption samples were prepared at a constant pH, ranging from pH 6 to pH 9, and aged in solution for 30 days. The pH was adjusted daily by addition of small amounts of 0.1 M or 0.01 M HCl/NaOH. After reaction, the suspensions were centrifuged (11000g, 15min) to separate the solid and solution. The supernatant was filtered through 0.2-μm PTFE membrane (Whatman, New Jersey) and analyzed for phosphorus by the Direct Coupled Plasma-Atomic Emission Spectroscopy (DCP-AES). The solid samples were quickly rinsed with a small volume of deionized water to remove residual salt and then air-dried for NMR measurements.

5.2.3. ^{31}P solid-state NMR

Solid-state ^{31}P single pulse (SP) MAS, $^{31}P\{^1H\}$ cross polarization magic angle spinning (CP/MAS) NMR spectra were collected with 7.5 mm Varian/Chemagnetics T3-type probe on a 400 MHz Varian Inova spectrometer (9.4 T), at operating frequencies of 161.8 MHz and 399.8 MHz for ^{31}P and ^{1}H, respectively. The ^{31}P SP/MAS spectra were obtained with a 90° excitation pulse of 8 μs and a 120 s relaxation delay. The $^{31}P\{^1H\}$ CP/MAS spectra were obtained with a spinning rate of 5 kHz and contact time of 1 ms. During the contact period the transverse ^{31}P field ($\gamma B_{1,P}$) was ramped linearly by ±5 kHz about the first sideband match. CP kinetics curves were measured at a spinning rate of 3 kHz with continuous wave (CW) irradiation at the n= -1 sideband match condition, with contact time varied from 0.3 ms to 7 ms. Proton decoupling was employed during acquisition of all $^{31}P\{^1H\}$ CP/MAS spectra. The ^{31}P chemical shifts are reported relative to external 85% H_3PO_4 solution, using hydroxylapatite as a secondary reference set to $\delta_{P\text{-}31}$ = 2.65 ppm.

2-D $^{31}P\{^1H\}$ heteronuclear correlation (HetCor) spectra were collected to obtain the ^{1}H spectra indirectly. The HetCor experiments employed a spinning rate of 10 kHz and a CP contact time of 1 ms, using a linear ramp of the ^{31}P B_1 field and 42 kHz ^{1}H field. We collected 150 hypercomplex points in t_1 with a 10 μs increment, corresponding to a 100 kHz spectral window in $F1$. For each spectrum, 300 to 400 scans were collected for each point at a 1 s relaxation delay. The spectra were acquired in ^{1}H-coupled mode, with no homonuclear ^{1}H decoupling pulses applied during t_1. Some HetCor experiments included a longer CP contact time (7 ms) to better distinguish signal from precipitates and adsorbates. The ^{1}H NMR chemical shifts ($\delta_{\text{H-1}}$) are referenced with respect to tetramethylsilane (TMS) using adamantane as a secondary reference set to $\delta_{\text{H-1}} = 2.0$ ppm.

^{31}P{^{1}H}/^{27}Al CP-REAPDOR [32] NMR spectra were obtained on a 500 MHz Varian Infinity plus spectrometer (11.7 T) with a 3-channel Varian/Chemagnetics T3 probe assembly configured for 4mm (o.d.) rotors. These experiments employed excitation of ^{31}P signal through ^{31}P{^{1}H} cross-polarization with a linear ramp of the ^{31}P field and 1 ms contact time. The ^{1}H 90° pulse length was 6 μs, and the relaxation delay 1 s. For REAPDOR, the ^{31}P 180° pulse length was 10 μs and the duration and strength of ^{27}Al pulse in the middle of the dephasing pulse train are 1/5 of the rotor period and 75 kHz.

5.2.4. Powder X-ray diffraction.

The powder X-ray diffraction (XRD) patterns were obtained on a Sintag powder diffractometer equipped with a copper target (Cu $K_{\alpha 1}$ radiation, $\lambda = 1.54060$ Å), a crystal graphite monochromator and a scintillation detector. The diffractometer was run at 45 kV and 25 mA. Dry powder samples were step-scanned from 5° to 80° 2θ with increments of 0.1° 2θ and a counting time of 6 s at each step, requiring about 6.5 hours to collect each pattern.

5.2.5. Scanning electron microscopy and energy dispersed X-ray spectroscopy

Scanning electron microscopy (SEM, Leo 1550, Japan) was employed to investigate the morphology of boehmite and any precipitates. Energy-dispersed X-ray (EDX) spectroscopy was used to estimate the Ca and P elemental distribution on the surface.

5.2.6. Speciation calculation

Thermodynamic calculations were carried out using the Geochemists' Workbench software package (Rockware, Inc.), to determine the aqueous phosphorus speciation in the initial solutions and the saturation state of possible solid precipitates. Saturation indexes (SI) for potential precipitates are listed in Table 1.

5.3. Results and discussion

5.3.1. Phosphorus speciation of in solution and solid state

Thermodynamic calculations indicate that a solution containing 1 mM [PO_4^{3-}] and 10 mM [Ca^{2+}] is over saturated. Thus, for all of our initial solution, for pH 6 to pH 9, the equilibrium phosphate concentration is controlled by Hap to a very low value. Calculated saturation indexes reveal that several other Ca-phosphate phases are also oversaturated within the pH range of 6-10, including brushite and amorphous calcium phosphate (ACP) (Table 1). In laboratory conditions, establishment of equilibrium is hindered due to the extremely slow crystallization kinetics of Hap at room temperature (Wang and Nancollas, 2008).

In this work, solutions with 10 mM [Ca^{2+}] and 1 mM [PO_4^{3-}] at pH 6-9 were prepared for comparison with adsorption experiments. At pH 6 and 7, no apparent precipitation phenomenon was observed. At pH 8 and pH 9, solutions were distinctly cloudy due to suspended white flocs. No discernible change was observed after saved for 30 days. These flocs could be colloidal ACP according to previous studies [23, 24, 33], which is a common product of mixing dissolved calcium and phosphate under conditions similar to those used here. Due to the extremely limited amount, we are unable to analyze the flocs in-situ, but their rapid appearance upon mixing is consistent with colloidal ACP. With high speed centrifugation (15,000 g), we have separated a very small amount of flocs at pH 9 for 30 days. Both ^{31}P SP/MAS (Figure. 5.1f) , $^{31}P\{^{1}H\}$ CP/MAS (Figure 5.2g) and $^{31}P\{^{1}H\}$ HetCor (Figure 5.5f) spectra were collected for air-dried sample to determine its strcuture.

5.3.2. Phosphate uptake

Table 5.2 summarizes the P-uptake results for the four samples prepared for NMR measurements. Phosphate is readily removed from solution under these conditions, with the uptake of phosphate varying from 87% at pH 6 and to almost 100% at pH 9

(Table 5.2). The pH effect on phosphate sorption with the $CaCl_2$ electrolyte solution differs from that with NaCl background where phosphate loading decreases with increasing pH. The elemental distribution on the particle surface as observed by SEM/EDX revealed that calcium co-adsorption is involved and might contribute the phosphate uptake. However, interaction between calcium and phosphate could not be discerned by such analytical methods. Mechanism for the mutual interaction between phosphate ions and calcium ions on boehmite surface is further investigated by ^{31}P solid state NMR spectroscopy.

5.3.3. ^{31}P single pulse NMR spectra

Figure 5.1 shows ^{31}P single pulse NMR spectra collected for four phosphate uptake samples reacted for 30 days at constant pH from pH 6 to pH 9 in 10 mM $CaCl_2$ background solution. A spectrum of commercial Hap (Figure 5.1g) is indicated for comparison.

The NMR spectra show changes with pH. At pH 6 (sample Cabmt6), a broad asymmetric peak with FWHM of ca. 12 ppm was observed. This broad resonance could be fitted with two distinct peaks, at 0 and -6 ppm, in which is supported by resolution of these two peaks in its 2-d HetCor spectrum. The two peaks are assigned to deprotonated and mono-protonated bidentate binuclear surface complexes respectively by comparison to previous results for phosphate adsorption on boehmite in the absence of calcium [20]. The spectrum for sample prepared at pH 7 (Cabmt7) differs remarkably from that of the Cabmt6 sample, with one appearance of a sharp peak at 2.6 ppm, 2.5 ppm FWHM and one broad peak centered near -6 ppm with FWMH of 7.5 ppm. The narrow peak observed for samples prepared at pH 7 (Cabmt7) to pH 9 (Cabmt9) resembles that of Hap, suggesting the presence of calcium phosphate precipitates. The peak at -6 ppm can be assigned to mono-protonated bidentate binuclear surface complexes as described above. For the samples Cabmt8 and Cabmt9, only the sharp peaks are apparent in the SP spectra, suggesting that precipitate is the major species. The narrow peak is similar to that for Hap in both chemical shift and peak width. In addition, for all samples this narrow peak also exhibits small intensity of spin sidebands observed in the spectra of the pH 7-9 samples, indicative of small chemical shift anisotropy (CSA), which is also confirmed with assignment to Hap. For the air-dried flocs, Figure 5.1f yields a single peak at 2.6 ppm with a full width at half maximum (FWHM) of 2.8 ppm, suggesting a possibility of the formation of Hap.

5.3.4. $^{31}P\{^1H\}$ CP/MAS spectra

The $^{31}P\{^1H\}$ CP/MAS NMR spectra (Figure 5.2) of those samples mentioned above are similar in chemical shift to the single pulse spectra (Figure 5.1) but with slight differences in line shape. For the sample Cabmt6, apparent two distinct two peaks were observed with chemical shifts at at 0 and -6 ppm respectively, with FWHM of 3.5 and 7 ppm. For sample Cabmt7, the two peaks at 0 and -6 ppm are still clearly observed. Besides those two peaks, an additional peak appears at about 2.6 ppm. For sample Cabmt8, the peak at 2.6 ppm become evident and overlaps severely with the peak at 0 ppm. There is still some signal from the peak at -6 ppm. The spectrum of sample Cabmt9 is similar to that of Cabmt8, but with intensity of the peak at 0 ppm and -6 ppm reduced. An additional CP/MAS spectrum (Figure 5.3f) was collected for Cabmt9 with longer CP contact time (7 ms), which only shows a single peak at 2.6 ppm with FWHM of 2 ppm, similar to that of commercial Hap (Figure 5.2h). In its $^{31}P\{^1H\}$ CP/MAS spectrum (Figure 2g), a peak at the same position (δ_P = 2.6 ppm) shows up with FWHM of 4.1 ppm, much broader than that of commercial Hap (Figure 5.2h), which is usually 1.5 – 1.8 ppm. This broad peak suggests that the flocs might contain ACP.

The ^{31}P signals in the $^{31}P\{^1H\}$ CP/MAS spectra are transferred from the closest ^1H through the ^1H-^{31}P dipolar coupling, so that the ^{31}P signals depends on the ^{31}P-^1H distance and numbers of neighboring protons [34]. The signal intensity varies with contact time according to the classical biexponential equation

$$I(\tau) = I_0\left[1 - \frac{T_{PH}}{T_{1\rho,H}}\right]^{-1}\left[1 - \exp\left(-\frac{T_{PH}}{\tau}\right)\right]\exp\left(-\frac{T_{1\rho,H}}{\tau}\right) \qquad (1)$$

where T_{PH} is the characteristic time for $^1H \rightarrow ^{31}P$ magnetization transfer, τ is the CP contact time and $T_{1\rho,H}$ is the time constant for decay of the ^1H magnetization in the rotating frame [35]. For Hap, ^{31}P and ^1H are weakly coupled and rigid, yielding large values for T_{PH} and $T_{1,\rho}$. As a result, the signals of adsorbed phosphate are more significantly magnified than that of Hap, so that the -6 ppm peak can be always observed at any pH in CP spectra but disappears in SP spectra at high pH. Quantitatively, CP kinetics suggested that different peaks showed different effect as a function of CP contact time (Figure 5.3). The peak at 0 ppm or -6 ppm build up the polarization of quickly in 1 ms CP contact time and decay significantly as contact time goes longer while the peak at 2.6 ppm builds up its polarization slightly slower but holds the maximum intensity for a long time to 7 ms. This explains the disappearance of the two peaks at 0 and -6 ppm in Figure 5.2f, where a 7 ms contact time is chosen and only signals from Hap remains.

3.5 ^{31}P{^{1}H} HetCor

We acquired ^{31}P{^{1}H} HetCor spectra of the Ca/P co-sorption samples to distinguish hydrogen environments near different phosphate sites. This experiment correlates ^{31}P peak with signals from 1H in close spatial proximity, from which polarization is transferred during the CP contact period.

Figure 5.4 shows a typical ^{31}P{^{1}H} HetCor spectrum, obtained for the boehmite/phosphate sample Cabmt9 at 1ms CP contact time. The spectrum in the centre is a typical 2-d contour plot with the sum projection of F2 (^{31}P) dimension on the left and the sum projction of F1 (^{1}H) on the top. The ^{31}P projection closely resembles the CP/MAS spectrum of the same sample (Figure 5.2e), and the ^{1}H projection contains signal only from H near phosphate. Another two slices of ^{1}H projection are taken at ^{31}P chemical shift of 0 ppm and 2.65ppm. Within the 2-d contour, two different domains are clearly distinguished. A more condensed contour density corresponds to correlation of the sharp peak at δ_{H-1} = 0.2 ppm in F1 with a peak at δ_{P-31} = 2.65 ppm in F2. These values correspond exactly to those reported for Hap [28], which are unique among Ca-phosphates. In particular, the hydroxyl group in Hap yields a narrow ^{1}H signal at 0.2 ppm that is unique. The domain centered atδ_{H-1} = +5 ppm andδ_{P-31} = 0 ppm (+5,0) is assigned to adsorbed phosphate on the boehmite surface because it is very similar to ^{31}P{^{1}H} HetCor spectra of phosphate/boehmite adsorption samples prepared in NaCl solution [20] in both contour shape and proton environment. Furthermore, the domain (+5, 0) is not observed in the spectrum collected at 7ms CP contact time (data not shown), consistent with the short $T_{1,\rho}$ of adsorbed phosphate, which shows a peak only for Hap.

It is worth noting that in the HetCor spectrum at 1 ms CP contact time, signal from adsorbed phosphate is clearly observed, overlapping the Hap peak in the ^{31}P dimension and in the CP/MAS spectra, but which is not discernable in the its corresponding ^{31}P single pulse spectrum. This result suggests that adsorbed phosphate co-exists with Hap but the amount is in very small amount and is greatly enhanced in the CP and HetCor spectra. The overlapped peaks in the ^{31}P dimension makes the accurate quantification challenging.

In Figure 5.5, ^{1}H slices taken at $\delta_{P\text{-}31}$ = 2.65 ppm from ^{31}P{^{1}H} HetCor spectra for different samples are stacked for comparison with (b) to (f) scaled to the height of the sharp peak at about δ_H = 0.2 ppm. From sample Cabmt7 to Cabmt9, ^{1}H slices that correlates to the 2.65 ppm speak in ^{31}P dimension. For both pH 7 (Cabmt7) and pH 8 samples (Cabmt8), the same sharp peak at 0.2 ppm and broad peak at 5 ppm indicating occurrence of both Hap precipitates and surface phosphate complexes, similar to the pH 9 sample (Cabmt9). However, the spectrum for the Cabmt7 is slightly different from that for the Cabmt8 sample in the relative intensity of the ^{1}H peak at 5 ppm. The difference suggests Cabmt7 contains less Hap and more surface adsorbed phosphate than the Cabmt8 does, which is in agreement with the quantitative analysis of ^{31}P single pulse spectra in Figure 5.1. The ^{1}H slice for Cabmt6 is much noisier and contains only a broad feature noticeable at about 5ppm. A closer inspection of the 2-d contour plots reveals great similarity with the ^{31}P{^{1}H} HetCor spectrum reported previously for those samples prepared in the NaCl [20]. Considering its ^{31}P single pulse spectrum as well, we conclude that only surface complexes formed at Cabmt6 with no Hap precipitates detected.

5.3.6. Powder X-ray diffraction

Given the strong evidence from NMR spectroscopy for the presence of apatite precipitates, powder X-ray diffraction patterns were obtained for several samples in an attempt to detect the Hap phase. Figure 5.6 shows the diffraction patterns of the initial boehmite sorbent and ca/phosphate sorbed sample prepapred at pH 9 (Cabmt9). The diffraction pattern for the adsorbent could be indexed well to pure boehmite with no evidence for impurities. The slightly broad peaks are consistent with the nano-sized particles observed by TEM. XRD patterns of sample Cabmt9 show additional peaks at 25-35° not evident in the diffraction patterns for the boehmite substrate. The two additional peaks, one at 27° and the other 32°, match the major peaks of hydroxylapatite, and can be indexed to (002) and (121) + (112) + (030) respectively. These reflections are diagnostic since other calcium phosphates do not yield major diffraction peaks near these position. This result confirms the surface precipitates observed by NMR as Hap. The diffraction peaks observed for Hap are distinctly broadened compared to well crystalline Hap, indicating poor crystallization and/or small particle size.

A systematic investigation of the samples prepared at different pH (inset of Figure 5.6) reveals that the intensities of the peaks at 27° and 32° decreases gradually from pH 9 to 6. This result confirms the observation of Hap in pH 7 and pH 8 samples by NMR spectroscopy. The observation indicates that Hap precipitates favor higher pH condition [36]. A very small feature near 32° 2θ occurs in the pattern of the pH 6 sample (Cabmt6) nearly within the noise, although no Hap was detected by NMR. It is possible that surface precipitates occur in the Cabmt6 sample at near or below the detection limit of the XRD and NMR methods used in this study. Nonetheless, the ^{31}P NMR data (Figure 5.1b and 5.2b) show that nearly all phosphate taken up at pH 6 occurs as surface complexes.

5.3.7. ^{31}P{^{27}Al} REAPDOR

The ^{31}P{^{27}Al} REAPDOR NMR experiments [32] were performed to qualitatively identify the structure of adsorbed phosphate bidendate or monodentate, by measuring the ^{31}P–^{27}Al heteronuclear dipolar interaction which depends on the interatomic distances and geometry [20]. Experimentally, sets of two ^{31}P-observed NMR spectra are acquired, one (S) obtained with a heteronuclear dipolar dephasing sequence and a control spectrum (S_0) acquired under identical conditions but without irradiation at the ^{27}Al frequency. The difference in peak intensity between the dephased spectrum and the control ($\Delta S = S_0 - S$) depends on the ^{31}P–^{27}Al heteronuclear dipolar coupling and the length of the dephasing period (τ). Figure 5.7 shows a typical set of ^{31}P–^{27}Al REAPDOR NMR spectra acquired for Ca/phosphate adsorbed sample prepared at pH 7 (Cabmt7) with 0.75 ms dephasing time (product of the number of rotor cycles and rotor period). The difference in peak intensity between the top and bottom spectra, ΔS, represents the influence of ^{31}P–^{27}Al dipolar coupling at this dephasing time. The REAPDOR fraction $\Delta S/S_0$ characterizes the magnitude of ^{31}P–^{27}Al heteronuclear dipolar coupling interactions and can be used to distinguish between bidentate and monodentate as described by Li et al. (2010) [20]. The $\Delta S/S_0$ for the peaks at 0 and -6 ppm are 0.69 and 0.64, respectively, similar to those observed previously for phosphate adsorbed on boehmite in NaCl solutions [20], supporting an assignment of the two peaks to the bridging bidentate surface complexes. For comparison, calculated monodentate structure models give a $\Delta S/S_0$ of 0.34, which differs from the experimental data. This result indicate that the presence of Ca does not alter the coordination of adsorbed phosphate to surface Al compared to that in NaCl solutions.

5.3.8. SEM and EDX analysis

SEM was employed to examine the morphology of Hap phases in the sample Cabmt9 (Figure 5.8) and EDX was used to examine the surface Ca/P distribution. In the SEM images (Figure 5.8), only fine particles of boehmite are observed, that no particles with distinct morphology could be identified as Hap crystals. This result suggests that the Hap is poorly crystallized and might be smaller size even than the boehmite particles. Some composition variation is observed between regions with differing brightness, labeled as ‘Dark’ (Figure 5.8b) and ‘Bright’ (Figure 5.8c). No significant difference in terms of morphology would be distinguished between the two regions, but EDX analysis reveal apparent differences in Ca/P content as well as in Ca/P ratio. The Ca /P ratio in the bright region is estimated to be 1.12, which is consistent with the co-existence of Hap and adsorbed phosphate. According to Wang and Nancollas (2008) [6], Ca/P ratio in Hap surface composition is around 1.5.

Nonetheless, no discernable Hap particles could be directly observed at this scale. It should be noted that the Ca/P content showed difference in the two regions, suggesting an inhomogeneous reaction process most possibly with adsorption and precipitation reactions happening simultaneously.

5.3.9. Effect of residence time

We prepared two calcium/phosphate co-adsorption samples with a short reaction time of 15 minutes at pH 7 and pH 9 respectively. Figure 5.9 shows ^{31}P single pulse NMR spectra collected for these two samples and the compared samples. The spectra show changes with reaction time. The -12 ppm peak arises from the rotor as background (Li et al., 2010)[20], and peaks at 0 and -6 ppm are assigned to adsorbed phosphate surface complexes. However, in a 30 day reaction sample (Figure 5.7b, also Figure 5.1c)), a major peak at 2.65 ppm is observed with an additional peak at -6 ppm, suggesting Hap forms after long time (days) reaction.

At pH 9, the spectrum for 15 minutes reaction sample (Figure 5.9c) is almost identical with that for 30 days reaction sample (Figure 5.9d), with only one single peak at 2.65 ppm. However, their $^{31}P\{^{1}H\}$ HetCor spectra show differences, as appeared in their ^{1}H sum projection (Figure 5.10). In Figure 5.10a, we observed one sharp peak at $\delta_H = 0.2$ ppm with FWHM of 0.2 ppm, one broad peak at $\delta_H = 5.4$ ppm with FWHM of 6 ppm and one small shoulder at about $\delta_H = 12$ ppm, which are clearly presented in the simulation spectrum (Figure 5.10c). The peak at 12 ppm could be assigned to be brushite, while the peak at $\delta_H = 0.2$ and 5.4 ppm arise from Hap and adsorbed phosphate. With clear inspection of peak intensity, we found that the ratio of the intensity of peak at 0.2 ppm over the total intensity in Figure 5.10b is larger than that in Figure 5.10a. This means longer time reaction sample contains more Hap precipitates. From the above analysis, we conclude that Hap mainly forms in long time reaction from the calcification adsorbed phosphate and crystallization of Ca-P flocs.

5.4. Conclusion

In this work, using ^{31}P solid state NMR spectroscopy and powder X-ray diffraction, we examined a long time phosphate adsorption behavior in 0.01 M $CaCl_2$ background electrolyte solution as a function of pH. Our objective was to characterize the phosphate speciation in those calcium/phosphate co-adsorption samples in a molecular level. Batch adsorption data indicate the presence of dissolved calcium facilitates phosphate removal by boehmite, especially at high pH conditions. Molecular scale information obtained from spectroscopic techniques demonstrates that adsorption reaction is main mechanism for phosphate immobilization at pH 6 and precipitation reaction dominates at higher pH. From pH 7 to pH 9, hydroxylapatite precipitates were identified by both ^{31}P NMR and XRD. According to SEM/EDX analysis of the sample prepared at pH 9, different Ca/P content was found between different regions, suggesting a heterogeneous reaction process.

To understand the formation of hydroxylapatite precipitates, flocs formed in mixture of dissolved calcium and phosphate solution prepared at pH 9 were analyzed after air-dried. ^{31}P NMR spectra suggest the flocs contain both amorphous calcium phosphate and poorly crystalline hydroxylapatite. Such flocs should have even more disordered structure in solution, since no apparent hydroxylapaite crystals were observed in the SEM images of adsorption samples.

References

[1] Barrow, N. J., *Soil Sci.* **1972**, *113*, 175-180.

[2] Barrow, N. J.; Bowden, J. W.; Posner, A. M.; Quirk, J. P., *Aust. J. Soil Res.* **1980**, *18*, 395-404.

[3] Gimsing, A. L.; Borggaard, O. K., *Clays Clay Miner.* **2001,** *49*, 270-275.

[4] Rietra, R. P. J. J.; Hiemstra, T.; Van Riemsdijk, W. H., *Environ. Sci. Technol.* **2001**, *35*, 3369-3374.

[5] Tunesi, S.; Poggi, V.; Gessa, C., *Nutr. Cycl. Agroecosys.* **1999**, *53*, 219-227.

[6] Wang, L. J.; Nancollas, G. H., *Chem. Rev.* **2008**, *108*, 4628-4669.

[7] Ronson, T. K.; McQuillan, A. J., *Langmuir* **2002**, *18*, 5019-5022.

[8] Hunger, S.; Cho, H.; Sims, J. T.; Sparks, D. L., *Environ. Sci. Technol.* **2004**, *38*,

674-681.

[9] Cade-Menun, B. J.; Navaratnam, J. A.; Walbridge, M. R., *Environ. Sci. Technol.* **2006**, *40*, 7874-7880.

[10] Hesterberg, D.; Zhou, W. Q.; Hutchison, K. J.; Beauchemin, S.; Sayers, D. E., *J. Synchrotron Rad.* **1999**, *6*, 636-638.

[11] Peak, D.; Sims, J. T.; Sparks, D. L., *Environ. Sci. Technol.* **2002**, *36*, 4253-4261.

[12] Hansen, J. C.; Cade-Menun, B. J.; Strawn, D. G., *J. Environ. Qual.* **2004**, *33*, 1521-1527.

[13] Sato, S.; Solomon, D.; Hyland, C.; Ketterings, Q. M.; Lehmann, J., *Environ. Sci. Technol.* **2005**, *39*, 7485-7491.

[14] Nooney, M. G.; Campbell, A.; Murrell, T. S.; Lin, X. F.; Hossner, L. R.; Chusuei, C. C.; Goodman, D. W., *Langmuir* **1998**, *14*, 2750-2755.

[15] Chusuei, C. C.; Goodman, D. W.; Van Stipdonk, M. J.; Justes, D. R.; Loh, K. H.; Schweikert, E. A., *Langmuir* **1999**, *15*, 7355-7360.

[16] Ingall, E. D.; Schroeder, P. A.; Berner, R. A., *Geochim. Cosmochim. Acta* **1990**, *54*, 2617-2620.

[17] Cade-Menun, B. J., *Talanta* **2005**, *66*, 359-371.

[18] Sannigrahi, P.; Ingall, E. D.; Benner, R., *Geochim. Cosmochim. Acta* **2006**, *70*, 5868-5882.

[19] Conte, P.; Smejkalova, D.; Piccolo, A.; Spaccini, R., *Eur. J. Soil Sci.* **2008**, *59*, 584-591.

[20] Li, W.; Feng, J.; Kwon, K. D.; Kubicki, J. D.; Phillips, B. L., *Langmuir* **2010**, *26*, 4753-4761.

[21] Negassa, W.; Kruse, J.; Michalik, D.; Appathurai, N.; Zuin, L.; Leinweber, P., *Environ. Sci. Technol.* **2010**, *44*, 2092-2097.

[22] Rothwell, W. P.; Waugh, J. S.; Yesinowski, J. P., *J. Amer. Chem. Soc.* **1980**, *102*, 2637-2643.

[23] Yesinowski, J. P., *J. Amer. Chem. Soc.* **1981**, *103*, 6266-6267.

[24] Yesinowski, J. P.; Benedict, J. J., *Calc. Tiss. Int.* **1983**, *35*, 284-286.

[25] Yesinowski, J. P.; Eckert, H., *J. Amer. Chem. Soc.* **1987**, *109*, 6274-6282.

[26] Yesinowski, J. P.; Eckert, H.; Rossman, G. R., *J. Amer. Chem. Soc.* **1988**, *110*, 1367-1375.

[27] Tseng, Y. H.; Zhan, J. H.; Lin, K. S. K.; Mou, C. Y.; Chan, J. C. C., *Solid State Nucl. Magn. Reson.* **2004**, *26*, 99-104.

[28] Tseng, Y. H.; Mou, C. Y.; Chan, J. C. C., *J. Amer. Chem. Soc.* **2006**, *128*, 6909-6918.

[29] Cho, G. Y.; Wu, Y. T.; Ackerman, J. L., *Science* **2003**, *300*, 1123-1127.

[30] Hartz, T. K.; Johnstone, P. R.; Smith, R. F.; Cahn, M. D. *Hort Sci.* **2007**, *42*, 1681-1684.

[31] Hawke, D.; Carpenter, P. D.; Hunter, K. A., *Environ. Sci. Technol.* **1989**, *23*, 187-191.

[32] Chopin, L.; Vega, S.; Gullion, T., *J. Amer. Chem. Soc.* **1998**, *120*, 4406-4409.

[33] Lee, Y. J.; Stephens, P. W.; Tang, Y.; Li, W.; Phillips, B. L.; Parise, J. B.; Reeder, R. J., *Am. Mineral.* **2009**, *94*, 666-675.

[34] Mehring, M., *Principles of High Resolution NMR in Solids*. 2nd ed ed.; Springer-Verlag: Berlin, 1983.

[35] Kolodziejski, W.; Klinowski, J., *Chem. Rev.* **2002**, *102*, 613-628.

[36] Chairat, C.; Schott, J.; Oelkers, E. H.; Lartigue, J. E.; Harouiya, N., *Geochim. Cosmochim. Acta* **2007**, *71*, 5901-5912.

Tables and figures

Table 5.1 Ionic activity products (IAP) and saturation indices (SI) of possible precipitates for initial solution compositions at 298K.

Mineral phases	CaP-pH6		CaP-pH7		CaP-pH8		CaP-pH9	
	Log(IAP)	SI	Log(IAP)	SI	Log(IAP)	SI	Log(IAP)	SI
$Ca_3(PO_4)_2$ (am1)	-28.42	-2.917	-25.26	0.244	-23.09	2.414	-21.79	3.709
$Ca_3(PO_4)_2$ (am2)	-28.42	-0.1670	-25.26	2.994	-23.09	5.164	-21.79	6.459
$Ca_3(PO_4)_2$ (beta)	-28.42	0.5030	-25.26	3.664	-23.09	5.834	-21.79	7.129
$Ca_4H(PO_4)_3{\bullet}3H_2O$	-47.48	0.4690	-43.73	4.217	-41.47	6.476	-40.53	7.424
$CaHPO_4$	-19.06	0.2120	-18.48	0.7980	-18.39	0.887	-18.74	0.540
$CaHPO_4{\bullet}2H_2O$	-19.06	-0.068	-18.48	0.5180	-18.39	0.607	-18.74	0.260
Hydroxyapatite	-37.77	6.561	-32.03	12.30	-27.78	16.55	-24.85	19.49
Lime	9.709	-22.99	11.70	-21.00	13.69	-19.01	15.68	-17.0
Portlandite	9.709	-13.00	11.70	-11.01	13.69	-9.013	15.68	-7.03

Table 5.2 Results of calcium/phosphate co-uptake experiments and from least-squares fits to corresponding ^{31}P NMR spectra

		P%	^{31}P NMR peak intensity		
Sample label	pH	uptake	2.65 ppm,	0 ppm,	-6 ppm
CaBmt6	6	87%	N/A	37%	63%
CaBmt7	7	97%	25%	49%	26%
CaBmt8	8	98%	81%	19%	N/A
CaBmt9	9	99%	100%	N/A	N/A
Hap	N/A	N/A	100%		
BmtpH6	5	72%		43%	57%

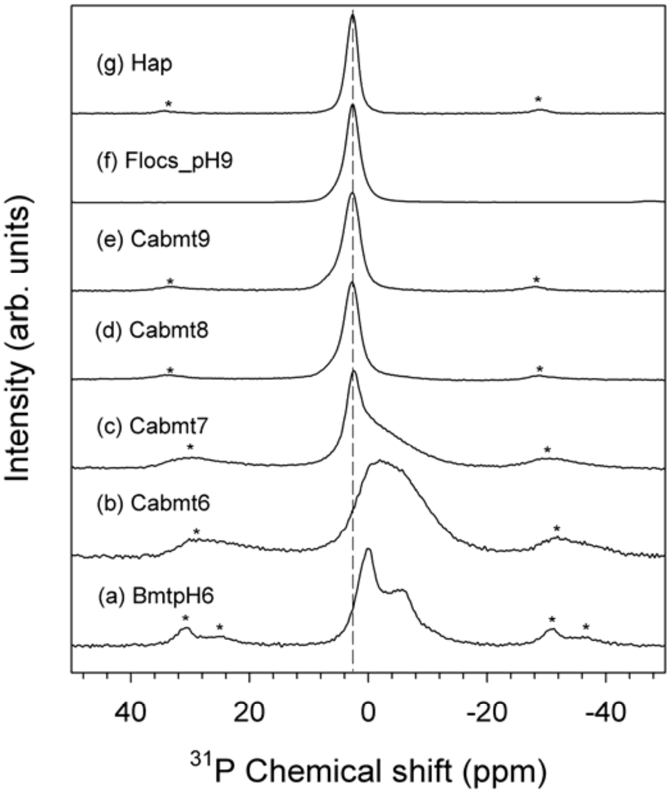

Figure 5.1 ^{31}P SP/MAS NMR spectra of phosphate adsorbed by boehmite at the indicated pH values (a-e), of flocs formed in solution at pH 9 (f) and commercial hydroxylapatite (g) for comparison. Background electrolyte was 10 mM $CaCl_2$ for b-e, and NaCl for a. Spectra were collected at a spinning rate of 5 kHz (a-e, g) and 8 kHz (f), pulse delay of 120s and about 300 - 400 scans.

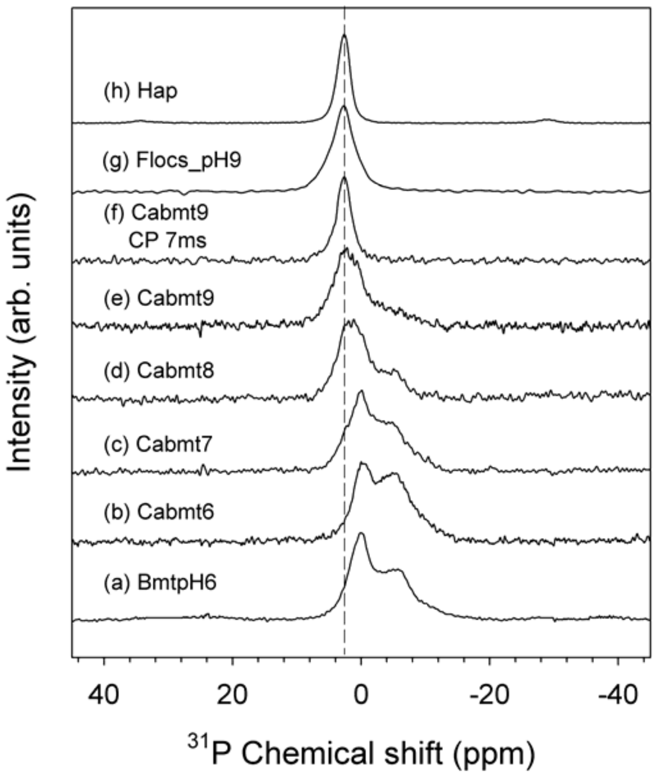

Figure 5.2 $^{31}P\{^{1}H\}$ CP/MAS NMR spectra of phosphate adsorbed by boehmite at the indicated pH values (a-f), of flocs form in solution at pH 9 (g) and of commercial hydroxylapatite (h) for comparison. Background electrolyte was 10 mM $CaCl_2$ for b-e , and NaCl for a. Spectra were collected at a spinning rate of 10 kHz (a-f) and 8 kHz (g), contact time of 1 ms, pulse delay of 1 s and about 200 - 300 scans.

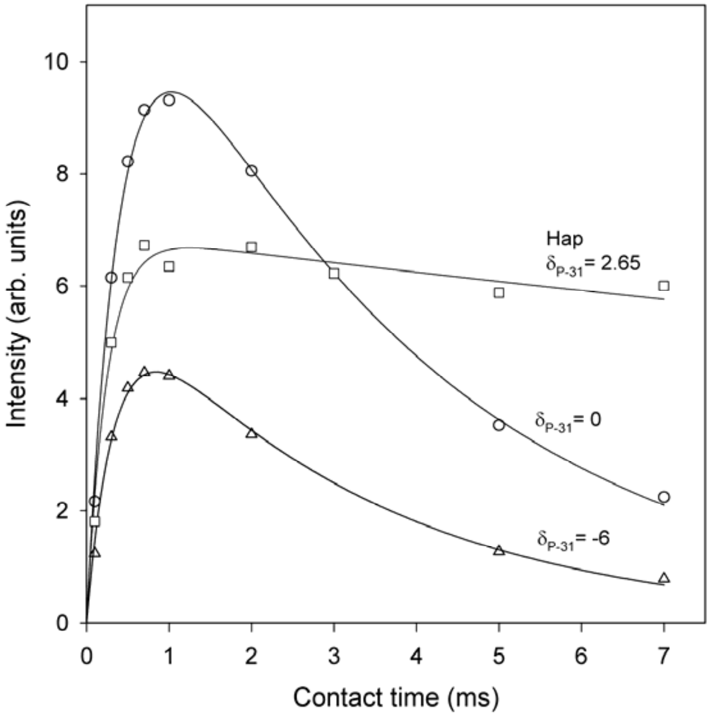

Figure 5.3 $^{31}P\{^1H\}$ CP/MAS kinetics of the peak at 2.65 ppm for commercial Hap and the two peaks at 0 and -6 ppm for the sample BmtpH6 in Figure 1a.

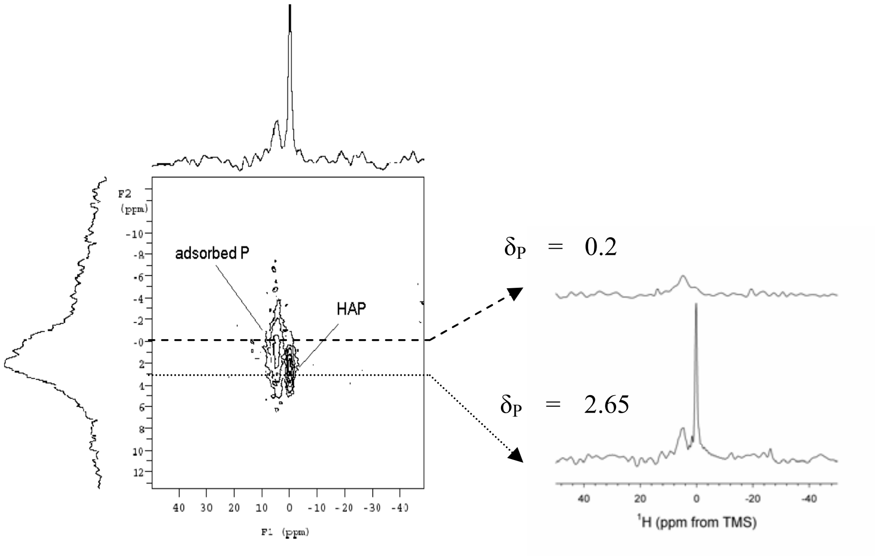

Figure 5.4 Left: $^{31}P\{^1H\}$ CP-HetCor spectrum of Ca/phosphate co-sorption sample prepared at pH 9 (Cabmt9). Typical 2-d contour plot at center; the spectra on top and on the right are summed projection of F1 (^{1}H) and F2 (^{31}P) respectively. Right: ^{1}H slices taken at δ_P of 0.2 and 2.65 ppm. Spectrum was collected with a spinning rate of 10 kHz, 1 ms CP contact time, 1s repetition delay and 382 scans for each point.

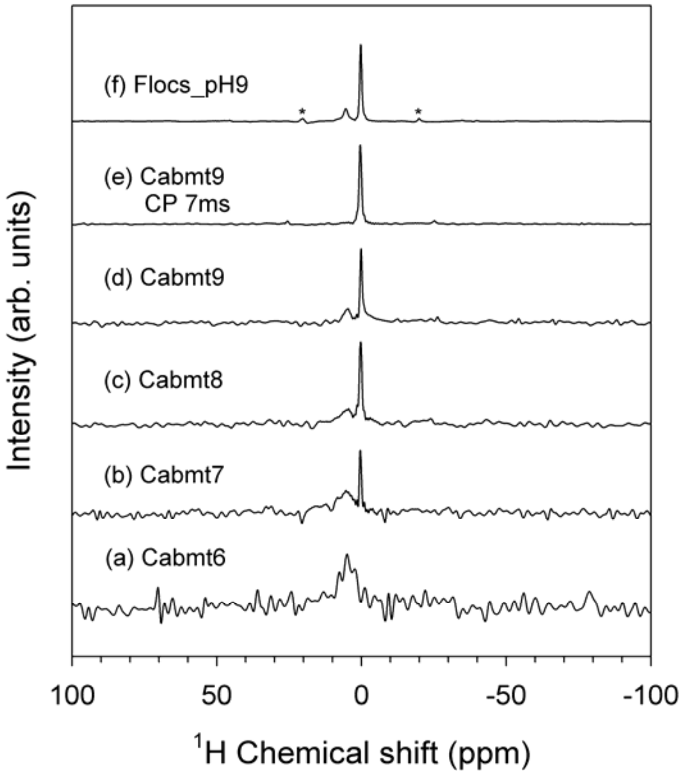

Figure 5.5 ^{1}H slices from 2-D ^{31}P{^{1}H} HetCor spectra of Ca/phosphate adsorbed samples (a-e) and of the flocs formed in solution at pH 9, taken at the ^{31}P position of 2.65 ppm. Spectra were collected at a spinning rate of 10 kHz (a-e) and 8 kHz (f), CP contact time of 1 ms, and ca. 300 scans. Spectrum (e) were collected at 7 ms CP contact time, with other conditions the same as (d).

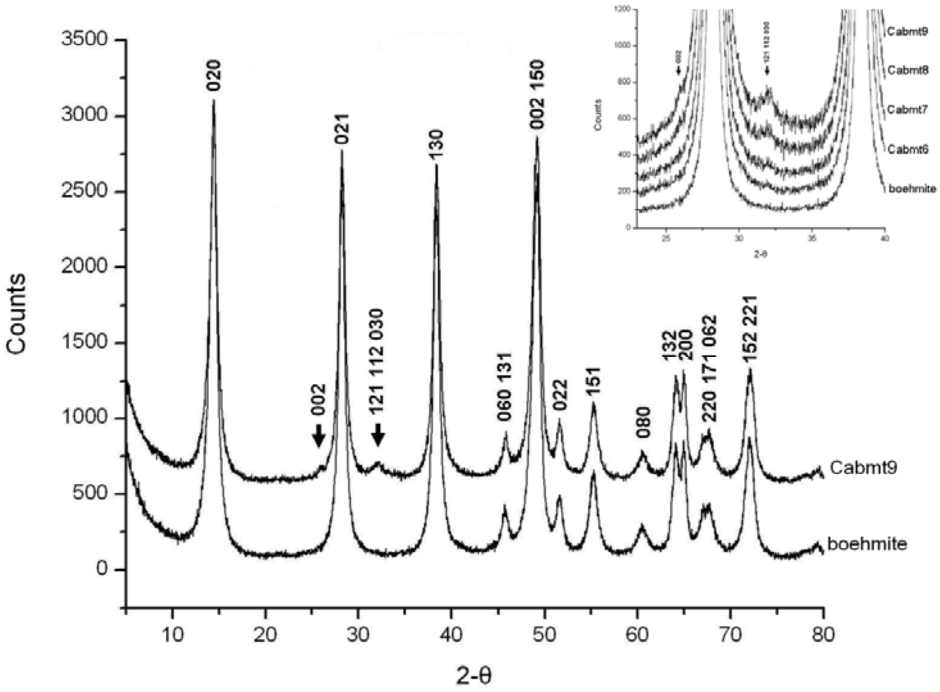

Figure 5.6 Powder X-ray diffraction patterns for boehmite and Ca/phosphate sorbed by boehmite at different pH 9 (Cabmt9). Reflections indexed to Hap are denoted by arrows. Inset: the diffraction patterns for boehmite and Ca/P adsorbed sample from pH 6 (Cabmt6) to pH 9 (Cabmt9) in the range between 20° to 40°.

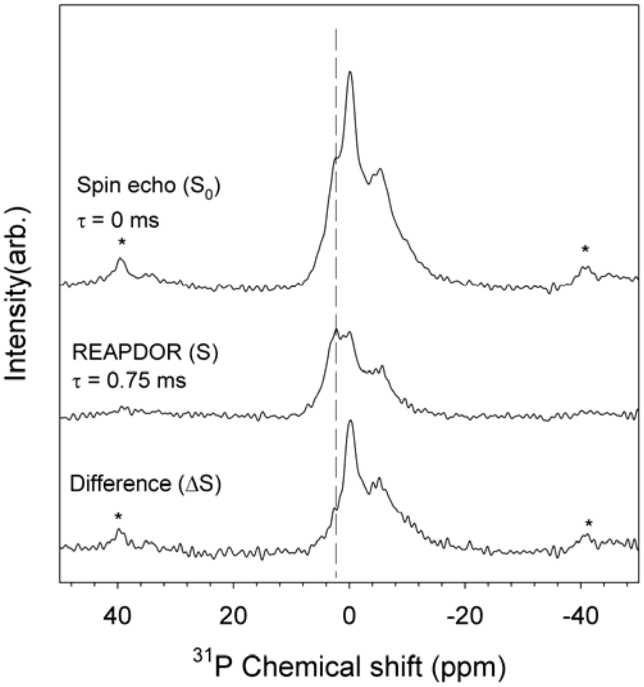

Figure 5.7 Typical $^{31}P\{^{1}H\}/^{27}Al$ CP-REAPDOR NMR dataset for Ca/phosphate adsorbed sample prepared at pH 7 (Cabmt7). Typical control (S_0) as Spin echo, ^{27}Al-dephased REAPDOR (S) and their difference spectrum (ΔS) and acquired with 8 kHz spinning rate, 2 s repetition delay, 1 ms CP contact time, 6 rotor cycles, and 14 588 scans. The dash line corresponds to 2.65 ppm.

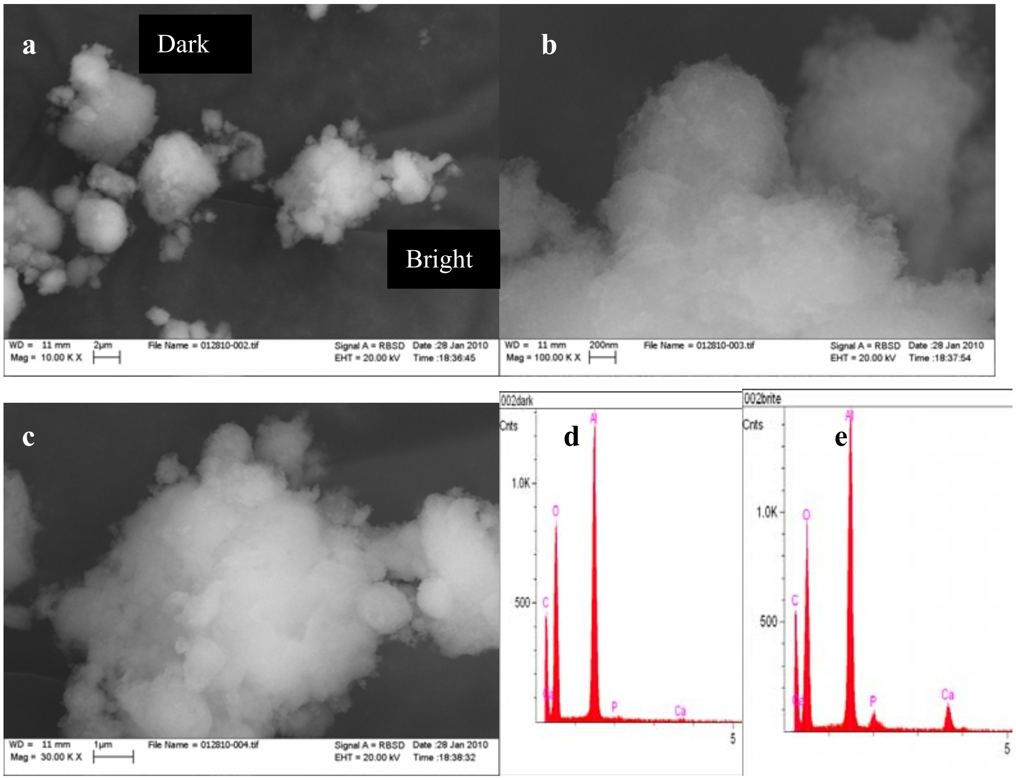

Figure 5.8 (a) SEM photos of Ca/phosphate adsorbed sample at pH 9 (Cabmt9); (b) the “Dark” region in photo (a); (c) the “Bright” region in photo (a); (d) EDX analysis for photo (b); (e) EDX analysis for photo (c).

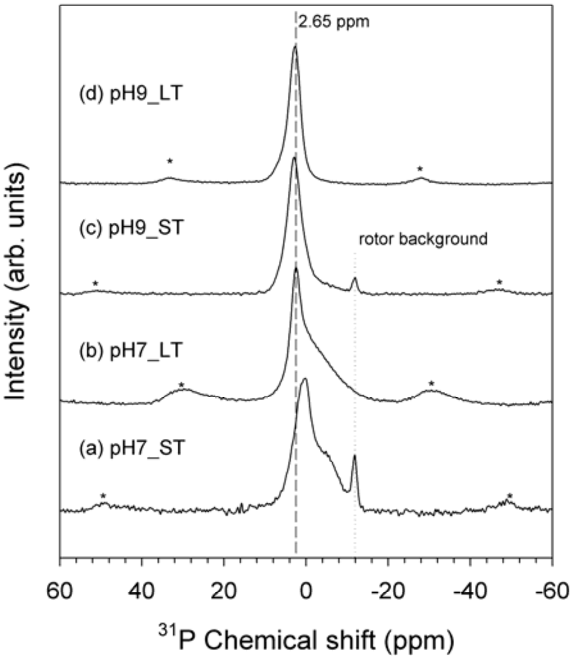

Figure 5.9 ^{31}P SP/MAS spectra of Ca/phosphate co-adsorbed samples prepared at pH 7 for 15 minutes (a) and for 30 days (b), as well as prepared at pH 9 for 15 minutes(c) and for 30 days (d). Spectra were collected at a spinning rate of 8 kHz (a, c) and 5 kHz (b, d), pulse delay of 120 s, and ca. 300 scans. The dash and dotted lines correspond to 2.65 and -12 ppm.

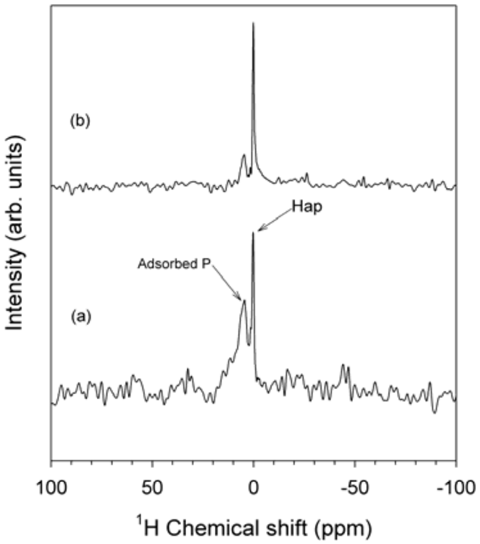

Figure 5.10 ^{1}H sum projection of ^{31}P{^{1}H} HetCor spectra of Ca/phosphate co-adsorbed samples prepared at pH 9 for for 15 minutes (a) and 30 days (b). Spectra were collected at a spinning rate of 10 kHz, CP contact time of 1 ms, and ca. 300 scans.

Chapter 6

General conclusions and future perspective

6.1. Implication of multiple sites adsorption

In the prior chapters, the NMR data reveal that the adsorbed phosphate exhibits more than one chemical environment. Take the boehmite system for example, samples prepared at different pH (3-11) and concentration (0.1-10 mM) show similar two distinct NMR peaks at 0 and -6 ppm. These two peaks were assigned to non-protonated bidentate phosphate surface complexes ($\equiv Al_2PO_4$) and single-protonated bidentate phosphate surface complexes ($\equiv Al_2PO_4H$). However, the evidence of different protontation state of the two peaks seems not strong enough to explain the 6 ppm difference in chemical shift, considering the difference between the chemical shift of Na_2HPO_4 and NaH_2PO_4 is about 3 ppm. Besides, this assignment raises a difficulty to understand the presence of a considerable amount of deprotonated species at acidic condition (e.g. pH 3 or pH 5). A plausible interpretation is that the two species are adsorbed on different adsorption sites, one more acidic and the other more basic.

The quantitative analysis of the NMR peak intensity could provide some support to the hypothesis of multiple sites adsorption. If these two species are binding on the same adsorption sites, then they should be related by a simple Brönsted reaction:

$$\equiv Al_2PO_4^- + H^+ \rightarrow \equiv Al_2PO_4H \qquad (1)$$

The equilibrium constant K can be expressed as

$$K = [\equiv Al_2PO_4H]/([\equiv Al_2PO_4]\,[H^+]) \qquad (2)$$

Based on equation (2), we obtain

$$\log([\equiv Al_2PO_4H]/[\equiv Al_2PO_4]) = \log K - pH \qquad (3),$$

in which the population ratio between the two species is pH dependent, and the slope is -1. However, this value is not in agreement with our experimental data when plotted in the pH diagram (Figure 6.1), which yields a slope of -0.17. This observation means the assumptions behind equation (1) to equation (3) are not be satisfied, suggesting that the two species do not occur at the same adsorption sites. The adsorption reaction at pH 5 might be illustrated as reactions at distinct adsorption sites:

$$2\ (\equiv Al_aOH) + H_2PO_4^- \rightarrow (\equiv Al_aO)_2PO_2 + 2\ H_2O \qquad (4)$$

$$2\ (\equiv Al_bOH) + H^+ + H_2PO_4^- \rightarrow (\equiv Al_bO)_2PO2_4H + 2\ H_2O \qquad (5)$$

The interpretation can be supported by the variation in the population of adsorbed species with phosphate concentration. Although the macroscopic isotherm for total phosphate uptake can be well fitted by the single-site Langmuir equation, each species resolved by NMR could be described by its own isotherm (Figure 6.2). The significant difference in fitting parameters among the three isotherms strongly supports the idea that phosphate adsorption occurs at multiple adsorptions sites. These sites may have different binding constants for phosphate and distinct acid/base chemistry. A simple multi-site adsorption model was proposed Hiemstra and van Riemsdijk [1] to describe phosphate adsorption behavior on goethite, which points out the (110) and (021) crystal surface contains different types of hydroxyl group and thus exhibits adsorption property.

Careful examination of the crystal structure of boehmite (Figure 6.3), shows that both (001) and (101) surfaces contain relatively high densities of paired terminal oxygens bonded to edge-shared Al octahedra with configuration suitable for forming bidentate binuclear complexes. Unfortunately direct evidence cannot be given here to demonstrate the two crystal surfaces contributed the two distinct NMR peaks observed on boehmite. Nonetheless, some previous studies provided some hint to support for this possibilities. Eggleston and Jordan [2] suggested that different crystal surfaces may have different charging property using scanning force microscopy (SFM) as a probe. With experimental acid-base titration and theoretical calculation based on multiple sites surface complexation model (MUSIC), Hiemstra et al. [3] systematically studied the surface charge of a series aluminum (hydro)xides. The results demonstrated the gibbsite (α-$Al(OH)_3$) (001) basal plane remains mainly uncharged below pH = 10 whereas the edges are charged over a wide pH range. Using second harmonic generration and surface titration together, Fitts et al [4] found the point of zero charge (PZC) is different for the (001) surface (pH 4.1 ± 0.4) and the (012) surface (pH 5.2 ± 0.4) of corundum (α-Al_2O_3). Inspired by these studies, some further investigation can be taken. First, if a large boehmite crystal can be grown up, I will measure the PZC of individual surfaces using the techniques mentioned above. In addition, I would like to synthesize a series of boehmite particles with different morphologies as adsorbents and compare the phosphate adsorption behavior among these adsorbents by solid state NMR spectroscopy. With these measurements, a better understanding of the relationship between crystal surfaces and phosphate adsorption would be achieved.

6.2. Comparison to previous studies

Past research of phosphate adsorption onto iron, aluminum and titanium (oxyhydr)oxides have consistently observed the formation of inner-sphere adsorption complexes [5-25]. In most recent experimental studies, bridging bidentate surface complexes have been observed on goethite, heamatite and ferryhydrite using in-situ attenuation total reflectance (ATR) FTIR at acidic condition [11-13, 21-23]. In certain condition, observations of monodentate mononuclear surface complexes [11, 20, 23] were also reported. A general agreement is that bidentate surface complexes form at acidic condition (pH 4-6), whereas monodentate mononuclear surface complexes dominant at alkaline environment (> pH 9) [26]. However, some researchers do not agree with this conclusion totally, who suggested that monodentate forms at low pH conditions and bidentate favors high pH conditions [20, 27]. Besides, at long time reaction with phosphate, surface precipitates of aluminum phosphates and were also suggested [14-17]. But direct experimental evidence for aluminum phosphate surface precipitates is sparse.

In this dissertation, I observed that bridging bidentate phosphate surface complexes are the dominant product of phosphate uptake on two typical aluminum hydroxides, boehmite (γ-AlOOH) and corundum (α-Al_2O_3). These results have confirmed the conclusions prior studies based on ex-situ IR data that bridging bidentate surface complexes are the dominant species on iron (hydr)oxides [25].

However, for a wet paste sample, a small amount of monodentate mononuclear surface complexes on boehmite surface has also been identified. This observation partially supports an early argument that varying the concentration of hydration water could change the phosphate coordination environment. It has been proposed for example that the drying process would alter the structure of adsorption surface complexes such as the transformation from monodentate mononuclear surface complexes to bidentate binuclear surface complexes [28]. It must be noted that in the Al/phosphate system investigated here, the monodentate mononuclear species accounts for only a very small fraction (ca. less than 1%) of the total phosphate adsorbed on the mineral surface, whereas bidentate binuclear surface complexes still dominate in wet conditions.

On the surface of corundum, I observed some aluminum phosphate surface precipitates, which are not apparent on the surface of boehmite. Although the formation mechanism for such surface precipitates is unclear, some insight may be obtained from the consideration the solubility and surface reactivity to explain why such surface precipitates form on corundum not boehmite. In comparison to boehmite, corundum has a higher solubility [29] according to following two equation:

$$0.5\alpha\text{-}Al_2O_3 + 3H^+ \rightarrow Al^{3+} + 1.5H_2O \quad \log K_{dis} = 9.73 \qquad (6)$$

$$\gamma\text{-}AlOOH + 3H^+ \rightarrow Al^{3+} + 2H_2O \quad \log K_{dis} = 8.13 \qquad (7).$$

This would enhance the possibility of dissolution of surface Al and subsequent precipitation of aluminum phosphate. Furthermore, according to thermochemical studies led by Navrotsky [30], corundum has greatest surface reactivity among corundum, γ-Al_2O_3 and boehmite as measured by their surface enthalpy. The authors suggested that although the bulk structure of corundum is more stable than that of boehmite, but the surface of corundum might be less stable than boehmite and tends to be more reactive.

6.3. Questions unresolved and future perspective

In this dissertation, I have determined the structure of phosphate adsorbed on aluminum hydroxides with novel solid state NMR techniques. I learned that the surface speciation of phosphate adsorbed on mineral surfaces is much more complicated than the commonly discussed bidentate binuclear and monodentate mononuclear surface complexes. Protonation state and the structure of mineral surfaces also contribute to the formation of distinctt species. All the environmental factors such as concentration, pH, ionic strength and reaction time would affect the macroscopic adsorption [25]; however, at the molecular level, the NMR results indicate these factors have very little effect on the phosphate bonding structure. In addition, I found that mineral surfaces definitely play significant roles in phosphate adsorption not only on the amount of uptake but also on the chemical environment of the adsorbed phosphate species. Whereas other methods such as infrared (IR) spectroscopy and extended X-ray absorption spectroscopy (EXAFS) could not show this effect clearly, NMR spectroscopy proves more sensitive to the details of surface complexes structure. To fully understand the impact of mineral surface on interfacial reactions, more work must be carried out on this direction. Only once a systematic link between materials structure and properties such as sorption and reactivity is developed, can the mobility and bioavailability of phosphate be predicted.

In the past three decades, understanding of cation/anion adsorption reactions at mineral/water interface has been largely improved by the surface complexation theory proposed by mainly Stumm and coworkers [31]. The theory postulates the adsorption reaction as essentially a surface complexation reaction of anion/cation with the surface hydroxyl group of minerals. Within this framework, this theory allows numerical simulation of adsorption reactions by surface complexation model, which can be used to predict the mobility of dissolved ions in aqueous environment. Results obtained in this dissertation support the basis of the surface complexation theory and further improved the understanding of the nature of surface adsorption reactions. The NMR results suggest that interfacial species has motional characteristics that differ from the rigid structure in solids and the rapid molecular tumbling in solution. Also, as mentioned above, the NMR results show the effect of mineral surfaces in adsorption reaction. These two aspects have not been clearly addressed and even rarely discussed before. The reason lies in the inability of the current methodology used in probing the interfacial species (reaction) at the mineral (solid)/water interface. NMR spectroscopy complements the current techniques (i.e. IR, EXAFS, etc) commonly used to probe chemical reactions at solid/water interface. No doubt, novel NMR techniques will certainly shed some light on the mysterious interfacial reactions.

The molecular motional feature of surface adsorbed species has rarely been investigated, and the mechanism remains largely unclear. In this dissertation, I found that the monodentate mononuclear surface complexes can be observed only by the spin echo sequence, suggesting that it exhibits a longer T_2 than bidentate binuclear surface complexes. The longer T_2 is consistent the mobile nature of its structural configuration, in which the phosphate group can rotate with the axis of P-O-Al bonds. However, in this dissertation, I cannot obtain more information to quantify its motional properties. The motional property is important for understanding phosphate desorption mechanism and aging effect of the inorganic pollutants. In contrast to the adsorption mechanism, the mechanism for desorption reaction is poorly understood. Formation of inner-sphere bridging bidentate surface complexes well explains the specific adsorption of phosphate on metal oxides, however, it cannot explain desorption hysterias phenomenon. Why only a small fraction of surface adsorbed phosphate is desorbed? Why only this part, not other part? Why surface adsorbed phosphate is more resistant to be desorbed upon long time aging? To answer these questions, structure information alone is not enough. The molecular dynamics of the interfacial species should be systematically studied to provide insight into adsorption/desorption reactions. Previous studies using FTIR and EXAFS cannot provide such information, but solid state NMR is well-suited for investigating the molecular motion at solid/water interface.

This dissertation focuses on orthophosphate mainly for the purpose of simplifying the research system and testing the feasibility of application of solid state NMR to interfacial geochemistry. In the natural environment, there are many other important P-bearing compounds such as glyphosate, the most widely used pesticide around the world. Many studies indicate glyphosate can strongly adsorb on metal oxides and clays. Solid state NMR methods used in this dissertation could be applied to elucidate the adsorption mechanism of glyphosate on soil minerals such as clays and carbonates. In addition, interaction between biological macromolecules such as ATP and DNA and mineral surfaces is a common phenomenon in soils and in the human body. To characterize the molecular structure of such macromolecules on solid surfaces is not very easy. FTIR is a useful tool with which to study interfacial species, but these macromolecules usually contain many IR-active functional groups which may cause severe spectral overlap and reduce resolution. But NMR can be readily applied to these studies, because its elemental specification can reduce the interference from mineral background and other functional groups.

6.4. General promises and constraints of solid state NMR

We found that solid state NMR spectroscopy, especially the advanced double resonance and two-dimensional NMR techniques, can provide fine details of structural information for interpretation of the reaction mechanism at mineral/water interface. The merits of solid state NMR on light elements such as ^{1}H and ^{31}P are pronounced in the case of phosphate sorption on aluminum (hydr)oxides. Interfacial water ordering and the proton environment are crucial to understand the mineral surface hydration and mineral surface structure. In this dissertation, ^{31}P{^{1}H} heteronuclear correlation (HetCor) certainly provides some structural information for the proton environment near adsorbed P molecules. Since P directly bonds to mineral surface as inner-sphere complexes, it can be deemed as a “molecular probe” that allows us to obtain information about the proton and water environment near the mineral surface indirectly. Due to the strong ^{1}H-^{1}H homonuclear dipolar coupling and the dominance mobile water molecules close to the surface of minerals, in our case, the indirectly observed ^{1}H spectra are poorly resolved. But in the future, we can employ surface deuteration methods to remove part of the interference from surface mobile water, and Lee-Goldberg Cross-polarization HetCor [32-33] and/or ultra-fast magic angle spinning to reduce the ^{1}H-^{1}H homonuclear dipolar coupling [34], such that well-resolved proton information could be obtained. Furthermore, specific pulse sequences can be developed to better resolve the proton environment. Another potential application of solid state NMR is to determine the solid state phosphorus speciation for real environmental samples with low Fe/Mn content. In the literature, Ca-P, Al-P and organic-P can be readily distinguished by solid state NMR in some biosolids [35-36]. Solid state NMR spectroscopy is complementary to the combination of solution-state NMR spectroscopy plus chemical extraction methods since some phosphorus remains in the solid during the extraction procedure or might experience an alteration in speciation.

Two fundamental factors that limit the application of solid state NMR to chemistry are sensitivity and resolution. These two limitations are even more pronounced in interfacial geochemistry, because interfacial species usually have low content, range in motional nature and wide distribution of chemical environments. In the case of phosphate uptake by corundum (Chapter 4), we found that it takes quite a long time to collect a spectrum with sufficient signal-to-noise ratio even in a CP condition owing to its low specific surface area. Furthermore, the broad feature observed of the ^{31}P spectra for phosphate adsorbed on corundum surface makes it rather difficult to interpret these spectra unambiguously. For adsorption studies, constraints also may arise from the observed nucleus. For instance, interaction of carbonate and organic acids in soils such citrate and malate with soil minerals is of interest for understanding interactions of natural organic matter and minerals in aqueous environment. However, in those compounds, the natural abundance for the NMR-active nucleus ^{13}C amounts to only 1.1%, making it difficult to observe ^{13}C signal in purely natural sample. To characterize the carbon environment for those compounds at mineral/water interface, isotope enrichment methods must be employed.

Also it must be noted that only a small amount element are easy to work with, although theatrically most element in the periodic table has at least one NMR-active isotope. Some widely studied NMR-active nuclei include ^{1}H, ^{7}Li ^{11}B, ^{13}C, ^{17}O, ^{19}F, ^{27}Al, ^{29}Si, and ^{31}P. As mentioned in Chapter one, quadrupolar nuclei with spin quantum number > ½ are normally difficult to work with. Besides, NMR is less sensitive to high-Z elements compared to X-ray techniques. High-Z elements, such as heavy metals, usually have many electrons surrounding the nucleus. More electrons mean stronger magnetic shielding effect on the nucleus. For instance, with spin quantum numbers = ½, ^{119}Cd and ^{207}Pb usually exhibit very large chemical shift anisotropy (CSA) in their compound, leading to much broad resonance lineshapes difficult to be resolved [37-38].

Another disadvantage of solid state NMR is the interference of Fe and other paramagnetic substances such as Mn and Ni, which cause the studies of phosphate (and/or other adsorbates) adsorption on iron-bearing minerals (e.g. goethite and ferryhydrite) extremely challenging. The magnetic interaction between nuclear spin and unpaired electrons can make the NMR signal very broad, further reducing resolution or even make the signal impossible to be observed. This effect also hinders the potential application of solid state NMR to natural geological samples which usually contain Fe and Mn. On the other hand, in the well-define systems, it is possible to observe well-separated signals for adsorbates on paramagnetic minerals, which might be another important application of NMR to determine adsorbate structure [39-41].

Reference

[1] Hiemstra, T.; Van Riemsdijk, W. H., *J. Colloid Interface Sci.* **1996**, *179*, 488-508.

[2] Eggleston, C. M.; Jordan, G., *Geochim. Cosmochim. Acta* **1998**, *62*, 1919-1923.

[3] Hiemstra, T.; Yong, H.; van Riemsdijk, W. H., *Langmuir* **1999**, *15*, 5942–5955.

[4] Fitts, J. P.; Shang, X. M.; Flynn, G. W.; Heinz, T. F.; Eisenthal, K. B., *J. Phys. Chem. B* **2005**, *109*, 7981-7986.

[5] Rajan, S. S. S.; Perrott, K. W.; Saunders, W. M. H., *J. Soil Sci.* **1974**, *25*, 438-447.

[6] Rajan, S. S. S., *Nature* **1975**, *253*, 434-436.

[7] Rajan, S. S. S., *Nature* **1976,** *262*, 45-46.

[8] Atkinson, R. J.; Quirk, J. P.; Posner, A. M., *J. Inorg. Nucl. Chem.* **1972**, *34*,

2201-2211.

[9] Kyle, J. H.; Posner, A. M.; Quirk, J. P., *J. Soil Sci.* **1975**, *26*, 32-43.

[10] Atkinson, R. J.; Parfitt, R. L.; Smart, R. S., *J. Chem. Soc. Faraday Trans. I* **1974**, *70*, 1472-1479.

[11] Tejedortejedor, M. I.; Anderson, M. A., *Langmuir* **1990**, *6*, 602-611.

[12] Connor, P. A.; McQuillan, A. J., *Langmuir* **1999**, *15*, 2916-2921.

[13] Arai, Y.; Sparks, D. L., *J. Colloid Interface Sci.* **2001,** *241*, 317-326.

[14] Ler, A.; Stanforth, R., *Environ. Sci. Technol.* **2003**, 37, 2694-2700.

[15] van Riemsdijk, W. H.; Lyklema, J., *J. Colloid Interface Sci.* **1980**, *76*, 55-66.

[16] Bleam, W. F.; Pfeffer, P. E.; Goldberg, S.; Taylor, R. W.; Dudley, R., *Langmuir* **1991**, *7*, 1702-1712.

[17] Kim, Y.; Kirkpatrick, R. J., *Eur. J. Soil Sci.* **2004**, *55*, 243-251.

[18] Khare, N.; Hesterberg, D.; Martin, J. D., *Environ. Sci. Technol.* **2005**, *39*, 2152-2160.

[19] Parfitt, R. L.; Atkinson, R. J., *Nature* **1976**, *264*, 740-742.

[20] Persson, P.; Nilsson, N.; Sjoberg, S., *J. Colloid Interface Sci.* **1996**, 177, 263-275.

[21] Ronson, T. K.; McQuillan, A. J., *Langmuir* **2002**, *18*, 5019-5022.

[22] **Luengo, C.; Brigante, M.; Antelo, J.; Avena, M.,** *J. Colloid Interface Sci.* **2006**, *300*, 511-518.

[23] Elzinga, E. J.; Sparks, D. L., *J. Colloid Interface Sci.* **2007**, *308*, 53-70.

[24] Khare, N.; Martin, J. D.; Hesterberg, D., *Geochim. Cosmochim. Acta* **2007**, *71*, 4405-4415.

[25] Goldberg, S.; Sposito, G., *Commun. Soil Sci. Plant Anal.* **1985**, *16*, 801-821.

[26] Kwon, K. D.; Kubicki, J. D., *Langmuir* **2004**, *20*, 9249-9254.

[27] Rahnemaie, R.; Hiemstra, T.; van Riemsdijk, W. H., *Langmuir* **2007**, *23*, 3680-3689.

[28] Laiti, E.; Persson, P.; Ohman, L.O., *Langmuir* **1996**, *12*, 2969-2975.

[29] Sparks, D.L., *Environmental Soil Chemistry* 2nd ed.; Academic Press: San Diego, CA, 2003.

[30] Navrotsky, A., *Rev. Mineral. Geochem.* **2001**, *44*, 73-103.

[31] Stumm, W. and Morgan, J. J.(1996): *Aquatic Chemistry, Chemical Equilibria and Rates in Natural Waters*, 3rd ed. John Wiley & Sons, Inc., New York

[32] Tseng, Y. H.; Zhan, J. H.; Lin, K. S. K.; Mou, C. Y.; Chan, J. C. C., *Solid State Nucl. Magn. Reson.* **2004**, 26, 99-104.

[33] Tseng, Y. H.; Mou, C. Y.; Chan, J. C. C., *J. Amer. Chem. Soc.* **2006**, 128, 6909-6918.

[34] Mehring, M., *Principles of High Resolution NMR in Solids*. 2nd ed.; Springer-Verlag: Berlin, 1983.

[35] Hunger, S.; Cho, H.; Sims, J. T.; Sparks, D. L., *Environ. Sci. Technol.* **2004**, *38*, 674-681.

[36] Cade-Menun, B. J.; Navaratnam, J. A.; Walbridge, M. R., *Environ. Sci. Technol.* **2006**, *40*, 7874-7880.

[37] Paola, D. L.; Javier C., *Clays Clay Miner.* **2003**, *51*, 403-414.

[38] Mason, H. E.; Hirner, J. J.; Xu, W.; Parise, J. B.; Phillips, B. L., *Magn. Reson. Chem.* **2009**, *47*, 1062-1070.

[39] Cole, K. E.; Paik, Y.; Reeder, R. J.; Schoonen, M.; Grey, C. P., *J. Phys. Chem. B.* **2004**, *108,* 6938-6940.

[40] Nielsen, U. G.; Paik, Y.; Julmis, K.; Schoonen, M. A. A.; Reeder, R. J.; Grey, C. P., *J. Phys. Chem. B* **2005**, *109*, 18310-18315.

[41] Kim, J.; Nielsen, U. G.; Grey, C. P., *J. Am. Chem. Soc.* **2008**, *130*, 1285-1295.

Figures

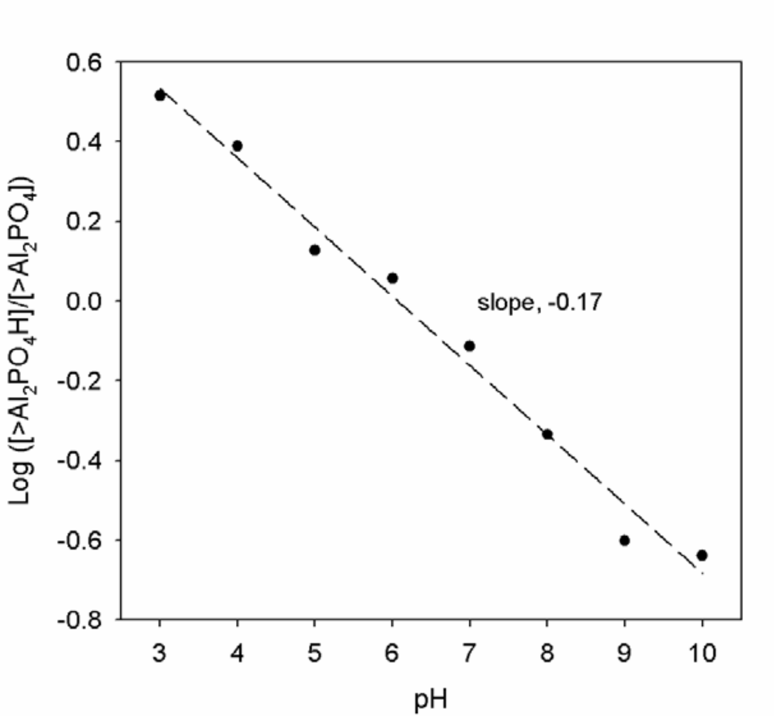

Figure 6.1 Population ratios between the two surface phosphate species on resolved boehmite by NMR as a function of pH. Data were fit to a line by least squares methods, yielding a slope of -0.17.

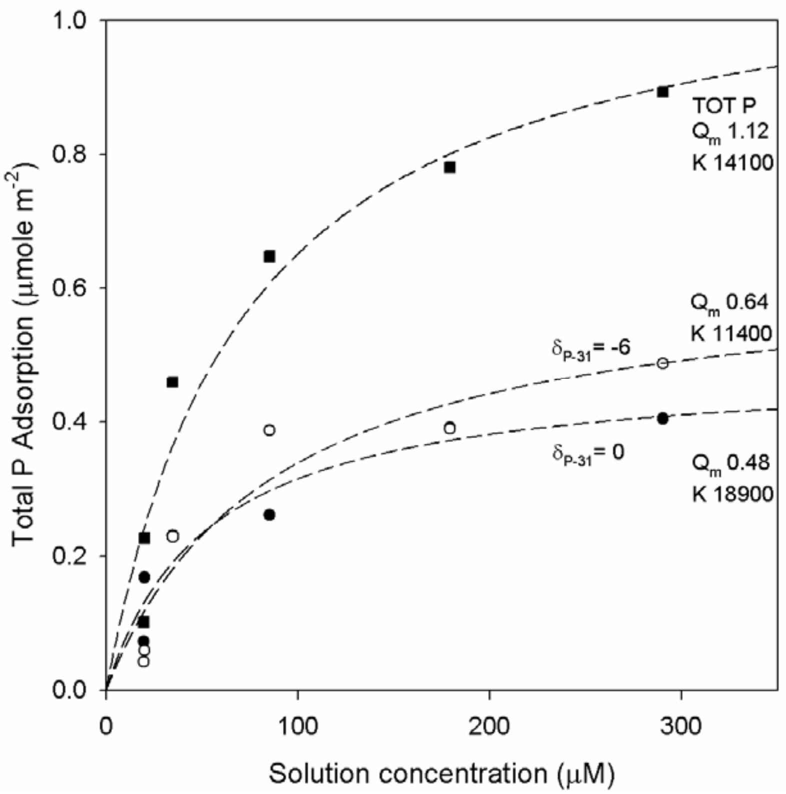

Figure 6.2 Adsorption isotherm of phosphate on boehmite. 10 mM NaCl background electrolyte, and 15 minute reaction time at room temperature.

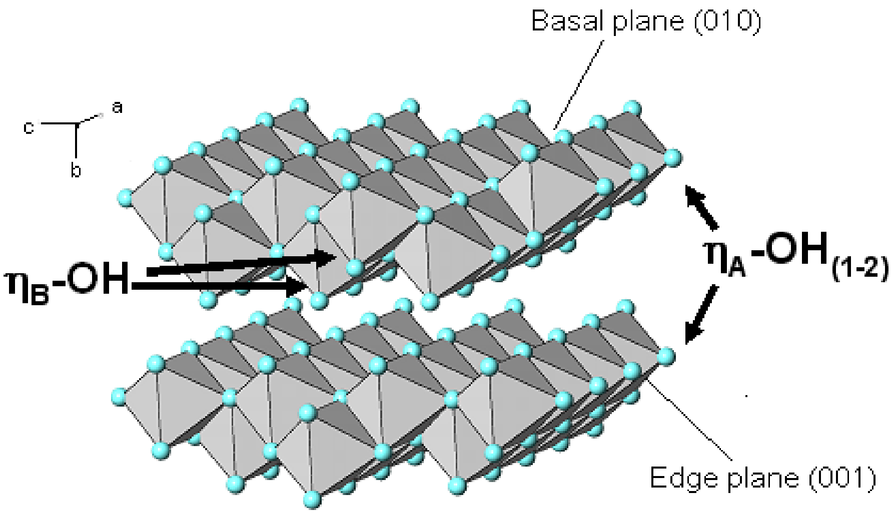

Figure 6.3 Polyhedral representation of boehmite (γ-AlOOH) Crystal structure, showing low-index faces. Two types of terminal hydroxyl groups are noted as η_A and η_B respectively. Grey polyhedra represents $Al(O,OH)_6$ and blue balls are oxygen.

Bibliography

Chapter 1.

[1] Slomp, C. P.; van Cappellen, P., *Biogeosciences* **2007**, *4*, 155-171.

[2] Arai, Y.; Sparks, D. L., *Adv. Agron.* **2007**, *94*, 135-179.

[3] Goldberg, S.; Sposito, G., *Commun. Soil Sci. Plant Anal.* **1985**. 16, 801-821.

[4] Kwon, K. D.; Kubicki, J. D., *Langmuir* **2004**, *20*, 9249-9254.

[5] Rahnemaie, R.; Hiemstra, T.; van Riemsdijk, W. H., *Langmuir* 2007, *23*, 3680-3689.

[6] Paytan, A.; McLaughlin, K., *Chem. Rev.* **2007**, *107*, 563-576.

[7] Mortlock, R. F.; Bell, A. T.; Radke, C. J., *J. Phys. Chem.* **1993**, *97*, 775-782.

[8] Cade-Menun, B. J., *Talanta* **2005**, *66*, 359-371.

[9] Cheetham, A. K.; Clayden, N. J.; Dobson C. M.; Jakeman, R. J. B., *Chem. Commun.* **1986**, 195-197.

[10] Turner, G. L.; Turner, G. L.; Smith, K. A.; Kirkpatrick, R. J.; Oldfield, E., *J. of Magn. Reson.* **1986**, *70*, 408-415.

[11] Rajan, S. S. S.; Perrott, K. W.; Saunders, W. M. H., *J. Soil Sci.* **1974**, *25*, 438-447.

[12] Rajan, S. S. S., *Nature* **1975**, *253*, 434-436.

[13] Rajan, S. S. S., *Nature* **1976**, *262*, 45-46.

[14] Atkinson, R. J.; Quirk, J. P.; Posner, A. M., *J. Inorg. Nucl. Chem.* **1972**, *34*, 2201-2211.

[15] Kyle, J. H.; Posner, A. M.; Quirk, J. P., *J. Soil Sci.* **1975**, *26*, 32-43.

[16] Atkinson, R. J.; Parfitt, R. L.; Smart, R. S., *J. Chem. Soc. Faraday Trans. I* **1974**, *70*, 1472-1479.

[17] Bleam, W. F.; Pfeffer, P. E.; Goldberg, S.; Taylor, R. W.; Dudley, R., *Langmuir* **1991,** *7*, 1702-1712.

[18] Tejedortejedor, M. I.; Anderson, M. A., *Langmuir* **1990**, *6*, 602-611.

[19] Connor, P. A.; McQuillan, A. J., *Langmuir* **1999**, *15*, 2916-2921.

[20] Arai, Y.; Sparks, D. L., *J. Colloid Interface Sci.* **2001**, *241*, 317-326.

[21] Gong, W. Q., *Int. J. Min. Proc.* **2001**, *63*, 147-165.

[22] Lefevre, G., *Adv. Colloid Interface Sci.* **2004,** *107*, 109-123.

[23] Catalano, J. G.; Park, C.; Fenter, P.; Zhang, Z., *Geochim. Cosmochim. Acta* **2008**, *72*, 1986-2004.

[24] Ler, A.; Stanforth, R., *Environ. Sci. Technol.* **2003**, *37*, 2694-2700.

[25] van Riemsdijk, W. H.; Lyklema, J., *J. Colloid Interface Sci.* **1980**, *76*, 55-66.

[26] Kim, Y.; Kirkpatrick, R. J., *Eur. J. Soil Sci.* **2004**, *55*, 243-251.

[27] Khare, N.; Hesterberg, D.; Martin, J. D., *Environ. Sci. Technol.* **2005**, *39*, 2152-2160.

[28] Parfitt, R. L.; Atkinson, R. J., *Nature* **1976**, *264*, 740-742.

[29] Nanzyo, M.; Watanabe, Y., *Soil Sci. Plant Nutri.* **1982**, *28*, 359-368.

[30] Nanzyo, M., *J. Soil Sci.* **1984**, *35*, 63-69.

[31] Persson, P.; Nilsson, N.; Sjoberg, S., *J. Colloid Interface Sci.* **1996**, *177*, 263-275.

[32] Ronson, T. K.; McQuillan, A. J., *Langmuir* **2002**, *18*, 5019-5022.

[33] Luengo, C.; Brigantea, M.; Antelo, J.; Avena, M., *J. Colloid Interface Sci.* **2006**, *300*, 511-518.

[34] Elzinga, E. J.; Sparks, D. L., *J. Colloid Interface Sci.* **2007**, 308, 53-70.

[35] Laiti, E.; Persson, P.; Ohman, L. O., *Langmuir* **1996**, 12, 2969-2975.

[36] Lookman, R.; Grobet, P.; Merckx, R.; Vlassak, K., *Eur. J. Soil Sci.* **1994**, 45, 37-44.

[37] Lookman, R.; Grobet, P.; Merckx, R.; Van Riemsdijk, W. H., *Geoderma* **1997**, 80, 369-388.

[38] Lookman, R.; Geerts, H.; Grobet, P.; Merckx, R.; Vlassak, K., *Eur. J. Soil Sci.* **1996**, 47, 125-130.

[39] Johnson, B. B.; Ivanov, A. V.; Antzutkin, O. N.; Forsling, W., *Langmuir* **2002**, *18*, 1104-1111.

[40] Harris R. K.; Thompson T. V.; Norman P. R.; Pottage C., *Carbon* **1999**, *37*, 1425-1430.

[41] Van Emmerik, T. J.; Sandstrom, D. E.; Antzutkin, O. N.; Angove, M. J.;

Johnson, B. B., *Langmuir* **2007**, *23*, 3205-3213.

[42] Fry, R. A.; Kwon, K. D.; Komarneni, S.; Kubicki, J. D.; Mueller, K. T., *Langmuir* **2006**, *22*, 9281-9286.

[43] Khare, N.; Hesterberg, D.; Beauchemin, S.; Wang, S. L., *Soil Sci. Soc. Am. J.* **2004**, *68*, 460-469.

[44] Khare, N.; Martin, J. D.; Hesterberg, D., *Geochim. Cosmochim. Acta* **2007**, *71*, 4405-4415.

[45] Laws, D. D.; Bitter H. M. L.; Jerschow, A., *Angew. Chem. Int. Ed.* **2002,** 41, 3096-3129.

[46] Ernst, R. R.; Anderson, W. A., *Rev. Sci. Instru.* **1966**, 37, 93-102.

[47] Waugh, J. S., *Anal. Chem.* **1993**, *65*, A725-A729.

[48] Dietrich, R.; Trahms, L., *J. Magn. Reson.* **1987**, *71*, 337-341.

[49] Herzfeld, J.; Berger, A. E., *J. Chem. Phys.* **1980**, *73*, 6021-6030.

[50] Pines, A.; Waugh, J. S.; Gibby, M. G., *J. Chem. Phys.* **1972**, *56*, 1776-1787.

[51] Pines, A.; Gibby, M. G.; Waugh, J. S., *J. Chem. Phys.* **1973**, *59*, 569-590.

[52] Andrew, E. R.; Bradbury, A.; Eades, R. G., *Nature* **1958**, *182*, 1659-1659.

[53] Lowe, I. J., *Phys. Rev. Lett.* **1959**, *2*, 285-287.

[54] Kolodziejski, W.; Klinowski, J., *Chem. Rev.s* **2002**, *102*, 613-628.

[55] Hartmann, S. R.; Hahn, E. L., *Phys. Rev.* **1962**, *128*, 2042-2053.

[56] Stejskal, E. O.; Schaefer, J.; Waugh, J. S., *J. Magn. Reson.* **1977**, *28*, 105-112.

[57] Schmidt-Rohr, K.; Clauss, J.; Spiess, H. W., *Macromolecules* **1992**, *25*, 3273-3277.

[58] Gullion, T., *Chem. Phys. Lett.* 1995, *246*, 325-330.

[59] Chopin, L.; Vega, S.; Gullion, T., *J. Amer. Chem. Soc.* 1998, *120*, 4406-4409.

[60] Gullion, T.; Schaefer, J., *J. Magn. Reson.* **1989**, *81*, 196-200.

[61] Grey, C. P.; Veeman, W.S.; Vega, A. J., *J. Chem. Phys.* **1993**, *98*, 7711-7724.

[62] Haase, J.; Conradi, M. S.; Grey, C. P.; Vega, A. J., *J. Magn. Reson. A* **1994**, *109*, 90-97.

[63] Bak, M.; Rasmussen, J. T.; Nielsen, N. C., *J. Magn. Reson.* **2000,** *147*, 296-330.

[64] Veshtort, M.; Griffin, R. G., *J. Magn. Reson.* **2006**, 178, 248-282.

[65] Pilkenton, S; Raftery, D., In *Environmental Catalysis*; Grassian, V. H., Ed.; CRC press: New York, 2005; p352.

Chapter 2.

[1] Goldberg, S.; Sposito, G., *Commun. Soil Sci. Plant Anal.* **1985**, *16*, 801-821.

[2] Brown, G. E.; Henrich, V. E.; Casey, W. H.; Clark, D. L.; Eggleston, C.; Felmy, A.; Goodman, D. W.; Gratzel, M.; Maciel, G.; McCarthy, M. I.; Nealson, K. H.; Sverjensky, D. A.; Toney, M. F.; Zachara, J. M., *Chem. Rev.* **1999**, *99*, 77-174.

[3] Rajan, S. S. S., *Nature* **1975**, *253*, 434-436.

[4] Rajan, S. S. S., *Nature* **1976**, *262*, 45-46.

[5] Khare, N.; Martin, J. D.; Hesterberg, D., *Geochim. Cosmochim. Acta* **2007**, *71*, 4405-4415.

[6] Rahnemaie, R.; Hiemstra, T.; van Riemsdijk, W. H., *Langmuir* **2007**, *23*, 3680-3689.

[7] Parfitt, R. L.; Atkinson, R. J.; Smart, R. S. C., *Soil Sci. Soc. Am. J.* **1975**, *39*, 837-841.

[8] Parfitt, R. L.; Atkinson, R. J., *Nature* **1976**, *264*, 740-742.

[9] Tejedor-Tejedor, M. I.; Anderson, M. A., *Langmuir* **1990**, *6*, 602-611.

[10] Persson, P.; Nilsson, N.; Sjoberg, S., *J. Colloid Interface Sci.* **1996**, *177*, 263-275.

[11] Arai, Y.; Sparks, D. L., *J. Colloid Interface Sci.* **2001**, *241*, 317-326.

[12] Hesterberg, D.; Zhou, W. Q.; Hutchison, K. J.; Beauchemin, S.; Sayers, D. E., *J. Synchrotron Radiat.* **1999**, *6*, 636-638.

[13] Khare, N.; Hesterberg, D.; Martin, J. D., *Environ. Sci. Technol.* **2005**, *39*, 2152-2160.

[14] Alvarez, R.; Fadley, C. S.; Silva, J. A., *Soil Sci. Soc. Am. J.* **1980**, *44*, 422-425.

[15] Kwon, K. D.; Kubicki, J. D., *Langmuir* **2004**, *20*, 9249-9254.

[16] Bleam, W. F.; Pfeffer, P. E.; Goldberg, S.; Taylor, R. W.; Dudley, R., *Langmuir* **1991**, *7*, 1702-1712.

[17] Lookman, R.; Grobet, P.; Merckx, R.; Vlassak, K., *Eur. J. Soil Sci.* **1994**, *45*, 37-44.

[18] Lookman, R.; Grobet, P.; Merckx, R.; Van Riemsdijk, W. H., *Geoderma* **1997**, *80*, 369-388.

[19] Johnson, B. B.; Ivanov, A. V.; Antzutkin, O. N.; Forsling, W., *Langmuir* **2002**, *18*, 1104-1111.

[20] Kim, Y.; Kirkpatrick, R. J., *Eur. J. Soil Sci.* **2004**, *55*, 243-251.

[21] Van Emmerik, T. J.; Sandstrom, D. E.; Antzutkin, O. N.; Angove, M. J.; Johnson, B. B., *Langmuir* **2007**, *23*, 3205-3213.

[22] Nordin, J.; Persson, P.; Laiti, E.; Sjoberg, S., *Langmuir* **1997**, *13*, 4085-4093.

[23] Gullion, T., *Chem. Phys. Lett.* **1995**, *246*, 325-330.

[24] Grey, C. P.; Vega, A. J., *J. Am. Chem. Soc.* **1995**, *117*, 8232-8242.

[25] Accelrys; *Cerius^2 Modeling Evnironment*; Accelrys, Inc.: San Diego CA, 2003.

[26] Frisch, M. J.; Trucks, G. W.; Schlegel, H. B.; Scuseria, G. E.; Robb, M. A.; Cheeseman, J. R.; Montgomery, J. A., Jr. ; Vreven, T.; Kudin, K. N.; Burant, J. C.; Millam, J. M.; Iyengar, S. S.; Tomasi, J.; Barone, V.; Mennucci, B.; Cossi, M.; Scalmani, G.; Rega, N.; Petersson, G. A.; Nakatsuji, H.; M. Hada; M. Ehara; K. Toyota; Fukuda, R.; Hasegawa, J.; Ishida, M.; Nakajima, T.; Honda, Y.; Kitao, O.; Nakai, H.; Klene, M.; Li, X.; Knox, J. E.; Hratchian, H. P.; Cross, J. B.; Adamo, C.; Jaramillo, J.; Gomperts, R.; Stratmann, R. E.; Yazyev, O.; Austin, A. J.; Cammi, R.; Pomelli, C.; Ochterski, J. W.; Ayala, P. Y.; Morokuma, K.; Voth, G. A.; Salvador, P.; Dannenberg, J. J.; Zakrzewski, V. G.; Dapprich, S.; Daniels, A. D.; Strain, M. C.; Farkas, O.; Malick, D. K.; Rabuck, A. D.; Raghavachari, K.; Foresman, J. B.; Ortiz, J. V.; Cui, Q.; Baboul, A. G.; Clifford, S.; Cioslowski, J.; Stefanov, B. B.; Liu, G.; Liashenko, A.; Piskorz, P.; Komaromi, I.; Martin, R. L.; Fox, D. J.; Keith, T.; Al-Laham, M. A.; Peng, C. Y.; Nanayakkara, A.; Challacombe, M.; Gill, P. M. W.; Johnson, B.; Chen, W.; Wong, M. W.; Gonzalez, C.; Pople, J. A.; *Gaussian 03, Revision C.02*; Gaussian, Inc.: Wallingford CT, 2004.

[27] Becke, A. D., *J. Chem. Phys.* **1997**, *107*, 8554-8560.

[28] Lee, C. T.; Yang, W. T.; Parr, R. G., *Phys. Rev. B* **1988**, *37*, 785-789.

[29] Hehre, W. J.; Ditchfie, R.; Pople, J. A., *J. Chem. Phys.* **1972**, *56*, 2257-2261.

[30] Wolinski, K.; Hinton, J. F.; Pulay, P., *J. Am. Chem. Soc.* **1990**, *112*, 8251-8260.

[31] Alam, T. M. *Ab Initio Calculation of Nuclear Magnetic Resonance Chemical Shift Anisotropy Tensors I. Influence of Basis Set on the Calculations of ^{31}P Chemical Shifts*; Sandia National Laboratories: Albequerque NM, 1998.

[32] Zhang, Y.; Oldfield, E., *J. Phys. Chem. B* **2004**, *108*, 19533-19540.

[33] McLean, A. D.; Chandler, G. S., *J. Chem. Phys.* **1980,** *72*, 5639-5648.

[34] Kolodziejski, W.; Klinowski, J., *Chem. Rev.* **2002**, *102*, 613-628.

[35] Mehring, M., *Principles of High Resolution NMR in Solids*; 2nd ed.; Springer-Verlag: Berlin, 1983.

[36] Chopin, L.; Vega, S.; Gullion, T., *J. Am. Chem. Soc.* **1998**, *120*, 4406-4409.

[37] Bak, M.; Rasmussen, J. T.; Nielsen, N. C., *J. Magn. Reson.* **2000**, *147*, 296-330.

[38] Fry, R. A.; Kwon, K. D.; Komarneni, S.; Kubicki, J. D.; Mueller, K. T., *Langmuir* **2006**, *22*, 9281-9286.

[39] Hartmann, P.; Vogel, J.; Schnabel, B., *J. Magn. Reson. A* **1994**, *111*, 110-114.

[40] Herzfeld, J.; Berger, A. E., *J. Chem. Phys.* **1980**, *73*, 6021-6030.

[41] Eichele, K.; Wasylishen, R. E.; *WSOLIDS*, 2.0.18; Dalhousie University: Halifax, 2000.

[42] Elzinga, E. J.; Sparks, D. L., *J. Colloid Interface Sci.* **2007**, *308*, 53-70.

[43] Mortlock, R. F.; Bell, A. T.; Radke, C. J., *J. Phys. Chem.* **1993**, *97*, 775-782.

[44] Holland, G. P.; Sharma, R.; Agola, J. O.; Amin, S.; Solomon, V. C.; Singh, P.; Buttry, D. A.; Yarger, J. L., *Chem. Mat.* **2007**, *19*, 2519-2526.

[45] Chiche, D.; Digne, M.; Revel, R.; Chaneac, C.; Jolivet, J. P., *J. Phys. Chem. C* **2008**, *112*, 8524-8533.

[46] Nordin, J. P.; Sullivan, D. J.; Phillips, B. L.; Casey, W. H., *Geochim. Cosmochim. Acta* **1999**, *63*, 3513-3524.

Chapter 3.

[1] Khare, N.; Hesterberg, D. L.; Martin, J. D., *Environ. Sci. Technol.* **2005**, 39, 2152-2160.

[2] Tejedor-Tejedor, M. I.; Anderson, M. A., *Langmuir* **1990**, 6, 602-611.

[3] Persson, P.; Nilsson, N.; Sjöberg, S., *J. Colloid Interface Sci.* **1996**, 177, 263–275.

[4] Kwon, K. D.; Kubicki, J. D., *Langmuir* **2004**, 20, 9249-9254.

[5] Rahnemaie, R.; Hiemstra, T.; van Riemsdijk, W. H., *Langmuir* **2007**, 23, 3680-3689.

[6] Bleam, W. F.; Pfeffer, P. E.; Goldberg, S.; Taylor, R. W.; Dudley, R., *Langmuir* **1991**, *7*, 1702-1712.

[7] Lookman, R.; Grobet, P.; Merckx, R.; Vlassak, K., *Eur. J. Soil Sci.* **1994**, *45*, 37-44.

[8] Lookman, R., Geerts, H., Grobet, P., Merckx, R., and Vlassak, K., *Eur. J. Soil Sci.* **1996**, 47, 125-130.

[9] Lookman, R.; Grobet, P.; Merckx, R.; Van Riemsdijk, W. H., *Geoderma* **1997**, *80*, 369-388.

[10] Johnson, B. B.; Ivanov, A. V.; Antzutkin, O. N.; Forsling, W., *Langmuir* **2002**, *18*, 1104-1111.

[11] Harris, R. K.; Thompsona, T. V.; Normanb P. R.; Pottageb C., *Carbon* **1999**, 37, 1425-1430.

[12] Kim, Y.; Kirkpatrick, R. J., *Eur. J. Soil Sci.* **2004**, *55*, 243-251.

[13] Van Emmerik, T. J.; Sandstrom, D. E.; Antzutkin, O. N.; Angove, M. J.; Johnson, B. B., *Langmuir* **2007**, *23*, 3205-3213.

[14] Fry, R. A.; Kwon, K. D.; Komarneni, S.; Kubicki, J. D.; Mueller, K. T., *Langmuir* **2006**, 22, 9281-9286.

[15] Li, W.; Feng, J.; Kwon, K. D.; Kubicki, J. D.; Phillips, B. L., *Langmuir* **2010**, 26, 4753-4761.

[16] Gullion, T., *Chem. Phys. Lett.* **1995**, 246, 325-330.

[17] Chopin, L.; Vega, S.; Gullion, T., *J. Am. Chem. Soc.* **1998**, 120, 4406-4409.

[18] Mortlock, R. F.; Bell, A. T.; Radke, C. J., *J. Phys. Chem.* **1993**, 97, 775-782.

[19] Bak, M.; Rasmussen, J. T.; Nielsen, N. C., *J. Magn. Reson.* **2000**, 147, 296-330.

[20] Kolodziejski, W.; Klinowski, J., *Chem. Rev.* **2002**, *102*, 613-628.

[21] Mehring, M., *Principles of High Resolution NMR in Solids*; 2nd ed.; Springer-Verlag: Berlin, 1983.

[22] Herzfeld, J.; Berger, A. E., *J. Chem. Phys.* **1980**, *73*, 6021-6030.

[23] Eichele, K.; Wasylishen, R. E.; *WSOLIDS*, 2.0.18; Dalhousie University: Halifax, 2000.

Chapter 4.

[1] Arai, Y.; Sparks, D. L., *Adv. Agron.* **2007,** 94, 135-179.

[2] Paytan, A.; McLaughlin K., *Chem. Rev.* **2007,** 107, 563–576.

[3] Strongin, D. R.; Grey, C. P.; Parise, J. B.; Kubicki, J. D., *Surf. Sci.* **2010,** 604, 1065-1071.

[4] Catalano, J. G.; Park, C.; Zhang, Z.; Fenter, P., *Langmuir* **2006**, 22, 4668-4673.

[5] Nero, M, D.; Galindo, C.; Barillon, R.; Halter, E.; Madé, B., *J. Colloid Interface Sci.* 342, 437-444.

[6] Atkinson, R. J.; Parfitt, R. L.; Smart, R. S. C., *J. Chem. Soc. Faraday Trans. I* **1974**, 70, 1472–1479.

[7] Parfitt, R. L.; Atkinson, R. J., *Nature* **1976**, 264, 740−742

[8] Tejedor-Tejedor, M. I.; Anderson, M. A., *Langmuir* **1990**, 6, 602-611.

[9] Arai, Y.; Sparks, D. L., *J. Colloid Interface Sci.* **2001**, *241*, 317-326

[10] Elzinga, E. J.; Sparks, D. L., *J. Colloid Interface Sci.* **2007**, *308*, 53-70.

[11] Kwon, K. D**.;** Kubicki, J. D., *Langmuir* **2004**, 20, 9249-9254.

[12] Bleam, W. F.; Pfeffer, P. E.; Goldberg, S.; Taylor, R. W.; Dudley, R., *Langmuir* **1991,** *7*, 1702-1712.

[13] Lookman, R.; Grobet, P.; Merckx, R.; Vlassak, K., *Eur. J. Soil Sci.* **1994,** *45*, 37-44.

[14] Lookman, R.; Grobet, P.; Merckx, R.; Van Riemsdijk, W. H., *Geoderma* **1997,** *80*, 369-388.

[15] Johnson, B. B.; Ivanov, A. V.; Antzutkin, O. N.; Forsling, W., *Langmuir* **2002,** *18*, 1104-1111.

[16] Kim, Y.; Kirkpatrick, R. J., *Eur. J. Soil Sci.* **2004,** *55*, 243-251.

[17] Van Emmerik, T. J.; Sandstrom, D. E.; Antzutkin, O. N.; Angove, M. J.; Johnson, B. B., *Langmuir* **2007,** *23*, 3205-3213.

[18] Fry, R. A.; Kwon, K. D.; Komarneni, S.; Kubicki, J. D.; Mueller, K. T., *Langmuir* **2006**, *22*, 9281-9286.

[19] Li, W.; Feng, J.; won, K. D.; Kubicki, J. D.; Phillips, B. L., *Langmuir* **2010**, *26*, 4753-4761.

[20] Gullion, T., *Chem. Phys. Lett.* **1995**, 246, 325-330.

[21] Frisch, M. J.; Trucks, G. W.; Schlegel, H. B.; Scuseria, G. E.; Robb, M. A.; Cheeseman, J. R.; Montgomery, J. A., Jr. ; Vreven, T.; Kudin, K. N.; Burant, J. C.; Millam, J. M.; Iyengar, S. S.; Tomasi, J.; Barone, V.; Mennucci, B.; Cossi, M.; Scalmani, G.; Rega, N.; Petersson, G. A.; Nakatsuji, H.; M. Hada; M. Ehara; K. Toyota; Fukuda, R.; Hasegawa, J.; Ishida, M.; Nakajima, T.; Honda, Y.; Kitao, O.; Nakai, H.; Klene, M.; Li, X.; Knox, J. E.; Hratchian, H. P.; Cross, J. B.; Adamo, C.; Jaramillo, J.; Gomperts, R.; Stratmann, R. E.; Yazyev, O.; Austin, A. J.; Cammi, R.; Pomelli, C.; Ochterski, J. W.; Ayala, P. Y.; Morokuma, K.; Voth, G. A.; Salvador, P.; Dannenberg, J. J.; Zakrzewski, V. G.; Dapprich, S.; Daniels, A. D.; Strain, M. C.; Farkas, O.; Malick, D. K.; Rabuck, A. D.; Raghavachari, K.; Foresman, J. B.; Ortiz, J. V.; Cui, Q.; Baboul, A. G.; Clifford, S.; Cioslowski, J.; Stefanov, B. B.; Liu, G.; Liashenko, A.; Piskorz, P.; Komaromi, I.; Martin, R. L.; Fox, D. J.; Keith, T.; Al-Laham, M. A.; Peng, C. Y.; Nanayakkara, A.; Challacombe, M.; Gill, P. M. W.; Johnson, B.; Chen, W.; Wong, M. W.; Gonzalez, C.; Pople, J. A.; *Gaussian 03, Revision C.02*; Gaussian, Inc.: Wallingford CT, 2004.

[22] Becke, A. D., *J. Chem. Phys.* **1997**, 107, 8554-8560.

[23] Lee, C. T.; Yang, W. T.; Parr, R. G., *Phys. Rev. B* **1988**, 37, 785-789.

[24] Hehre, W. J.; Ditchfie, R.; Pople, J. A., *J. Chem. Phys.* **1972**, 56, 2257-2261.

[25] Scott, A. P.; Radom, L., *J. Phys. Chem.* **1996**, 100, 16502-16513.

[26] Schaftenaar, G.; Noordik, J. H., *J. Comput. Aided Mol. Design* **2000**, 14, 123-134.

[27] Mortlock, R. F.; Bell, A. T.; Radke, C. J., *J. Phys. Chem.* **1993**, 97, 775-782.

[28] Cade-Menun, B.J. *Talanta* **2005**, 66, 359-371.

[29] Conte, P.; Šmejkalová, D.; Piccolo, A.; Spaccini, R., *Eur. J. Soil Sci.* **2008**, 59, 584 – 591.

[30] Kolodziejski, W.; Klinowski, J., *Chem. Rev.* **2002**, 102, 613-628.

[31] Mehring, M., *Principles of High Resolution NMR in Solids;* 2nd ed.; Springer-Verlag: Berlin, 1983.

[32] Bak, M.; Rasmussen, J. T.; Nielsen, N. C., *J. Magn. Reson.* **2000**, 147, 296-330.

[33] Loring, J. S.; Sandstrom, M. H.; Noren, K.; Persson, P., *Chem. Eur. J.* **2009**, 15, 5063-5072.

[34] Sherman, D. M.; Randall, S. R., *Geochim. Cosmochim. Acta* **2003**, 67, 4223-4230.

Chapter 5.

[1] Barrow, N. J., *Soil Sci.* **1972**, *113*, 175-180.

[2] Barrow, N. J.; Bowden, J. W.; Posner, A. M.; Quirk, J. P., *Aust. J. Soil Res.* **1980**, *18*, 395-404.

[3] Gimsing, A. L.; Borggaard, O. K., *Clays Clay Miner.* **2001,** *49*, 270-275.

[4] Rietra, R. P. J. J.; Hiemstra, T.; Van Riemsdijk, W. H., *Environ. Sci. Technol.* **2001**, *35*, 3369-3374.

[5] Tunesi, S.; Poggi, V.; Gessa, C., *Nutr. Cycl. Agroecosys.* **1999**, *53*, 219-227.

[6] Wang, L. J.; Nancollas, G. H., *Chem. Rev.* **2008**, *108*, 4628-4669.

[7] Ronson, T. K.; McQuillan, A. J., *Langmuir* **2002**, *18*, 5019-5022.

[8] Hunger, S.; Cho, H.; Sims, J. T.; Sparks, D. L., *Environ. Sci. Technol.* **2004**, *38*, 674-681.

[9] Cade-Menun, B. J.; Navaratnam, J. A.; Walbridge, M. R., *Environ. Sci. Technol.* **2006**, *40*, 7874-7880.

[10] Hesterberg, D.; Zhou, W. Q.; Hutchison, K. J.; Beauchemin, S.; Sayers, D. E., *J. Synchrotron Rad.* **1999**, *6*, 636-638.

[11] Peak, D.; Sims, J. T.; Sparks, D. L., *Environ. Sci. Technol.* **2002**, *36*, 4253-4261.

[12] Hansen, J. C.; Cade-Menun, B. J.; Strawn, D. G., *J. Environ. Qual.* **2004**, *33*, 1521-1527.

[13] Sato, S.; Solomon, D.; Hyland, C.; Ketterings, Q. M.; Lehmann, J., *Environ. Sci. Technol.* **2005**, *39*, 7485-7491.

[14] Nooney, M. G.; Campbell, A.; Murrell, T. S.; Lin, X. F.; Hossner, L. R.; Chusuei, C. C.; Goodman, D. W., *Langmuir* **1998**, *14*, 2750-2755.

[15] Chusuei, C. C.; Goodman, D. W.; Van Stipdonk, M. J.; Justes, D. R.; Loh, K. H.; Schweikert, E. A., *Langmuir* **1999**, *15*, 7355-7360.

[16] Ingall, E. D.; Schroeder, P. A.; Berner, R. A., *Geochim. Cosmochim. Acta* **1990**, *54*, 2617-2620.

[17] Cade-Menun, B. J., *Talanta* **2005**, *66*, 359-371.

[18] Sannigrahi, P.; Ingall, E. D.; Benner, R., *Geochim. Cosmochim. Acta* **2006**, *70*, 5868-5882.

[19] Conte, P.; Smejkalova, D.; Piccolo, A.; Spaccini, R., *Eur. J. Soil Sci.* **2008**, *59*, 584-591.

[20] Li, W.; Feng, J.; Kwon, K. D.; Kubicki, J. D.; Phillips, B. L., *Langmuir* **2010**, *26*, 4753-4761.

[21] Negassa, W.; Kruse, J.; Michalik, D.; Appathurai, N.; Zuin, L.; Leinweber, P., *Environ. Sci. Technol.* **2010**, *44*, 2092-2097.

[22] Rothwell, W. P.; Waugh, J. S.; Yesinowski, J. P., *J. Amer. Chem. Soc.* **1980**, *102*, 2637-2643.

[23] Yesinowski, J. P., *J. Amer. Chem. Soc.* **1981**, *103*, 6266-6267.

[24] Yesinowski, J. P.; Benedict, J. J., *Calc. Tiss. Int.* **1983**, *35*, 284-286.

[25] Yesinowski, J. P.; Eckert, H., *J. Amer. Chem. Soc.* **1987**, *109*, 6274-6282.

[26] Yesinowski, J. P.; Eckert, H.; Rossman, G. R., *J. Amer. Chem. Soc.* **1988**, *110*, 1367-1375.

[27] Tseng, Y. H.; Zhan, J. H.; Lin, K. S. K.; Mou, C. Y.; Chan, J. C. C., *Solid State*

Nucl. Magn. Reson. **2004**, *26*, 99-104.

[28] Tseng, Y. H.; Mou, C. Y.; Chan, J. C. C., *J. Amer. Chem. Soc.* **2006**, *128*, 6909-6918.

[29] Cho, G. Y.; Wu, Y. T.; Ackerman, J. L., *Science* **2003**, *300*, 1123-1127.

[30] Hartz, T. K.; Johnstone, P. R.; Smith, R. F.; Cahn, M. D. *Hort Sci.* **2007**, *42*, 1681-1684.

[31] Hawke, D.; Carpenter, P. D.; Hunter, K. A., *Environ. Sci. Technol.* **1989**, *23*, 187-191.

[32] Chopin, L.; Vega, S.; Gullion, T., *J. Amer. Chem. Soc.* **1998**, *120*, 4406-4409.

[33] Lee, Y. J.; Stephens, P. W.; Tang, Y.; Li, W.; Phillips, B. L.; Parise, J. B.; Reeder, R. J., *Am. Mineral.* **2009**, *94*, 666-675.

[34] Mehring, M., *Principles of High Resolution NMR in Solids*. 2nd ed ed.; Springer-Verlag: Berlin, 1983.

[35] Kolodziejski, W.; Klinowski, J., *Chem. Rev.* **2002**, *102*, 613-628.

[36] Chairat, C.; Schott, J.; Oelkers, E. H.; Lartigue, J. E.; Harouiya, N., *Geochim. Cosmochim. Acta* **2007**, *71*, 5901-5912.

Chapter 6.

[1] Hiemstra, T.; Van Riemsdijk, W. H., *J. Colloid Interface Sci.* **1996**, *179*, 488-508.

[2] Eggleston, C. M.; Jordan, G., *Geochim. Cosmochim. Acta* **1998**, *62*, 1919-1923.

[3] Hiemstra, T.; Yong, H.; van Riemsdijk, W. H., *Langmuir* **1999**, *15*, 5942–5955.

[4] Fitts, J. P.; Shang, X. M.; Flynn, G. W.; Heinz, T. F.; Eisenthal, K. B., *J. Phys. Chem. B* **2005**, *109*, 7981-7986.

[5] Rajan, S. S. S.; Perrott, K. W.; Saunders, W. M. H., *J. Soil Sci.* **1974**, *25*, 438-447.

[6] Rajan, S. S. S., *Nature* **1975**, *253*, 434-436.

[7] Rajan, S. S. S., *Nature* **1976,** *262*, 45-46.

[8] Atkinson, R. J.; Quirk, J. P.; Posner, A. M., *J. Inorg. Nucl. Chem.* **1972**, *34*, 2201-2211.

[9] Kyle, J. H.; Posner, A. M.; Quirk, J. P., *J. Soil Sci.* **1975**, *26*, 32-43.

[10] Atkinson, R. J.; Parfitt, R. L.; Smart, R. S., *J. Chem. Soc. Faraday Trans. I* **1974**, *70*, 1472-1479.

[11] Tejedortejedor, M. I.; Anderson, M. A., *Langmuir* **1990**, *6*, 602-611.

[12] Connor, P. A.; McQuillan, A. J., *Langmuir* **1999**, *15*, 2916-2921.

[13] Arai, Y.; Sparks, D. L., *J. Colloid Interface Sci.* **2001,** *241*, 317-326.

[14] Ler, A.; Stanforth, R., *Environ. Sci. Technol.* **2003**, 37, 2694-2700.

[15] van Riemsdijk, W. H.; Lyklema, J., *J. Colloid Interface Sci.* **1980**, *76*, 55-66.

[16] Bleam, W. F.; Pfeffer, P. E.; Goldberg, S.; Taylor, R. W.; Dudley, R., *Langmuir* **1991**, *7*, 1702-1712.

[17] Kim, Y.; Kirkpatrick, R. J., *Eur. J. Soil Sci.* **2004**, *55*, 243-251.

[18] Khare, N.; Hesterberg, D.; Martin, J. D., *Environ. Sci. Technol.* **2005**, *39*, 2152-2160.

[19] Parfitt, R. L.; Atkinson, R. J., *Nature* **1976**, *264*, 740-742.

[20] Persson, P.; Nilsson, N.; Sjoberg, S., *J. Colloid Interface Sci.* **1996**, 177, 263-275.

[21] Ronson, T. K.; McQuillan, A. J., *Langmuir* **2002**, *18*, 5019-5022.

[22] **Luengo, C.; Brigante, M.; Antelo, J.; Avena, M.,** *J. Colloid Interface Sci.* **2006**, *300*, 511-518.

[23] Elzinga, E. J.; Sparks, D. L., *J. Colloid Interface Sci.* **2007**, *308*, 53-70.

[24] Khare, N.; Martin, J. D.; Hesterberg, D., *Geochim. Cosmochim. Acta* **2007**, *71*, 4405-4415.

[25] Goldberg, S.; Sposito, G., *Commun. Soil Sci. Plant Anal.* **1985**, *16*, 801-821.

[26] Kwon, K. D.; Kubicki, J. D., *Langmuir* **2004**, *20*, 9249-9254.

[27] Rahnemaie, R.; Hiemstra, T.; van Riemsdijk, W. H., *Langmuir* **2007**, *23*, 3680-3689.

[28] Laiti, E.; Persson, P.; Ohman, L.O., *Langmuir* **1996**, *12*, 2969-2975.

[29] Sparks, D.L., *Environmental Soil Chemistry* 2nd ed.; Academic Press: San Diego, CA, 2003.

[30] Navrotsky, A., *Rev. Mineral. Geochem.* **2001**, *44*, 73-103.

[31] Stumm, W. and Morgan, J. J.(1996): *Aquatic Chemistry, Chemical Equilibria and Rates in Natural Waters*, 3rd ed. John Wiley & Sons, Inc., New York

[32] Tseng, Y. H.; Zhan, J. H.; Lin, K. S. K.; Mou, C. Y.; Chan, J. C. C., *Solid State Nucl. Magn. Reson.* **2004**, 26, 99-104.

[33] Tseng, Y. H.; Mou, C. Y.; Chan, J. C. C., *J. Amer. Chem. Soc.* **2006**, 128, 6909-6918.

[34] Mehring, M., *Principles of High Resolution NMR in Solids*. 2nd ed.; Springer-Verlag: Berlin, 1983.

[35] Hunger, S.; Cho, H.; Sims, J. T.; Sparks, D. L., *Environ. Sci. Technol.* **2004**, *38*, 674-681.

[36] Cade-Menun, B. J.; Navaratnam, J. A.; Walbridge, M. R., *Environ. Sci. Technol.* **2006**, *40*, 7874-7880.

[37] Paola, D. L.; Javier C., *Clays Clay Miner.* **2003**, *51*, 403-414.

[38] Mason, H. E.; Hirner, J. J.; Xu, W.; Parise, J. B.; Phillips, B. L., *Magn. Reson. Chem.* **2009**, *47*, 1062-1070.

[39] Cole, K. E.; Paik, Y.; Reeder, R. J.; Schoonen, M.; Grey, C. P., *J. Phys. Chem. B.* **2004**, *108,* 6938-6940.

[40] Nielsen, U. G.; Paik, Y.; Julmis, K.; Schoonen, M. A. A.; Reeder, R. J.; Grey, C. P., *J. Phys. Chem. B* **2005**, *109*, 18310-18315.

[41] Kim, J.; Nielsen, U. G.; Grey, C. P., *J. Am. Chem. Soc.* **2008**, *130*, 1285-1295.